Theses - Daytona Beach

Dissertations and Theses

Spring 2010

# Optical Properties of Type III-V Semiconductor Spherical Quantum Dot Heterostructures

Nathan Haluska
*Embry-Riddle Aeronautical University - Daytona Beach*

Follow this and additional works at: https://commons.erau.edu/db-theses

Part of the Atomic, Molecular and Optical Physics Commons

# OPTICAL PROPERTIES OF TYPE III-V SEMICONDUCTOR SPHERICAL QUANTUM DOT HETEROSTRUCTURES

By

Nathan Haluska

A Thesis Submitted to the

Physical Sciences Department

In Partital Fulfillment of the Requirements for the Degree of

Master of Science in Engineering Physics

Embry-Riddle Aeronautical University

Daytona Beach, Florida

Spring 2010

UMI Number: EP31915

INFORMATION TO USERS

The quality of this reproduction is dependent upon the quality of the copy submitted. Broken or indistinct print, colored or poor quality illustrations and photographs, print bleed-through, substandard margins, and improper alignment can adversely affect reproduction.

In the unlikely event that the author did not send a complete manuscript and there are missing pages, these will be noted. Also, if unauthorized copyright material had to be removed, a note will indicate the deletion.

UMI®

# OPTICAL PROPERTIES OF TYPE III-V SEMICONDUCTOR SPHERICAL QUANTUM DOT HETEROSTRUCTURES

by

Nathan Haluska

This thesis was prepared under the direction of the candidate's thesis committee chair, Dr. Bereket H. Berhane, Department of Physical Sciences, and has been approved by the members of the thesis committee. It was submitted to the Department of Physical Sciences and was accepted in partial fulfillment of the requirements of the Degree of

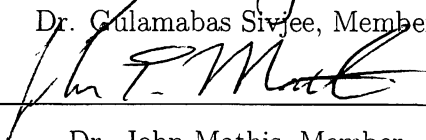Master of Science in Engineering Physics

THESIS COMMITTEE:

_____
Dr. Bereket H. Berhane, Chair

_____
Dr. Gulamabas Sivjee, Member
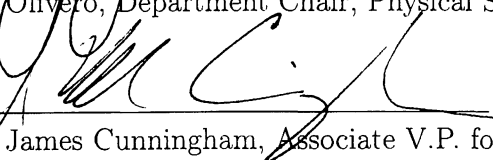
_____
Dr. John Mathis, Member

_____
Dr. Erdman, MSEP Graduate Program Coordinator

_____
Dr. Olivero, Department Chair, Physical Sciences

_____                    5-06-10
Dr. James Cunningham, Associate V.P. for Academics      Date

iii

# ABSTRACT

| | |
|---|---|
| Author | Nathan Haluska |
| Title | Optical Properties of Type III-V Semiconductor Spherical Quantum Dot Heterostructures |
| Institution | Embry-Riddle Aeronautical University |
| Degree | Master of Science in Engineering Physics |
| Year | 2010 |

In recent years quantum dots (QD) have attracted increasing interest because of their wide variety of revolutionary applications  Such applications include high speed optical communication lasers, infrared photodetectors, and single photon emitters  One promising immediate application is QD solar cells  Proper analysis of the optical absorption characteristics in these solar cells requires a rigorous modeling of the electronic structure and optical properties of semiconductor heterostructures  Our emphasis will be on type III-V semiconductors  Such structures, have a great potential for increasing efficiencies, but they also possess highly degenerate and complex valence band structures  Therefore, we seek to develop a model of spherical QD band structure for type III-V Semiconductor materials, and with such results we obtain the absorption properties of the simulated QDs  We assume stress and strain effects are negligible  We also assume the conduction and spin-orbit bands are treated as distant  We utilize the spherically symmetric, single and multiple band effective mass equations along with previously developed analytical methods to simplify the problem, then we obtain the eigenfunctions and eigenenergies of the QD, and use them to model optical transitions  We assume a quasi-equilibrium Fermi-Dirac distribution for electrons and holes and obtain the microscopic transition rates and absorption coefficients  Furthermore, we implement this in Matlab with a robust graphical user interface which allows for arbitrary configurations of materials and QD sizes  With this tool, the eigenenergies, eigenfunctions, and absorption coefficients may be calculated

# ACKNOWLEDGEMENT

First, I would like to thank my thesis committee, whose valued support and expertise greatly added to my understanding of the subject matter. In particular, I would like to thank my advisor Dr. Berhane, for his endless hours of discussions and explanations. His knowledge and lectures on the subject provided me with the background required to complete an otherwise daunting task.

Furthermore, I would also like to express my gratitude towards my family, for their unending support which allowed me to focus on my studies. Most important of all, I would like to thank my future wife Lee Ann, who is back owed many weekends of time and affection, and apparently a cow–a little brown one I'm told, possibly with a white spot on its nose. I know God has also helped me in many ways, but he wasn't very specific as to how.

Nathan Haluska
6 May 2010

# Nomenclature

$\alpha$      Optical Absorption Coefficient

$\delta_{ab}$      Kronecker Delta Function

$\left( \begin{smallmatrix} F & J & L \\ F_z & J_z & L_z \end{smallmatrix} \right)_{cg}$    Clebsch Gordan Coeffficient

$\left( \begin{smallmatrix} L & L' & L'' \\ m & m' & m'' \end{smallmatrix} \right)$    Wigner 3-j Symbol

$\vec{A}$      Vector Potential

$\vec{E}(\vec{r}, t)$   Electric Field

$\vec{H}(\vec{r}, t)$   Magnetic Field

$\vec{P}(\vec{r}, t)$   Poynting Vector

$E_g$      Band Gap Enegry (eV)

$E_p$      Optical Matrix Parameter

$I$      Intensity$(W/m^2)$

$j_l$      Spherical Bessel Functions

$k_{op}$      optical wave vector

$m^*$      Effective mass

$m_e^*$      Conduction band Effective mass

$m_{hh}^*$      Heavy Hole Effective mass

$m_{lh}^*$      Light Hole Effective mass

$m_{so}^*$      Spin-Orbit Split-off Hole Effective mass

$m_0$      Electron Mass

$P$      Kane's Parameter

$P_{cv}$      Bloch component of Momentum Matrix Element

$u_{n\vec{k}}(\vec{r})$      Bloch function

$Y_L^M$      Spherical Harmonic (Normalised)

H      Hamiltonian

# Contents

# List of Tables

# List of Figures

# Chapter 1

# Introduction

In the last two decades, quantum dots have attracted increasing interest because of their wide variety of revolutionary applications. Such applications include high speed optical communication lasers [1; 2], infrared detectors [3], and single photon emitters [4]. They have been suggested to serve as platforms for qubits in quantum computation. Recently, they have also been used as imaging dyes in biomedical applications. Quantum dots are very versatile because they are essentially synthetic atoms.

Perhaps, the most promising immediate application of quantum dots is in solar cells. It has been shown [5] that quantum dot solar cells can produce efficiencies more than double the Shockley-Queisser [6] limit. Such efficiencies are possible with quantum dots because of their highly discrete density of states, temperature stability, long exciton lifetimes, and multiple exciton generations [7; 8; 9].

Semiconductors offer a very effective platform for optoelectronic applications. Here, we concentrate on type III-V semiconductors. In the past few decades, the technology required for the growth and fabrication of type III-V semiconductors has matured, and their band structure lends itself easily to the optical spectrum needed for photovoltaic and other optical (visible and near infrared) applications. Such semiconductors are known to have many advantages over conventional silicon; but these

advantages come at the price of a complex and degenerate band structure. To exploit the full potential application of III-V semiconductor heterostructures, a detailed knowledge of their quantum-optical properties is very important.

Although, there are relatively simple models for quantum dots [10; 11], these methods do not provide realistic enough models. An effective model for a type III-V semiconductor quantum dot must include band mixing and the influence of the multiple materials. In order to obtain a realistic optical absorption spectrum, the effective mass equation–a set of coupled partial differential equations–must be solved to find eigenfunctions and eigenenergies. In most geometries this must be done numerically. Here we consider a spherically symmetric system which can be simplified analytically by exploiting the spherical symmetry [12; 13; 14], and we obtain semi-analytical results. With the eigenfunctions and eigenenergies, we consider dipole transitions, and compute the dipole matrix elements. We assume a quasi-equilibrium Fermi-Dirac distribution for electrons and holes, and then obtain the microscopic transition rates and absorption coefficients.

The thesis is organized as follows: In the first chapter, we introduce the concept of a semiconductor quantum dot and some relevant background on perturbation theory. In chapter 2, we develop and discuss $\vec{k} \cdot \vec{p}$ theory for a bulk semiconductors, then expand the theory to heterostructures and obtain the effective mass equation. In Chapter 3, we use the effective mass equation to develop a model for obtaining eigenfunctions and eigenenergies; we implement this model in Matlab. We also give the results for many common types of quantum dots. In chapter 4, we cover the methodology required to calculate the optical transition rates and absorption coefficients, and present relevant results. In the final chapter, we give an overview of quantum dot solar cells and the relevance of our results to such applications.

## 1.1 Semiconductors

A Semiconductor is a material that has an electrical conductivity between that of a conductor and an insulator. Semiconductor materials absorb and emit photons by undergoing transitions among allowed energy levels. Because of the proximity of the

atoms in the crystal lattice, the energies belong to the system as a whole and not just the single atoms. Depending on the arrangement, density, and type of atoms in the crystal, various symmetry conditions exist which lead to closely spaced energy levels or bands. Silicon for example has a comparatively simple structure to that of type III-V semiconductors. Discussions on semiconductors can be found in many texts such as [15; 11].

It is important to introduce the concept of a *hole*–the absence of an electron. A *hole* is actually a rather intricate concept from quantum field theory. If we were to consider the electrons in the valence band as a large system of identical particles then we would have to insure that the total wave function of all the particles was antisymmetric (which is a huge problem). The second quantized method [16; 17] of quantum field theory alleviates this problem and essentially allows us to model holes instead, which are much fewer in number. Thus we can say that the absorption of a photon can create an electron-hole pair– which is also referred to as an exciton. Recombination of an electron-hole pair can result in the emission of a photon.

The band structure of type III-V semiconductors lends itself nicely to optoelectronic applications. If we consider a single bulk semiconductor, we can model it macroscopically as a crystal with infinite periodic potentials, and from this we model electrons in the conduction band, and holes in the valence band. The band structures for our case are complicated and highly degenerate. We show a unit cell of type III-V semiconductors in Figure 1.1. This unit cell represents the most basic form of the crystal lattice, and we can construct a bulk lattice by stacking them in all directions. We shall return to bulk semiconductors in chapter 2, but first we introduce the concept of a heterostructures of two semiconductor materials.

## 1.1.1 Semiconductor Heterostructures

Semiconductor heterostructures are formed by a juxtaposition of two semiconductor materials (e.g. GaAs in AlAs). This leads to a potential difference in the band edges which serve as confining potentials, creating quantum wells, quantum wires, or quantum dots (Figure 1.2).
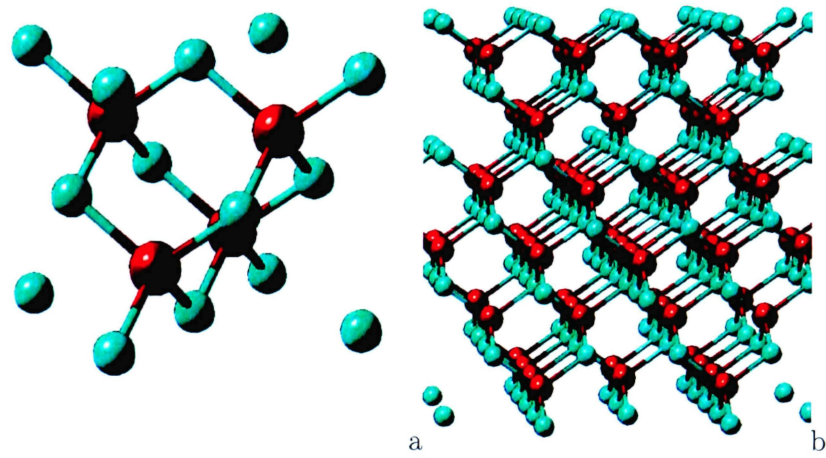
Figure 1.1: a) Zinc blende unit cell. b) Bulk lattice.
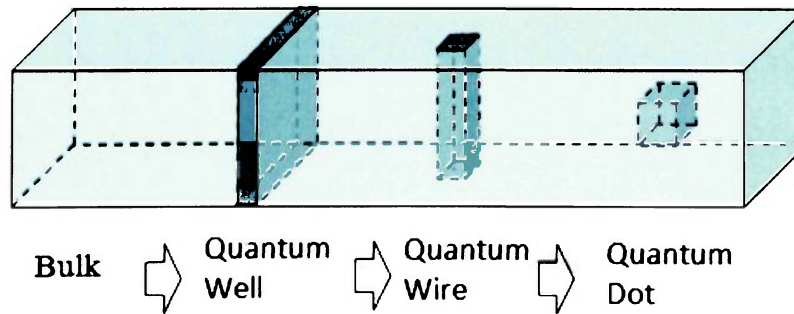


Figure 1.2: Confining a Semiconductor Heterostructure.

As a side note, we point out that experimental and theoretical physicists describe quantum confined structures differently. Experimentalists refer to the geometrical dimensionality of a quantum-confined structure–a quantum well has two dimensions, a quantum wire has one dimension, and a quantum dot has zero dimensions. Theoretical physicists depict these structures by number of confinement dimensions. A quantum well possesses one dimension of confinement, a quantum wire contains two dimensions of confinement, and a quantum dot has three dimensions of confinement. For our purposes, we focus on the electronic structure of quantum dots; therefore, we refer to a quantum dot as a 3D structure.

## Semiconductor Quantum Wells and Wires

In a quantum well, electrons are confined in one direction (dimension) by a potential and unconfined in the other two. This is illustrated in Figure 1.3.
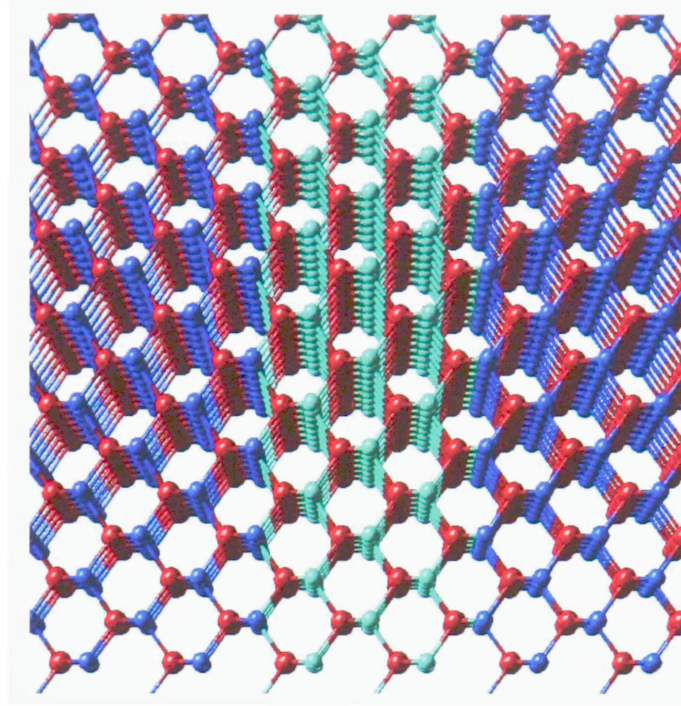
Figure 1.3: A 1D Semiconductor Quantum Well of about 1nm; the intent of this figure is to illustrate the concept of a 1D heterojunction. In most cases a width of $\approx 2$ nm is needed for confined levels to exist.

A quantum wire is confined by a potential in two directions, and unconfined in a third direction. Nanotubes are a common example.

### Semiconductor Quantum Dot

A quantum dot is characterized by a three dimensional confining potential. We illustrate a spherical case in Figure 1.4
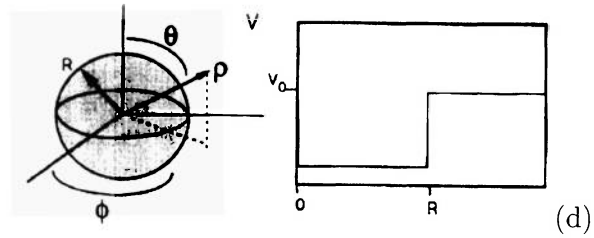
Figure 1.4: The quantum dot and quantum dot confining potential

Since, spherical quantum dots are the focus of our discussion, we have created some structural examples in Matlab whose sizes are comparable to those in our discussion. In the next three figures, we give plots of what a III-V quantum dot would look like on the atomic scale, ignoring the outside material. We build these dots by stacking unit cells together into spheres with radii of a specified number of unit cells.
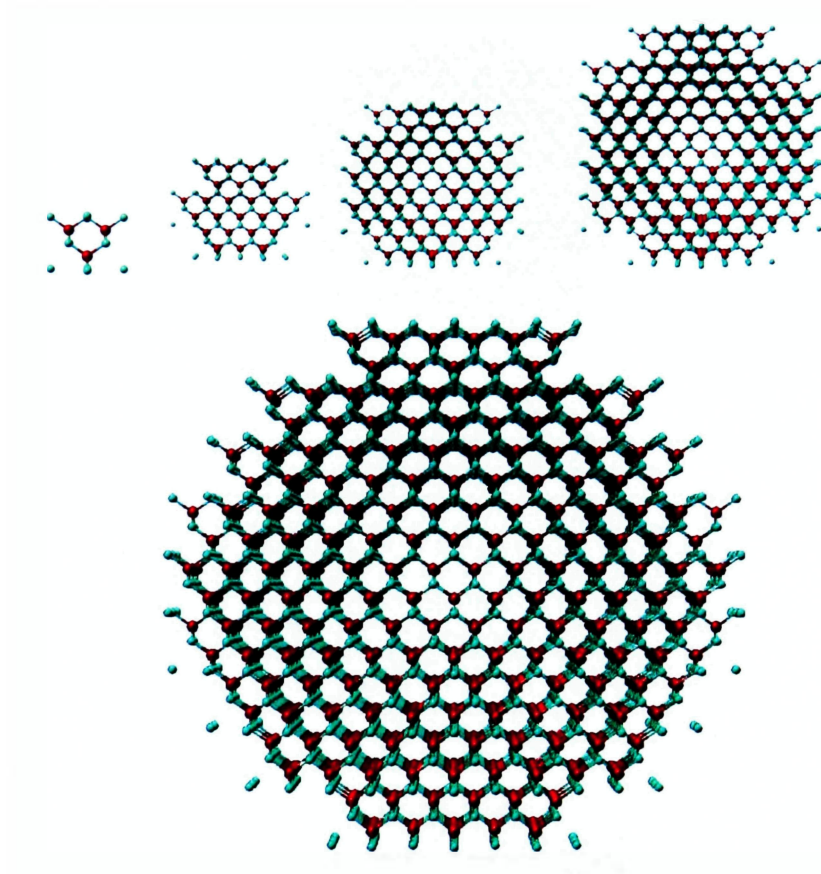
Figure 1.5: Quantum dots with radii of 1,2,3,4, and 5 unit cells. Essentially we build spheres out of unit cells, and only plot those that are within a specified radius. Two unit cells equates to about 1 nm for an average type III-V semiconductor.
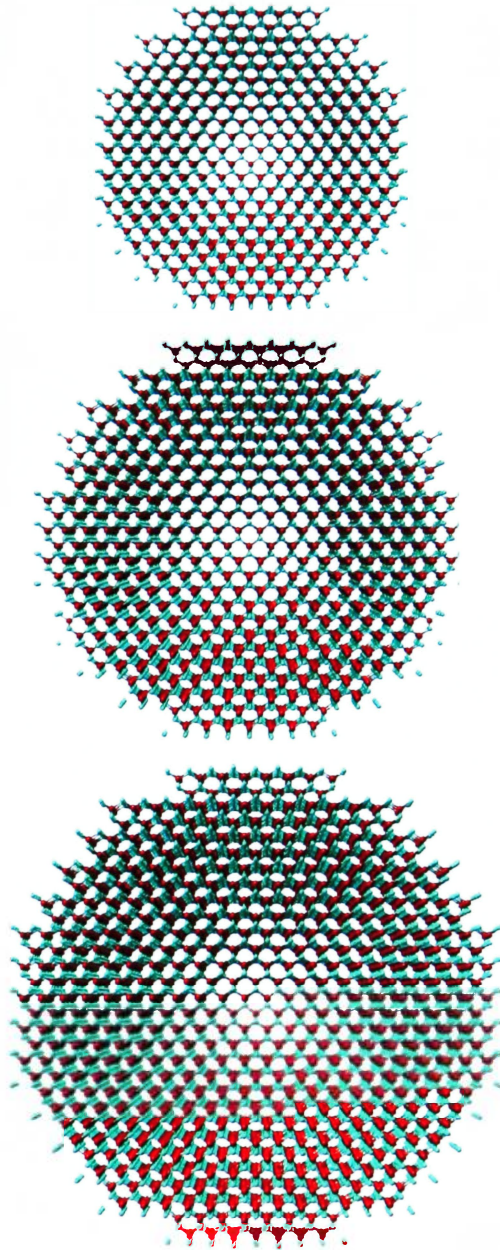
Figure 1.6: Quantum dots of 6 to 8 unit cells of radius
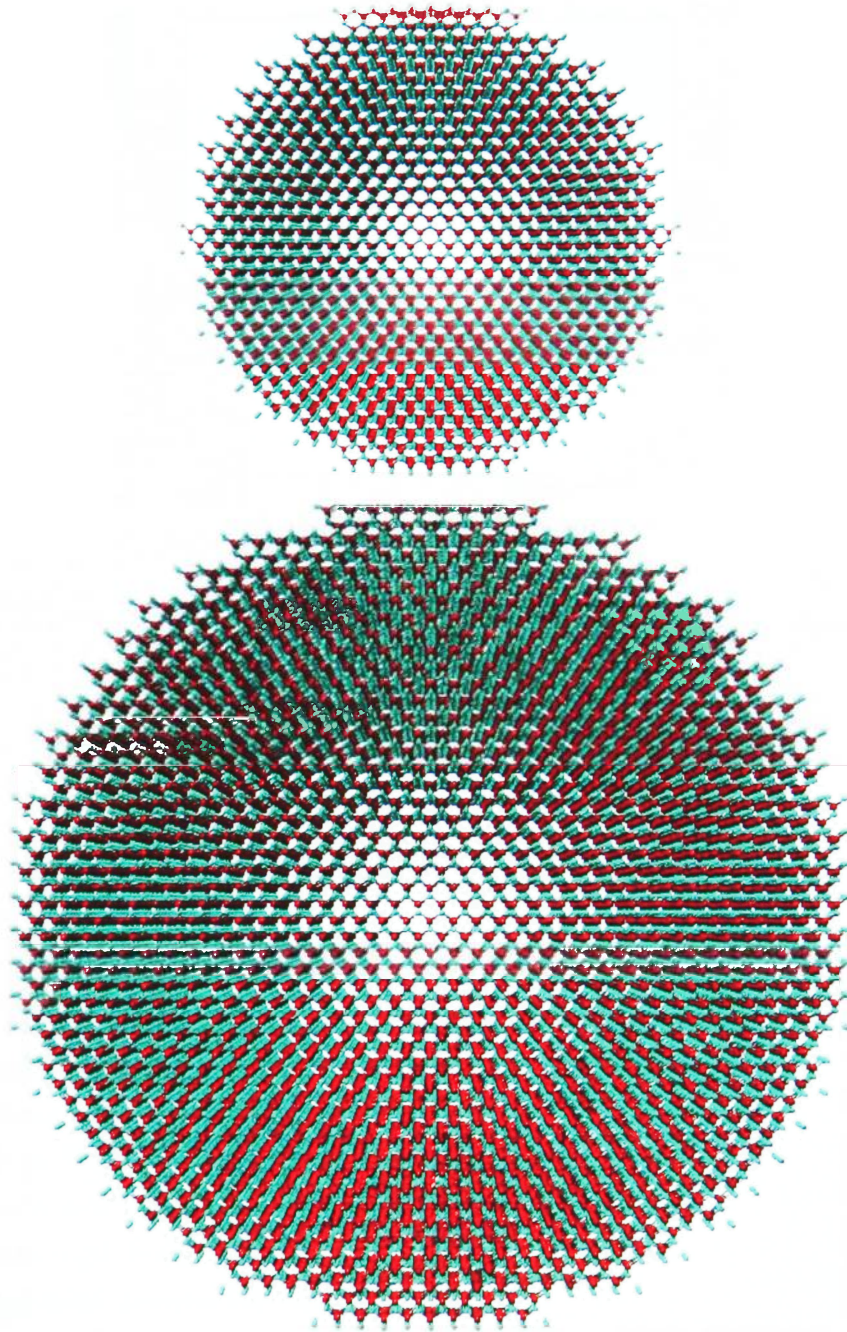
Figure 1.7: Quantum dots of 9 and 13 unit cells of radius, for GaAs a radius of 13 unit cells corresponds to about 7.3 nm.
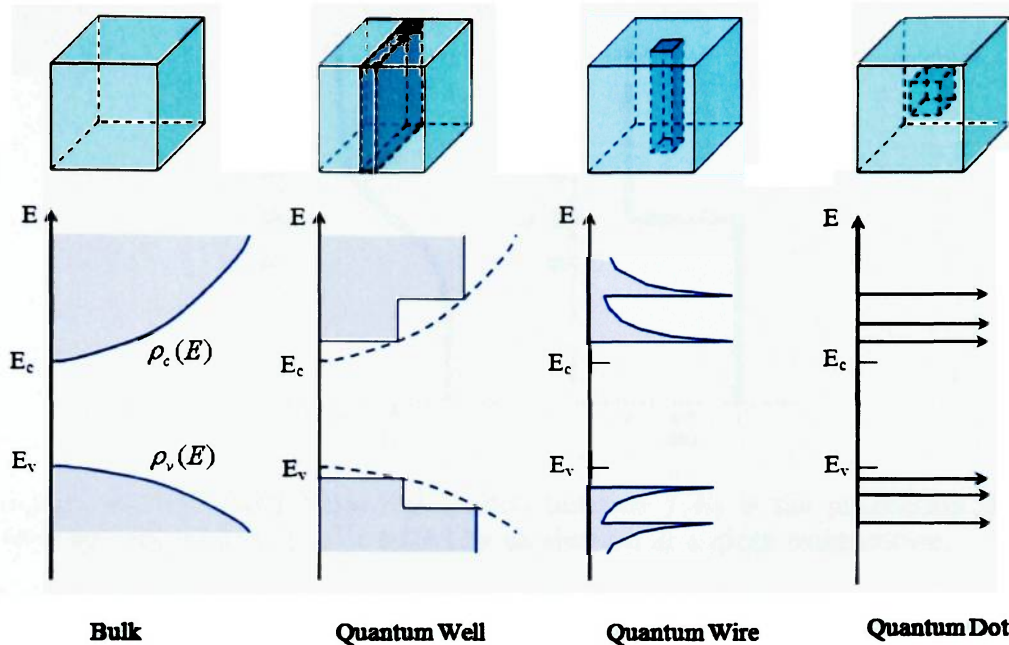
Figure 1.8: The effect of quantum confinement on the density of states. The y-axis specifies the energy levels, and the x-direction (not-shown) specifies the number of states that exist at that energy level.

# 1.2 Density of States in Quantum-Confined Structures

One of the most important characteristics of a band structure is the density of states. The density of states refers to the population of electrons in the conduction band and valence band at a given temperature. It is highly influenced by confinement [10, 11], as illustrated in Figure 1.8. Note that for bulk semiconductors, the density of states is nearly continuous–it's actually discrete but the fluctuations are small at the macroscopic level. As we increase the confinement, we eventually end up with the Dirac-delta distribution for the quantum dots. The high degree of confinement leads to very discrete states, making quantum dots very useful in producing a laser with a very low number of modes.
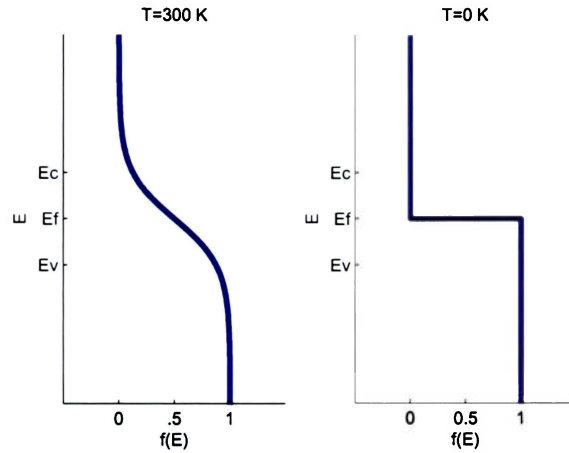
Figure 1.9: The Fermi-Dirac distribution function $f(E)$ is the probability that a particular energy level E is occupied by an electron at a given temperature.

We make the approximation that the crystal is in quasi-equilibrium. Under these conditions the probability of occupancy is given by the Fermi-Dirac distribution. The Fermi-Dirac distribution–or Fermi-Dirac statistics–gives the probability that a state is occupied for a given energy level and temperature:

$$f(E) = \frac{1}{e^{\frac{E-E_f}{k_b T}} + 1}$$

where $E_f$ is the Fermi energy and $k_b$ is Boltzmann's constant.; for a semiconductor in thermal-equilibrium this is usually half the separation between the conduction and valence band. We illustrate this distribution in Figure 1.9. Note that at 0 K there are no electrons in the conduction band.

## 1.3   Time-Independent Perturbation theory

In most practical physical systems, the Schrödinger equation does not have a exact or analytical solution. Therefore, we find solutions through perturbation methods. We shall first look at cases where the eigenvalues of the unperturbed Hamiltonian are non-degenerate.

## 1.3.1 Non-Degenerate Case

Suppose we know the eigenfunctions of some unperturbed Hamiltonian,

$$H^{(0)}\phi_n^{(0)} = E_n^{(0)}\phi_n^{(0)}$$

and consider a perturbation Hamiltonian H, where

$$H = H^{(0)} + H'$$

In order to find solutions to

$$H\psi = E\psi$$

it is convenient to introduce the parameter $\lambda$, which we set equal to 1 later

$$H = H^{(0)} + \lambda H'$$

We look for solutions of the form

$$
\begin{aligned}
E &= E^{(0)} + \lambda E^{(1)} + \lambda^2 E^{(2)} + \cdots \\
\psi &= \psi^{(0)} + \lambda\psi^{(1)} + \lambda^2\psi^{(2)} + \cdots
\end{aligned}
$$

and substitute them for $H$,$E$, and $\psi$ into $H\psi = E\psi$:

Zeroth order $H^{(0)}\psi^{(0)} = E^{(0)}\psi^{(0)}$

First order $\quad H^{(0)}\psi^{(1)} + H'\psi^{(0)} = E^{(0)}\psi^{(1)} + E^{(1)}\psi^{(0)}$

Second order $H^{(0)}\psi^{(2)} + H'\psi^{(1)} = E^{(0)}\psi^{(2)} + E^{(1)}\psi^{(1)} + E^{(2)}\psi^{(0)}$

**Zeroth-Order Solutions**

It is straight forward to see that

$$
\begin{aligned}
\psi_n^{(0)} &= \phi_n^{(0)} \\
E_n^{(0)} &= E_n^{(0)}
\end{aligned}
$$

## First-Order Solutions

We simply include the final result but more information can be found in quantum mechanics textbooks such as [10; 18; 19]

$$\psi_n^{(1)} = \phi_n^{(0)} + \sum_{m \neq n} \frac{H'_{mn}}{E_n^{(0)} - E_m^{(0)}} \phi_m^{(0)} \tag{1.1}$$

$$E_n^{(1)} = E_n^{(0)} + H'_{nn} \tag{1.2}$$

where

$$H'_{mn} = \int \phi_m^{(0)*} H' \phi_n^{(0)} d^3 \vec{r}$$

## Second-Order Solutions

Again, we just note the final results

$$\psi_n^{(2)} = \phi_n^{(0)} + \sum_{m \neq n} \frac{H'_{mn}}{E_n^{(0)} - E_m^{(0)}} \phi_m^{(0)} + \sum_{m \neq n} \left[ \left( \sum_{k \neq n} \frac{H'_{mk} H'_{kn}}{\left( E_n^{(0)} - E_m^{(0)} \right) \left( E_n^{(0)} - E_k^{(0)} \right)} \right. \right.$$
$$\left. \left. - \frac{H'_{mn} H'_{nn}}{\left( E_n^{(0)} - E_m^{(0)} \right)^2} \right) \phi_m^{(0)} - \frac{\left( H'_{mn} \right)^2}{2 \left( E_n^{(0)} - E_m^{(0)} \right)^2} \phi_n^{(0)} \right]$$
$$E_n^{(2)} = E_n^{(0)} + H'_{nn} + \sum_{m \neq n} \frac{\left( H'_{nm} \right)^2}{E_n^{(0)} - E_m^{(0)}} \tag{1.3}$$

Note that in all cases beyond the zeroth order, if $E_n^{(0)} \approx E_m^{(0)}$, then singularities will result.

## 1.3.2 Degenerate Case: Löwdin's Renormalization Method

In the prior sub-section we saw that if the energy level $E_n^{(0)}$ approached the energy level $E_m^{(0)}$, then the perturbation theory breaks down. We can mitigate this with Löwdin's Method [20]. Löwdin's method is readily applicable to semiconductors with a single conduction band and highly degenerate valence bands.

Consider the time-independent Schrödinger equation

$$H = \left( H^{(0)} + H' \right) \psi = E\psi$$

we start with known solutions to an unperturbed Hamiltonian

$$H^{(0)}\phi_n^{(0)} = E_n^{(0)}\phi_n^{(0)}$$

where $\left\{ \phi_n^{(0)} \right\}$ form a complete set of orthonormal functions. We can let $\psi$ be a linear combination of the unperturbed eigenfunctions

$$\psi = \sum_n a_n \phi_n^{(0)}$$

Next we substitute this into $H\psi = E\psi$ and take the inner product with respect to $\phi_k^{(0)}$ where $k = 1, \cdots, N$ and from the condition of orthonormality we have

$$\sum_n \left( H_{kn} - E\delta_{kn} \right) a_n = 0 \qquad (1.4)$$

where $\delta_{nk}$ is the Kronecker delta function, $\delta_{ab} = 0$ if $a \neq b$ and $\delta_{ab} = 1$ if $a = b$. Next we rewrite equation 1.4 as

$$(E - H_{nn}) a_n = \sum_{m \neq n}^{A} H_{nm} a_m + \sum_{\alpha \neq n}^{B} H_{n\alpha} a_\alpha$$

Now we can utilize Löwdin's renormalization method [20] to solve

$$\sum_n^A \left( H_{kn} - E\delta_{kn} \right) a_n = 0$$

by transforming it into

$$\sum_n \left( U_{kn}^A - E\delta_{kn} \right) a_n = 0$$

where

$$U_{kn}^A = H_{kn} + \sum_\alpha^B \frac{H_{k\alpha}' H_{\alpha n}'}{E_A - H_{\alpha\alpha}}$$

The details of the above results can be found in [10].

## 1.4 Time-Dependent Perturbation theory

Since our main focus is optical properties of quantum dots, we wish to address single photon transitions [21; 10; 16]. The emission and absorption of photons requires transitions between the valence and conduction band. Therefore, we consider transitions in time between the states (eigenvectors) in our system by adding a perturbation Hamiltonian $H'(\vec{r}, t)$ due to some external electromagnetic field. We start with the time-dependent Schrödinger equation

$$i\hbar \frac{\partial}{\partial t} \psi(\vec{r}, t) = H \psi(\vec{r}, t)$$

where the Hamiltonian consists of

$$H = H_0 + H'(r, t)$$

We assume we know the solutions to

$$i\hbar \frac{\partial}{\partial t} \phi_n(\vec{r}, t) = H_0 \phi_n(\vec{r}, t)$$
$$\phi_n(\vec{r}, t) = \phi_n(\vec{r}) e^{-\imath E_n t/\hbar}$$

For convenience we assume that we have a time-harmonic perturbation which "turns on" at $t = 0$. In other words, we have considered the states of the system quantum mechanically, and the applied electric field classically. With these assumptions we have

$$H'(\vec{r}, t) = \begin{cases} H'(\vec{r}) e^{-\imath \omega t} + H'^\dagger(\vec{r}) e^{-\imath \omega t} & t \geq 0 \\ 0 & t < 0 \end{cases}$$

where the supper script † indicates the hermitian conjugate. To find $\psi(\vec{r}, t)$ we expand the wave function as a linear superposition of the eigenfunctions of the unperturbed Hamiltonian

$$\psi(\vec{r}, t) = \sum_n a_n(t)\phi_n(\vec{r})e^{-iE_n t/\hbar}$$

We define the initial electron state with the subscript $i$ and the final state as $f$. At $t = 0$

$$a_i(t = 0) = 1; \qquad a_m(0) = 0, \quad m \neq i$$

If we let

$$a_n(t) = a_n^{(0)}(t) + a_n^{(1)}(t) + a_n^{(2)}(t) + \cdots$$

then it can be shown [10; 16; 18; 21], that the transition rate from state $i$ to $f$

$$
\begin{aligned}
W_{if} &= \frac{d}{dt}\left|a_f^{(1)}(t)\right|^2 \\
&= \frac{2\pi}{\hbar}\left|H'_{fi}\right|^2 \delta(E_f - E_i - \hbar\omega) + \frac{2\pi}{\hbar}\left|H'^{\dagger}_{fi}\right|^2 \delta(E_f - E_i + \hbar\omega)
\end{aligned}
\tag{1.5}
$$

This is Fermi's Golden rule in a form convenient for our purposes.

# Chapter 2

# $\vec{k} \cdot \vec{p}$ Theory and the Effective Mass Equation

In order to investigate the optical properties of semiconductors in the presence of an external field, we must first obtain their electronic band structures. (The discusion below is based on work done by Luttenger and Kohn [22, 23], and further discusion can be found in *The Physics of Photonic Devices* [10].)

The objective of this chapter is to utilize the well developed theory of bulk semiconductor properties and structures. From these well known and experimentally verified parameters, we approximate the band structure in a bulk semiconductor. In the last section, we expand the theory to hetrojunctions by considering a perturbation to the bulk structure.

## 2.1 The $\vec{k} \cdot \vec{p}$ method for Bulk Semiconductors

An important result from solid states physics is that a periodic potential, $V(\vec{r}) = V(\vec{r} + \vec{R})$, will give a Hamiltonian with eigenfunctions of the form [15]:

$$\psi_{n\vec{k}} = e^{i\vec{k}\cdot\vec{r}} u_{n\vec{k}}(\vec{r}) \tag{2.1}$$

18

The subscript n, in $u_{n\vec{k}}(\vec{r})$, refers to the band, and $\vec{k}$ is the wave vector of the electron. We refer to $u_{n\vec{k}}(\vec{r})$ as the Bloch function, which is illustrated in Figure 2.1. In Figure 2.1a, we see an unperturbed periodic potential of atomic nuclei. Figure 2.1b illustrates the pseudo potential caused by the combination of the Bloch potential and the periodic potential. In reality this function occurs in three dimensions so we also included an Equipotential surface in the Si lattice in figure 2.1c.



(a)

(b)

(c)
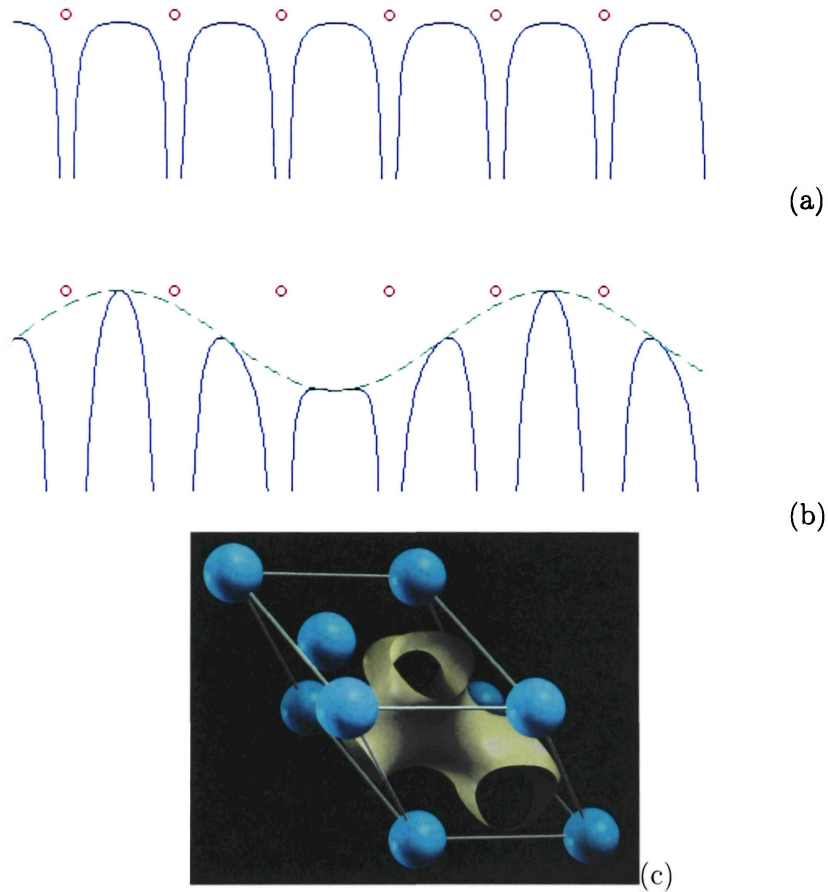
Figure 2.1: (a) A 1D periodic potential. (b) A partial representation of a periodic potential with modified Bloch $u_{n\vec{k}}(\vec{r})$ component, this is not realistic just conceptual. (c) A 3D equipotential in the Si bulk lattice
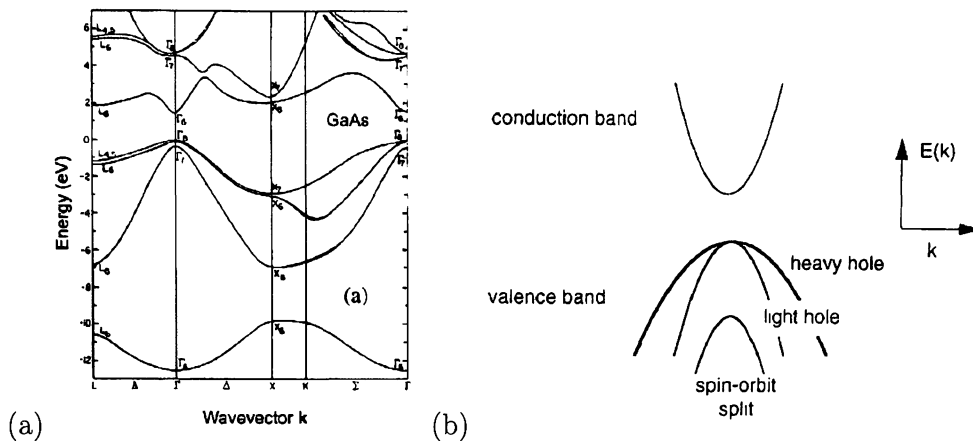
Figure 2.2: (a) GaAs Band Structure. (b) Zoomed in region of $\Gamma$ symmetry point. $\vec{k} \cdot \vec{p}$ theory attempts to approximate the band structure of a semiconductor in this region by using the parabolic nature of the known structure.

In order to obtain an accurate description of the band structure, numerical methods from solid state physics [15] are required. The GaAs band structure calculated by the pseudopotential method is shown in figure 2.2a, from [24], which represents the energy bands along different $\vec{k}$. In k-space, the Fourier transform of the zinc-blende unit cell, the face centered cubic (FCC) structure of the bulk becomes a body centered cubic structure which has may forms of mirror and rotational symmetries. this plays an important factor in the band structure. For our purposes, the region of interest is the $\Gamma$ symmetry point which is highlighted in Figure 2.2b [9]. The $\Gamma$ symmetry point is a highly symmetric point of the reciprocal crystal lattice. The names "light hole" and "heavy hole" refer to the parabolic dispersion relations which describe the states. Essentially the "effective masses" of holes in the heavy hole band are larger then the effective mass of the light holes.

The Bloch function oscillates on the order of the unit cell. The zinc blende unit cell and bulk lattice are shown in figure 1.1. If we use equation 2.1 in the time independent Schrödinger equation

$$H\Psi(\vec{r}) = \left( \frac{\hbar^2}{2m_0} \nabla^2 + V(\vec{r}) \right) \psi(\vec{r}) = E(\vec{k})\psi(\vec{r}) \qquad (2.2)$$

we obtain (note $\vec{p} = -\imath\hbar\nabla$)

$$\left(\frac{p^2}{2m_0} + V(\vec{r})\right)\psi_{n\vec{k}}(\vec{r}) = E_n(\vec{k})\psi_{n\vec{k}}(\vec{r})$$

$$\left(\frac{p^2}{2m_0} + V(\vec{r})\right)e^{\imath\vec{k}\cdot\vec{r}}u_{n\vec{k}}(\vec{r}) = E_n(\vec{k})e^{\imath\vec{k}\cdot\vec{r}}u_{n\vec{k}}(\vec{r}) \qquad (2.3)$$

$$\left(\frac{p^2}{2m_0} + \frac{\hbar}{m_0}\vec{k}\cdot\vec{p} + V(\vec{r})\right)u_{n\vec{k}}(\vec{r}) = \left[E_n(\vec{k}) - \frac{\hbar^2 k^2}{2m_0}\right]u_{n\vec{k}}(\vec{r})$$

When a unit-cell/lattice possesses a high degree of symmetry, the spin-orbit coupling plays a larger role [15]. Such is the case with type III-V semiconductors; therefore, we must include spin-orbit coupling in the Hamiltonian.

## The $\psi$ Basis

In addition to the Hamiltonian, a complete description of the system requires a maximum set of commuting observables. As in the basic example of the hydrogen atom we start with the observables

$$L^2 \quad , \quad L_z \quad , \quad S^2 \quad , \quad S_z \text{ (without L·S coupling)} \qquad (2.4)$$

However, if we include spin-orbit interaction, not all of these observables commute with the Hamiltonian. To correct this, we introduce the total angular momentum $\vec{J}$

$$\vec{J} = \vec{L} + \vec{S}$$

which yields the new set of commuting observables:

$$H, J^2 \quad , \quad J_z \quad , \quad L^2 \quad , \quad L_z \text{ (with L·S coupling)} \qquad (2.5)$$

Therefore, we use the new basis states$\{|\psi\rangle\}$, where

$$|\psi\rangle = e^{\imath\vec{k}\cdot\vec{r}}u_{n\vec{k}}(\vec{r}) \qquad (2.6)$$

In equation 2.6, $e^{\imath\vec{k}\cdot\vec{r}}$ represents an envelope function, and $u_{n0}(\vec{r}) = |J, J_z\rangle$.

The conduction band Bloch functions are given by

$$|J, J_z\rangle = \left|\frac{1}{2}, \frac{1}{2}\right\rangle = |iS, \uparrow\rangle$$

$$and \qquad\qquad\qquad (2\,7)$$

$$|J, J_z\rangle = \left|\frac{1}{2}, \frac{-1}{2}\right\rangle = |iS, \downarrow\rangle$$

Here, we use[1] S because the conduction band Bloch functions have spherical symmetry (an S-state as in and $\ell=0$ orbital)

For the valence band, with no spin orbit interaction, the Bloch functions for a type III-V semiconductor are given by

$$|X, \uparrow\rangle, \quad |Y, \uparrow\rangle, \quad |Z, \uparrow\rangle, \quad |X, \downarrow\rangle, \quad |Y, \downarrow\rangle, \quad |Z, \downarrow\rangle$$

for further explanation see [25]  These functions (X, Y, Z) are related to spherical harmonics  For more information see appendix A 2  From solid state physics, we know that along the $\Gamma$ symmetry point ($\vec{k} = 0$), the Bloch functions take the form

$$\text{heavy hole 1} \quad u_{10}(\vec{r}) = \left|\frac{3}{2}, \frac{3}{2}\right\rangle = \frac{-1}{\sqrt{2}}|X + iY, \uparrow\rangle$$

$$\text{light hole 1} \quad u_{20}(\vec{r}) = \left|\frac{3}{2}, \frac{1}{2}\right\rangle = \frac{-1}{\sqrt{6}}|X + iY, \downarrow\rangle + \sqrt{\frac{2}{3}}|Z, \uparrow\rangle$$

$$\text{light hole 2} \quad u_{30}(\vec{r}) = \left|\frac{3}{2}, \frac{-1}{2}\right\rangle = \frac{1}{\sqrt{6}}|X - iY, \uparrow\rangle + \sqrt{\frac{2}{3}}|Z, \downarrow\rangle$$

$$\text{heavy hole 2} \quad u_{40}(\vec{r}) = \left|\frac{3}{2}, \frac{-3}{2}\right\rangle = \frac{1}{\sqrt{2}}|X - iY, \downarrow\rangle \qquad (2\,8)$$

$$\text{Spin-orbit 1} \quad u_{50}(\vec{r}) = \left|\frac{1}{2}, \frac{1}{2}\right\rangle = \frac{1}{\sqrt{3}}|X + iY, \downarrow\rangle + \sqrt{\frac{1}{3}}|Z, \uparrow\rangle$$

$$\text{Spin-orbit 2} \quad u_{60}(\vec{r}) = \left|\frac{1}{2}, \frac{-1}{2}\right\rangle = \frac{1}{\sqrt{3}}|X - iY, \uparrow\rangle - \sqrt{\frac{1}{3}}|Z, \downarrow\rangle$$

---

[1]This is a new S, not the S for the spin observable mentioned above in equations 2 4 and 2 5

The above developments are closely related to the work done by Luttenger and Kohn [22]; however, it is worth noting that the same results were obtained by Dresselhaus [26].[2]

### 2.1.1   The $\vec{k} \cdot \vec{p}$ Model with Spin-Orbit Interaction

The Hamiltonian with the additional spin-orbit term[3] is given by

$$H = \frac{\hbar^2}{2m_0}\nabla^2 + V(\vec{r}) + \frac{\hbar}{4m_0^2c^2}\sigma \ \nabla V \times \vec{p} \qquad (2.9)$$

where $\sigma$ is the Pauli spin matrix vector with components

$$\sigma_x = \begin{bmatrix} 0 & 1 \\ 1 & 0 \end{bmatrix} \quad \sigma_y = \begin{bmatrix} 0 & -i \\ i & 0 \end{bmatrix} \quad \sigma_z = \begin{bmatrix} 1 & 0 \\ 0 & -1 \end{bmatrix} \qquad (2.10)$$

Using the same process as equation 2.3, we solve $H\psi = E\psi$ using $\psi = e^{i\vec{k}\cdot\vec{r}}u_{n\vec{k}}(\vec{r})$ and we obtain a new eigenvalue-eigenvector relationship

$$\left(\frac{p^2}{2m_0} + \frac{\hbar}{m_0}\vec{k} \cdot \vec{p} + V(\vec{r}) + \frac{\hbar}{4m_0^2c^2}[\nabla V \times \vec{p}]\cdot\sigma + \frac{\hbar^2}{4m_0^2c^2}\nabla V \times \vec{k}\cdot\sigma\right) u_{n\vec{k}}(\vec{r})$$
$$= \left[E_n(\vec{k}) - \frac{\hbar^2 k^2}{2m_0}\right] u_{n\vec{k}}(\vec{r}) \quad (2.11)$$

### Single band with $\vec{k} = k\hat{z}$

We first consider a single, non-degenerate band. This single band approximation means we consider "distant" bands such as the conduction band, where we can ignore coupling between bands. In equation 2.11, the last term on the left hand side contains a $\vec{k}$-dependent spin-orbit interaction. Because the (pseudo) crystal lattice momentum,

---

[2]They both derived these functions within a few months of each other in 1954. However Dresselhaus focused on the all the states along the $\Gamma$ symmetry point. For our purposes we only need to reuse 2.8 from. [22].

[3]Note that for a spherically symmetric V, $\nabla V = \frac{dV}{d\vec{r}}\hat{r} = \frac{dV}{d\vec{r}}\frac{\vec{r}}{r}$, $\frac{1}{r}\frac{dV}{dr}\vec{L} = \nabla V \times \vec{p} \Rightarrow \frac{\hbar}{4m_0^2c^2}\sigma \ \nabla V \times \vec{p} = \frac{1}{2m_0^2c^2}\left(\frac{1}{r}\frac{dV}{dr}\right)\vec{L} \cdot \vec{S}$

$\hbar\vec{k} \ll \vec{p}$ (where $\vec{p}$ is the electron's momentum) we neglect the last term[4] and equation 2 11 becomes

$$\left(\frac{p^2}{2m_0} + \frac{\hbar}{m_0}\vec{k} \quad \vec{p} + V(\vec{r}) + \frac{\hbar}{4m_0^2c^2}[\nabla V \times \vec{p}] \quad \sigma\right) u_{n\vec{k}}(\vec{r}) = \left[E_n(\vec{k}) - \frac{\hbar^2k^2}{2m_0}\right] u_{n\vec{k}}(\vec{r}) \tag{2 12}$$

Therefore, our $\vec{k}$ $\vec{p}$ Hamiltonian is

$$H = H_0 + \frac{\hbar}{m_0}\vec{k} \quad \vec{p} + \frac{\hbar^2k^2}{2m_0} + \frac{\hbar}{4m_0^2c^2}\sigma \quad \nabla V \times \vec{p} \tag{2 13}$$

where $H_0 = \frac{p^2}{2m_0} + V(\vec{r})$ We solve equation 2 13 using perturbation theory (introduced in section 1 3 1)

The conduction band has a minimum at $\vec{k} = 0$ (called the $\Gamma$ symmetry point) We investigate states with $\vec{k}$ values near the $\Gamma$ symmetry point (see figure 2 2b) We define the perturbation Hamiltonian, and effective energy to be

$$H' = \frac{\hbar}{m_0}\vec{k} \quad \vec{p} + \frac{\hbar}{4m_0^2c^2}\sigma \quad \nabla V \times \vec{p}$$

$$E' = E_n(\vec{k}) - \frac{\hbar^2k^2}{2m_0}$$

The correction to the energies near the conduction band edge due to $H'$, can be found using perturbation theory

$$E_n = E_n^{(0)} + H'_{nn} + \sum_{m\neq n} \frac{(H'_{nm})^2}{E_n^{(0)} - E_m^{(0)}} +$$

(See section 1 3 1 and equation 1 3) For conduction band states, the first order correction $H'_{nn} = 0$ because the $|iS,\uparrow\rangle$ state is a constant, so differential operators make

$$\left\langle iS \left| -i\hbar\frac{\partial}{\partial x} \right| iS \right\rangle = 0$$

---

[4]$\hbar\vec{k}$ is very small compared to the electron's momentum $\vec{p}$ in the far interior of the atom where the spin-orbit interaction occurs

Therefore, to the second order

$$
\begin{aligned}
E_n &= E_n^{(0)} + \sum_{m \neq n} \frac{(H'_{nm})^2}{E_n^{(0)} - E_m^{(0)}} = E' = E_n(\vec{k}) - \frac{\hbar^2 k^2}{2m_0} \Rightarrow \\
E_n(\vec{k}) &= E_n^{(0)} + \frac{\hbar^2 k^2}{2m_0} + \sum_{m \neq n} \frac{(H'_{nm})^2}{E_n^{(0)} - E_m^{(0)}}
\end{aligned}
$$

We know from solid state physics and extensive experimental results the band edge energies:

$$
\begin{aligned}
\text{Conduction band: } & E_c^{(0)} = E_c(\vec{k} = 0) = E_c \\
\text{Light/Heavy Holes: } & E_v^{(0)} = E_v(\vec{k} = 0) = E_v \\
\text{Spin-Orbit Holes: } & E_{so}^{(0)} = E_{so}(\vec{k} = 0) = E_v - \Delta \\
\text{Band gap Enegry: } & E_g = E_c - E_v
\end{aligned}
$$

( $\Delta$ is the spin-orbit split off energy. Values for $E_v$, $E_c$, $\Delta$, and $E_g$ can be found in table B.2.) Therefore

$$
E_c(\vec{k}) = E_c + \frac{\hbar^2 k^2}{2m_0} + \sum_{m \neq c} \frac{(H'_{cm})^2}{E_c^{(0)} - E_m^{(0)}} \tag{2.14}
$$

To evaluate the above, it is convenient to define Kane's Parameter $P$ and the spin-orbit split off energy $\Delta$ as

$$
\begin{aligned}
P &\equiv \frac{\hbar}{m_0} \left\langle \imath S \left| -\imath\hbar \frac{\partial}{\partial x} \right| X \right\rangle = \frac{\hbar}{m_0} \left\langle \imath S \left| -\imath\hbar \frac{\partial}{\partial y} \right| Y \right\rangle = \frac{\hbar}{m_0} \left\langle \imath S \left| -\imath\hbar \frac{\partial}{\partial z} \right| Z \right\rangle \\
\Delta &\equiv \frac{3\hbar\imath}{4m_0^2 c^2} \left\langle X \left| \frac{\partial V}{\partial x} p_y - \frac{\partial V}{\partial y} p_x \right| Y \right\rangle
\end{aligned}
$$

The values of these parameters can be found experimentally. It is also helpful to note that[5]

$$0 = \left\langle iS \left| \frac{\partial V}{\partial x}p_y - \frac{\partial V}{\partial y}p_x \right| iS \right\rangle$$

$$0 = \left\langle iS \left| \frac{\partial V}{\partial x}p_y - \frac{\partial V}{\partial y}p_x \right| X \text{ or } Y \text{ or } Z \right\rangle$$

With the above definitions, equation 2.14 takes the form

$$E_c(\vec{k}) = E_c + \frac{\hbar^2 k^2}{2m_0} + \frac{k^2 P^2}{3} \frac{(3E_g + 2\Delta)}{E_g (E_g + \Delta)} \tag{2.15}$$

We can take this an important step further by introducing the concept of effective mass $m^*$ For the conduction band we can write the electron dispersion relation, equation 3.4, in the form

$$E_c(\vec{k}) = E_c + \frac{\hbar^2 k^2}{2m_e^*}$$

where $m_e^*$ is the effective mass of electrons in the conduction band. Because the effective mass is a combination of experimentally known parameters, the effective mass is also a known material parameter. Suppose we had replaced the electron mass $m_0$ in our original Hamiltonian, with $m^*$ and we obtain the eigenvector-eigenvalue solutions for $(H_0 + H')\psi = E\psi$. Then it is as if the perturbation Hamiltonian is identical to unperturbed electron motion with a different mass. Therefore, we can say the electron flow in the semiconductor has an effective mass $m^*$ .

Values for the effective masses can be found in table B.2. Unfortunately, this formulation does not include band coupling between the conduction and valence band. If we applied this single band formulation to the degenerate valence band, we would obtain incorrect dispersion relations [10].

---

[5]The term $\left| \frac{\partial V}{\partial x_1}p_{x_2} - \frac{\partial V}{\partial x_2}p_{x_1} \right|$ is known to be hermitian and therefore we can interchange the conduction and valence band states. Because the term now operates on a constant the result is zero.

## 2.1.2 Luttinger-Khon $\vec{k} \cdot \vec{p}$ Model for Degenerate Bands

Single band perturbation theory has two major shortcomings. It contains no coupling between bands, and produces an incorrect dispersion relation for the heavy-hole energies.[6] When formulating the Hamiltonian in equation 2.12, we set the last term equal to zero and obtained the Hamiltonian in equation 2.13. This time, we consider this term. For $Hu_{n\vec{k}} = Eu_{n\vec{k}}$ we have

$$H = H_0 + \frac{\hbar^2 k^2}{2m_0} + \frac{\hbar}{4m_0^2 c^2}\sigma \cdot \nabla V \times \vec{p} + H'$$

where

$$H' = \frac{\hbar}{m_0}\vec{k} \cdot \left(\vec{p} + \frac{\hbar}{4m_0^2 c^2}\sigma \times \nabla V\right)$$

Again, this Hamiltonian is not solvable analytically. Therefore, we utilize perturbation theory for degenerate bands. If we treat the conduction band as distant (does not couple with valence band), we can separate the problem into two regions. Typically these regions are referred to as Class A (degenerate region) and Class B (non-degenerate region). In our case, class A refers to the valence band with the basis from equation 2.8; and class B refers to the conduction band. With this concept we can express $u_{n\vec{k}}$ as

$$u_{n\vec{k}} = \sum_{j'}^{A} a_{j'}(\vec{k})u_{j'0}(\vec{r}) + \sum_{\gamma}^{B} a_{\gamma}(\vec{k})u_{\gamma 0}(\vec{r})$$

Where $j'$ goes from 1 to 6 for the corresponding $H(\vec{k} = 0)u_{j0}(\vec{r}) = E_j(0)u_{j0}(\vec{r})$ and

$$E_j(0) = E_v \qquad \text{for } j = 1, 2, 3, 4$$
$$E_j(0) = E_v - \Delta \quad \text{for } j = 5, 6$$

We apply Löwdin's method (section 1.3.2) and solve

$$\sum_{j'}^{A} \left(U_{jj'}^{A} - E\delta_{jj'}\right) a_{j'}(\vec{k}) = 0$$

---

[6]We will point out how the Luttinger-Khon model gives the correct method.

instead of

$$\sum_{j'}^{A} \left( H_{jj'} - E\delta_{jj'} \right) a_{j'}(\vec{k}) = 0$$

A more detailed discusion of this can be found in [10], but the important result is

$$U_{jj'}^{A} = D_{jj'} = E_j(0)\delta_{jj'} + \sum_{\alpha} \sum_{\beta} D_{jj'}^{\alpha\beta} k_\alpha k_\beta \qquad (2.16)$$

Where $\alpha$ and $\beta$ represent the directions $\hat{x}$, $\hat{y}$, and $\hat{z}$. The expression $D_{jj'}^{\alpha\beta}$ is defined as

$$D_{jj'}^{\alpha\beta} = \frac{\hbar^2}{2m_0} \left( \delta_{jj'}\delta_{\alpha\beta} + \sum_{\gamma}^{B} \frac{p_{j\gamma}^{\alpha} p_{\gamma j'}^{\beta} + p_{j\gamma}^{\beta} p_{\gamma j'}^{\alpha}}{m_0 (E_0 - E_\gamma)} \right)$$

From this we can obtain the Luttenger-Khon Hamiltonian (in all we have gone from $U^A \equiv D \equiv H^{LK}$)

$$H^{LK} = - \begin{bmatrix} P+Q & -S & R & 0 & \frac{-1}{\sqrt{2}}S & \sqrt{2}R \\ -S^\dagger & P-Q & 0 & R & -\sqrt{2}Q & \sqrt{\frac{3}{2}}S \\ R^* & 0 & P-Q & S & \sqrt{\frac{3}{2}}S^\dagger & \sqrt{2}Q \\ 0 & R^\dagger & S^\dagger & P+Q & -\sqrt{2}R^\dagger & \frac{-1}{\sqrt{2}}S^\dagger \\ \frac{-1}{\sqrt{2}}S^\dagger & -\sqrt{2}Q^\dagger & \sqrt{\frac{3}{2}}S & -\sqrt{2}R & P+\Delta & 0 \\ \sqrt{2}R^\dagger & \sqrt{\frac{3}{2}}S^\dagger & \sqrt{2}Q^\dagger & \frac{-1}{\sqrt{2}}S & 0 & P+\Delta \end{bmatrix} \qquad (2.17)$$

(Note that the valence band edge is set to 0 instead of the general $E_v$, i.e. $E_v = 0$ )
and

$$P = \frac{\hbar^2 \gamma_1}{2m_0} \left( k_x^2 + k_y^2 + k_z^2 \right)$$

$$Q = \frac{\hbar^2 \gamma_2}{2m_0} \left( k_x^2 + k_y^2 - 2k_z^2 \right)$$

$$R = \frac{\hbar^2}{2m_0} \left[ -\sqrt{3}\gamma_2 \left( k_x^2 - k_y^2 \right) + i2\sqrt{3}\gamma_3 k_x k_y \right]$$

$$S = \frac{\hbar^2 \gamma_3}{m_0} \sqrt{3} \left( k_x - i k_y \right) k_z$$

Note that this P is different from Kane's parameter. The Luttinger-Khon parameters
or band-structure parameters $\gamma_1$, $\gamma_2$, and $\gamma_3$ are found experimentally (see table B.2)
They play a larger role in going from equation 2.16 to equation 2.17. However, for our
purposes they are experimentally known parameters. Also, if we now set $\vec{k} = k\hat{z}$ we
obtain the aforementioned dispersion relations from equation2.19, but now with the
correct heavy hole dispersion relation. With $\vec{k} = k\hat{z}$, $R = S = 0$ and $H^{LK}$ becomes

$$H^{LK} = - \begin{bmatrix} P+Q & 0 & 0 & 0 & 0 & 0 \\ 0 & P-Q & 0 & 0 & 0 & 0 \\ 0 & 0 & P-Q & 0 & 0 & 0 \\ 0 & 0 & 0 & P+Q & 0 & 0 \\ 0 & 0 & 0 & 0 & P+\Delta & 0 \\ 0 & 0 & 0 & 0 & 0 & P+\Delta \end{bmatrix} \tag{2.18}$$

From this we can write additional effective mass dispersion relations for the valence
band. We summarize the results in equation 2.19.

Conduction Band
$$E^{(c)}(k) = E_c + \frac{\hbar^2 k^2}{2m_e^*}$$

Valence Band: $\qquad$ (2.19)

Heavy Hole (corrected using $H^{LK}$) $E^{(hh)}(k) = E_v - \dfrac{\hbar^2 k^2}{2m_{hh}^*}$

Light Hole $\qquad E^{(lh)}(k) = E_v - \dfrac{\hbar^2 k^2}{2m_{lh}^*}$

Spin-Orbit Split-off Hole $\qquad E^{(so)}(k) = E_v - \Delta - \dfrac{\hbar^2 k^2}{2m_{so}^*}$

These four parabolic dispersions relations (when the heavy-hole band is corrected) approximately reproduce Figure 2.2b. The light-hole and heavy-hole effective masses are given by

$$\frac{m_{hh}^*}{m_0} = \frac{1}{\gamma_1 - 2\gamma_2}$$
$$\frac{m_{lh}^*}{m_0} = \frac{1}{\gamma_1 + 2\gamma_2}$$

The spin orbit hole is a more complicated case, from equation 2.18 we obtain

$$\frac{m_{so}^*}{m_0} = \frac{1}{\gamma_1}$$

However, if we applied single band effective mass theory ( as in the last sub- section) we would obtain

$$\frac{m_{so}^*}{m_0} = \frac{1}{\frac{E_p}{3(E_g + \Delta)} - 1}$$

Where $E_p = \frac{2m_0}{\hbar^2} P^2$ This P is again Kane's parameter. These expressions are not identical, and the exact expression for the spin-orbit effective mass is not well understood. Further discussion on this is given in [24], where the spin-orbit effective mass is defined as

$$\frac{m_{so}^*}{m_0} = \left[\gamma_1 - \frac{E_p \Delta}{3E_g(E_g + \Delta)}\right]^{-1}$$

We shall use this definition for the spin orbit effective mass.

It is also possible to include the conduction band to obtain an 8x8 $H^{LK}$. However we must make changes in the Luttinger parameters to do so. Also, a more general degenerate perturbation theory must be used as Löwdin's method does not apply to this case. The 8x8 $H^{LK}$ can be found in many appendixes in papers published in the field such as [12]. Note that the 8x8 $H^{LK}$ is usually given in atomic units where $\hbar = m_0 = 1$. Next, we shall consider the effect of a perturbation on the periodic lattice, which will generalize our discussion to hetrojunctions.

## 2.2  The Effective Mass equation

In this section, we introduce hetrojunctions into our formulation. We shall summarize the effective mass theory [22] for single and degenerate bands.

### Single band Effective Mass Equation

In equation 2 19, we introduced the concept of effective mass. However, we confined our discussion only to the $\hat{z}$ direction. The effective mass is actually dependent on the direction. The true form of the effective mass, $m^*$, is actually a tensor. We can generalize the equations in 2.19 to

$$E_n(\vec{k}) = E_n(0) + \sum_\alpha \sum_\beta \frac{\hbar^2}{2} \left( \frac{1}{m^*} \right)_{\alpha\beta} k_\alpha k_\beta$$

where $\alpha$ and $\beta$ indicate that the summations run over $\hat{x}$, $\hat{y}$, and $\hat{z}$. We model a hetrojunctions by treating an impurity (an additional material in the lattice) as an additional perturbation potential $U(\vec{r})$. Therefore, in heterostructures the bulk properties get modified. We no longer have an infinite periodic crystal, because we have added a small portion of an additional material. In addition, $U(\vec{r})$ can act as a confining potential. This is how we solve for the energy eigenvalues and eigenfunctions in quantum wells, wires and dots. Because we no loner have an infinite periodic crystal, the envelope function is no longer $e^{i\vec{k}\cdot\vec{r}}$ but some unknown function $F(\vec{r})$. The wave

function is now given by

$$\psi_n(\vec{r}) = F_n(\vec{r})u_{n0}(\vec{r})$$

To formulate the effective mass equation, we make the following replacement to k. ( Further details of this are given in [15, 25].)

$$k_\alpha \rightarrow -i\frac{\partial}{\partial\alpha} \quad \text{and} \quad k_\beta \rightarrow -i\frac{\partial}{\partial\beta}$$

For a single band, $F(\vec{r})$ is found by solving the single band effective mass equation:

$$\left[\sum_\alpha\sum_\beta \frac{\hbar^2}{2}\left(\frac{1}{m^*}\right)_{\alpha\beta}\left(-i\frac{\partial}{\partial\alpha}\right)\left(-i\frac{\partial}{\partial\beta}\right) + U(\vec{r})\right]F(\vec{r}) = (E - E_n(0))F(\vec{r}) \quad (2.20)$$

To summarize: the periodic potential $V(\vec{r})$ determines the energy bands and the effective masses, which are known. Therefore, we only need to solve equation 2.20 to account for the confinement potential $U(\vec{r})$. This method works well for analyzing the conduction band in quantum confined structures.

## Degenerate band Effective Mass Equation

Next, we shall apply the same process as above for degenerate bands. When dealing with the 6 coupled valence bands, we return to the Löwdin's method and $H^{LK}$. In this case, we can solve the coupled band effective mass equation with

$$\psi(\vec{r}) = \sum_{j=1}^{6} F_j(\vec{r})u_{j0}(\vec{r})$$

and

$$\sum_{j'=1}^{6}\left[E_j(0)\delta_{jj'} + \sum_\alpha\sum_\beta D_{jj'}^{\alpha\beta}\left(-i\frac{\partial}{\partial\alpha}\right)\left(-i\frac{\partial}{\partial\beta}\right) + U(\vec{r})\delta_{jj'}\right]F_{j'}(\vec{r}) = EF(\vec{r}) \quad (2.21)$$

(Derivation of this equation can be found in [15, 25].) For example, if we have a well in the $\hat{z}$ direction of width L ( a potential that gives confinement in the $\hat{z}$ direction and is unbounded in the $\hat{x}$ and $\hat{y}$ directions.)

$$U_n(z) = \begin{cases} 0 & z < 0 \\ E - (E_{v_{out}} - \Delta_{out}\delta_{n,n'=5,6}) & z \geq L \end{cases}$$

the $\Delta_{out}$ is added for the spin orbit energy outside the well, this forms a well with $\Delta_{in}$ which is already in $H^{LK}$  The eigenfunctions and eigenvalues are found by solving

$$\left[ H^{LK}\left( k_x, k_y, k_z = -i\frac{\partial}{\partial z} \right) + U(z)I \right] \begin{bmatrix} F_1 \\ F_2 \\ F_3 \\ F_4 \\ F_5 \\ F_6 \end{bmatrix} = E \begin{bmatrix} F_1 \\ F_2 \\ F_3 \\ F_4 \\ F_5 \\ F_6 \end{bmatrix}$$

where I is the identity matrix and $F_n(\vec{r}) = F_n'(z)e^{ik_x x + ik_y y}$. Because there is no confinement in the $\hat{x}$ and $\hat{y}$ directions, the original envelope components in those directions subsist. An example of performing these calculations can be found in [27].

# Chapter 3

# Model

We shall now construct a model that will allows us to obtain the energy eigenvalue-eigenvector relationships of a quantum dot. In section 2.2, we demonstrated how the single-band effective mass equation allows us to solve the eigenvalue-eigenvector problem,

$$H\psi = E\psi$$

for heterostructures when the band under consideration is isolated from the other bands. In a semiconductor, the conduction band is separated from the valence band by a band gap, $E_g$; if this gap is sufficiently large, the coupling of the conduction and valence bands can be ignored. Such rational is employed in section 3.2.

We also showed that multiple-band effective mass theories allow us to solve for eigenvalues and eigenvectors in a coupled system, such as the tripplely degenerate $\Gamma$ point in the type III-V valence band. This will be discussed in section 3.3.

The zinc blende structures formed by type III-V semiconductors have unit cells whose sizes are material dependent. The unit cell sizes are given in table B.2, in appendix B, where $a_0$ is the cell width. When two different materials are used to form a heterojunction, a lattice mismatch will occur if the two materials do not have the same unit cell dimensions. Thus, if we consider spherical hetrojunctions, the differences in unit cell size will lead to a stress or strain on the semiconductor lattice, which in turn will affect the electronic properties. The hetrojunctions we consider

are made from materials with unit cells of similar size (GaAs in AlAs). Therefore, we ignore the effects of stress and strain.

## 3.1    Possible Models

In order to account for the 3D confinement, we make the substitution

$$k_x \rightarrow -i\frac{\partial}{\partial x}, \quad k_y \rightarrow -i\frac{\partial}{\partial y}, \quad k_z \rightarrow -i\frac{\partial}{\partial z}$$

in the Luttinger-Khon Hamiltonian, $H^{LK}$; and solve equation 2.21.

Perhaps, the most common way to consider a semiconductor quantum dot is the infinite potential box. In this basic model, the potential outside the well is treated as infinite and the band mixing is ignored. Under this assumption, the wave function for the electron, vanishes outside quantum dot. For some semiconductors, this approximation is reasonable; however, for type III-V crystals, the valence band contains a tripplely degenerate valence band. The rectangular structure is easily analyzed in Cartesian coordinates, for a box of dimensions a x b x c, the eigenenergies and eigenfunctions for the conduction band are [10, 11]

$$E^{(c)}_{n_x n_y n_z} = E_{c0} + \frac{\hbar^2}{2m^*_{e,in}}\left[\left(\frac{\pi n_x}{a}\right)^2 + \left(\frac{\pi n_y}{b}\right)^2 + \left(\frac{\pi n_z}{c}\right)^2\right]$$

and

$$\psi^{(c)}_{n_x n_y n_z}(x,y,z) = \sqrt{\frac{8}{abc}}\sin\left(\frac{\pi n_x}{a}x\right)\sin\left(\frac{\pi n_y}{b}y\right)\sin\left(\frac{\pi n_z}{c}z\right)u_{c0}(\vec{r})$$

and for the valence band

$$E^{(v)}_{n_x n_y n_z} = E_{v0} - \frac{\hbar^2}{2m^*_{h,in}}\left[\left(\frac{\pi n'_x}{a}\right)^2 + \left(\frac{\pi n'_y}{b}\right)^2 + \left(\frac{\pi n'_z}{c}\right)^2\right]$$

and

$$\psi^{(v)}_{n'_x n'_y n'_z}(x,y,z) = \sqrt{\frac{8}{abc}}\sin\left(\frac{\pi n'_x}{a}x\right)\sin\left(\frac{\pi n'_y}{b}y\right)\sin\left(\frac{\pi n'_z}{c}z\right)u_{v0}(\vec{r})$$

If the quantum dot is spherically symmetric, the analysis is best done in spherical coordinates. For a dot of radius $r_{well}$ we have for the conduction band

$$E_{nl}^{(c)} = E_{c0} + \frac{\hbar^2}{2m_{e,in}^* r_{well}^2}\beta_{nl}^2 \quad \text{and} \quad \psi_{nlm}^{(c)}(r, \theta, \phi) = A_{nl}j_l\left(\frac{\beta_{lm}}{r_{well}}r\right)Y_l^m(\theta, \phi)u_{c0}(\vec{r}) \tag{3.1}$$

and for the valence band

$$E_{n'l'}^{(v)} = E_{v0} - \frac{\hbar^2}{2m_{h,in}^* r_{well}^2}\beta_{n'l'}^2 \quad \text{and} \quad \psi_{n'l'm'}^{(v)}(r, \theta, \phi) = A_{n'l'}j_{l'}\left(\frac{\beta_{lm}}{r_{well}}r\right)Y_{l'}^{m'}(\theta, \phi)u_{v0}(\vec{r}) \tag{3.2}$$

where $\beta_{nl}$ is the nth zero of the lth spherical Bessel function $j_l(\beta_{nl})$. $A_{nl}$ is a normalization constant, $E_{c0}$ and $E_{v0}$ are the band edge energies, and $u_i(\vec{r})$ are the Bloch functions. More information on spherical Bessel functions is given in appendix C.1. The general solution for the infinite spherical potential well can be found in [18].

These two infinite potential formulations give us very quick and easy means to approximate band structures. However, the results do not depend on any parameters of the host material; that is the results are independent of the effective mass and band edges of the material the dot is embedded in. In addition, these models do not include any band coupling, which is an important consequence when considering degenerate bands.

In order to account for band mixing and finiteness of the confining potential, we apply the effective mass theory in three dimensions where the finite wells are formed by the conduction band edges and valence band edges. Furthermore, we limit our consideration to spherically symmetric cases as in references [12, 13, 14] for mathematical simplicity. The advantage of the spherical symmetry is that we can analytically reduce the problem to a set of coupled of differential equations in the radial direction and factor out the angular components as spherical harmonics. In our work we follow the developments of Sercel and Vahala [12] very closely.

## 3.2   Conduction Band Model

To model the conduction band, we utilize the single band effective mass equation in spherical coordinates. Our spherically symmetric confinement potential is given by the conduction band edges of our inside material, $E_c^{in}$ and our outside material $E_c^{out}$

$$U(r) = \begin{cases} 0 & r < r_{well} \\ E_c^{out} - E_c^{in} & r > r_{well} \end{cases}$$

From section 2 2, we know our states are given by

$$\psi_{nS}(r, \theta, \phi) = F_n(r, \theta, \phi) u_{S0}(r, \theta, \phi)$$

the S subscript is added to denote the two conduction band Bloch functions $u_{S0}(r, \theta, \phi) = |iS, \uparrow\downarrow\rangle$. The envelope function $F_n(r, \theta, \phi)$ is found by solving

$$\left[ \sum_\alpha \sum_\beta \frac{\hbar^2}{2} \left( \frac{1}{m^*} \right)_{\alpha\beta} \left( -i\frac{\partial}{\partial\alpha} \right) \left( -i\frac{\partial}{\partial\beta} \right) + U(r) \right] F_n(r, \theta, \phi) = (E - E_c^{in}) F_n(r, \theta, \phi)$$

We assume that the effective mass tensor is independent of direction, therefore:

$$(m_e^*)_{\alpha\beta} = m_e^* \begin{bmatrix} 1 & 0 & 0 \\ 0 & 1 & 0 \\ 0 & 0 & 1 \end{bmatrix} = m_e^* I$$

With this assumption, our effective mass equation becomes

$$\left[ \frac{\hbar^2}{2m_e^*} \sum_\alpha \sum_\beta I \left( -i\frac{\partial}{\partial\alpha} \right) \left( -i\frac{\partial}{\partial\beta} \right) + U(r) \right] F_n(r, \theta, \phi) = (E_n - E_c^{in}) F_n(r, \theta. \phi)$$

$$\left[ -\frac{\hbar^2}{2m_e^*} \nabla^2 + U(r) \right] F_n(r, \theta, \phi) = (E_n - E_c^{in}) F_n(r, \theta. \phi)$$

We can absorb $E_c^{in}$ into the potential and obtain

$$U'(r) = \begin{cases} E_c^{in} & r < r_{well} \\ E_c^{out} & r > r_{well} \end{cases}$$

and

$$\left[ -\frac{\hbar^2}{2m_e^*}\nabla^2 + U'(r) \right] F_n(r, \theta, \phi) = (E_n)F_n(r, \theta, \phi)$$

Next, we transform the potential again by setting

$$U''(r) = \begin{cases} -V_0 & r < r_{well} \\ 0 & r > r_{well} \end{cases}$$

where $V_0 = E_c^{out} - E_c^{in}$, $E_n = E_n' + E_c^{out}$ and

$$\left[ -\frac{\hbar^2}{2m_e^*}\nabla^2 + U''(r) \right] F_n(r, \theta, \phi) = (E_n')F_n(r, \theta, \phi) \tag{3.3}$$

We review and further explain this problem in appendix C.2. Equation 3.3 is identical to Schrödinger's time independent equation with one important caveat: the effective mass is a function of r

$$m_e^*(r) = \begin{cases} m_e^{*in} & r < r_{well} \\ m_e^{*out} & r > r_{well} \end{cases}$$

That is, the effective mass changes from the inside material to the outside material. We must insure that the probability current density across the hetrojunctions is conserved. We also show this in appendix C.2. The eigenenergies from equation 3.3 can be found using the numerically efficient form

$$\frac{l}{r_{well}} - K\frac{j_{l+1,n}(Kr_{well})}{j_{ln}(Kr_{well})} = \frac{m_{in}^*}{m_{out}^*}\left[ \frac{l}{r_{well}} - \lambda\frac{\sum_{m=0}^{l+1}\frac{1}{m!(2\lambda r_{well})^m}\frac{(l+m+1)!}{(l-m+1)!}}{\sum_{m=0}^{l}\frac{1}{m!(2\lambda r_{well})^m}\frac{(l+m)!}{(l-m)!}} \right] \tag{3.4}$$

(m is a dummy index not the mass or the spherical eigenvalue) where

$$K = \sqrt{\frac{2m_{in}^*}{\hbar^2}(E_n' + V_0)} \quad , \quad i\lambda = \sqrt{\frac{2m_{out}^*}{\hbar^2}(E_n')} \quad \text{and} \quad E_{nl} = E_{nl}' + E_c^{out}$$

Equation 3.4 must be solved numerically for all $l$ and $n$. (Note that there are multiple n values for each L value.) Hence, each energy level is degenerate with respect to spin and $m$, where $m \in [-l, -l+1, ..., l]$ .

The wave functions are given by

$$\psi_{Snlm} = R_{nl}(r)Y_l^m(\theta, \phi)u_{s0}(r, \theta, \phi)$$

where, $R_{nl(r)}$ is given by[1]

$$R_{nl}(r) = \begin{cases} Aj_l(Kr) & r < r_{well} \\ B_{nl}h_l^{(1)}(i\lambda r) & r > r_{well} \end{cases}$$

and $B_{nl}$ must be found by solving $j_l(Kr_{well}) = B_{nl}h_l^{(1)}(i\lambda r_{well})$ using the values found for $E_{nl}'$   It is also useful to define the basis in Dirac notation $(L = \ell, \text{ and } L_z = m)$[2]

$$\{|L, L_z, J, J_z\rangle\}$$

which has the position representation

$$\langle r, \theta, \phi \,|L, L_z, J, J_z\rangle = R_{nl}(r)Y_L^{L_z}(\theta, \phi)u_{s0}(r, \theta, \phi)$$

---

[1]we set$A = 1$ and normalize later
[2]$|J, J_z\rangle = |iS, \uparrow\downarrow\rangle$

## 3.3   Valence Band Model

In order to construct a model for the valence band under a spherically symmetric confining potential, it is convenient to obtain the matrix elements of the Luttinger-Khon $\vec{k} \cdot \vec{p}$ Hamiltonian in a spherically symmetric basis. From section 2.2, we saw that the wave functions take the form

$$|\psi(\vec{r})\rangle = \sum_{J,J_z} F_{JJ_z}(\vec{r}) u_{n0}(\vec{r})$$

which we can rewrite as

$$|\psi(\vec{r})\rangle = \sum_{J,J_z} F_{JJ_z}(\vec{r}) |J, J_z\rangle$$

To exploit the spherical symmetry of the problem, we introduce a new angular momentum $\vec{L}$, which is associated with the envelope component of the wavefunction, and varies on the order of the quantum dot. In terms of the eigenfunctions of $L^2$ and $L_z$

$$|\psi(\vec{r})\rangle = \sum_{J,J_z} C_{JJ_z} R_L(r) Y_L^{L_z}(\theta, \phi) |J, J_z\rangle$$

or using Dirac notation

$$|\psi(\vec{r})\rangle = \sum_{J,J_z} C_{JJ_z} |L, L_z\rangle |J, J_z\rangle$$

This formulation allows us to factor out the spherical harmonic components; however, the components of J and L do not commute with the Hamiltonian. If we introduce a new angular momentum $\vec{F}$

$$\vec{F} = \vec{J} + \vec{L}$$

It follows that $F^2$ and $F_z$ commute with the Hamiltonian [12]. We define a new basis set in terms of the old basis using Clebsch Gordan coefficients with

$$|F, F_z, L, J\rangle = \sum_{L_z, J_z} \left( \begin{array}{ccc} F & J & L \\ F_z & J_z & L_z \end{array} \right)_{cg} |L, L_z\rangle \otimes |J, J_z\rangle$$

For simplicity, in some-cases we use the notation $|L, L_z\rangle \otimes |J, J_z\rangle =$ $|L, L_z, J, J_z\rangle$ or $|L, L_z\rangle|J, J_z\rangle$   If $|F, F_z\rangle$ is a simultaneous eigenstate of $F^2$ and $F_z$, the matrix element[3]

$$\langle F, F_z, L, J \left| H_{FF_z} \right| F', F_z', L', J'\rangle$$

is equal to zero unless $F = F'$ and $F_z = F_z'$  If the set $\{|F, F_z, L, J\rangle\}$ is used as a basis, the matrix representation of $H^{LK}$ is block-diagonal, that is, we have separate blocks for $F = F_{1/2}, F_{3/2}, F_{5/2},$    Each block is increasingly larger, and for a particular $F$, there are multiple degenerate $F_z$ Hamiltonians  (For $H_{\frac{1}{2}, \pm\frac{1}{2}}$ there exists a two-fold degeneracy, i e  $H_{\frac{1}{2}, \frac{1}{2}} = H_{\frac{1}{2}, -\frac{1}{2}}$ )  For example,

$$H_{FF_z} = \begin{vmatrix} H_{\frac{1}{2}, \pm\frac{1}{2}} & 0 & 0 & 0 \\ 0 & H_{\frac{3}{2}, \pm\frac{3}{2}\pm\frac{1}{2}} & 0 & 0 \\ 0 & 0 & H_{\frac{5}{2}, \pm\frac{5}{2}\pm\frac{3}{2}\pm\frac{1}{2}} & 0 \\ 0 & 0 & 0 & \ddots \end{vmatrix}$$

The matrix elements can be evaluated using a plain wave expansion of the original bulk wave functions, $|\psi\rangle = e^{i\vec{k}\cdot\vec{r}}u_{n\vec{k}}(\vec{r})$, to spherical components  We can express the matrix element for $H^{LK}$ as[4] $(K = \vec{k})$

$$\langle K, J, J \left| H^{LK} \right| K, J', J_z'\rangle$$

We want to express this in a spherically symmetric basis, so we rewrite the envelope component $e^{i\vec{k}\cdot\vec{r}}$ with the plain wave expansion

$$e^{i\vec{k}\cdot\vec{r}} = \sum_{L=0}^{\infty} \sum_{m=-L}^{L} 4\pi i^L Y_L^{m*}(\theta_k, \phi_k) Y_L^m(\theta, \phi) j_L(kr) \tag{3 5}$$

---

[3]As we will explain, this is not the 6x6 (or 8x8) $H^{LK}$ from chapter 2
[4]This $H^{LK}$ is the Hamiltonian introduced in chapter 2

1 e

$$e^{i\vec{k}\cdot\vec{r}}\,|J, J_z\rangle \;=\; \sum_{L=0}^{\infty}\sum_{L_z=-L}^{L} 4\pi i^L Y_L^{L_z *}(\theta_k, \phi_k) Y_L^{L_z}(\theta, \phi) j_L(kr)\,|J, J_z\rangle$$

$$=\; \sum_{L=0}^{\infty}\sum_{m=-L}^{L} C_{k,L\,L_z}\,|L, L_z\rangle\,|J, J_z\rangle$$

where $|L\ L_z\rangle = Y_L^{L_z}(\theta, \phi) j_L(kr)$ and $C_{k\,L,L_z} = 4\pi i^L Y_L^{L_z *}(\theta_k, \phi_k)$

Using the closure relation (I is an identity matrix)

$$I = \sum_i |\xi_i\rangle\langle\xi_i|$$

we can express the matrix elements of $H^{LK}$ as $\widetilde{H}^{LK}$ $(K = \vec{k})$

$$\langle L, L_z, J, L\,|\widetilde{H}^{LK}|\,L', L_z', J', J_z'\rangle =$$

$$\sum_{J\,J_z}\sum_{J'',J_z''}\langle L, L_z, J, J\,|K, J, J_z\rangle\,\langle K, J, J_z\,|H^{LK}|\,K, J'', J_z''\rangle\,\langle K, J'', J_z''|\,L', L_z', J', J_z'\rangle$$

where the $\langle L, L_z, J, J\,|K, J, J_z\rangle$ integrals are evaluated with the plain-wave expansion formula, equation 3 5  The matrix elements can be rewritten a final time as $H_{F,F_z}$

$$\langle F, F_z, L, J\,|H_{F,F_z}|\,F, F_z, L', J'\rangle = \sum_{L,L_z}\sum_{J,J_z}\big[\langle F, F_z, L, J\,|L, L_z, J, J_z\rangle$$

$$\langle L, L_z, J, J_z\,|H^{LK'}|\,L'', L_z'',\, ,J'', J_z''\rangle\,\langle L'', L_z'', J'', J_z''|\,F, F_z, L', J'\rangle\big]$$

where the integral $\langle F, F_z, L, J\,|L, L_z, J, J_z\rangle$ is evaluated using the Clebsch Gordan coefficients  Sercel and Vahala [12], show that this produces a block diagonal Hamiltonian which is separated into blocks for different $F$  The $F_{1/2}$ space has a two fold degeneracy and is given by

$H_{\frac{1}{2},\pm\frac{1}{2}} =$

$$
\begin{bmatrix}
E_c + \frac{1}{2}K^2 & 0 & 0 & -i\sqrt{\frac{2}{3}}PK & -i\sqrt{\frac{1}{3}}PK & 0 \\
0 & E_c + \frac{1}{2}K^2 & -i\sqrt{\frac{2}{3}}PK & 0 & 0 & -i\sqrt{\frac{1/3}{3}}PK \\
0 & i\sqrt{\frac{2}{3}}PK & LH & 0 & 0 & -2\sqrt{2}\gamma_2\frac{K^2}{2} \\
i\sqrt{\frac{2}{3}}PK & 0 & 0 & LH & -2\sqrt{2}\gamma_2\frac{K^2}{2} & 0 \\
i\sqrt{\frac{1}{2}}PK & 0 & 0 & -2\sqrt{2}\gamma_2\frac{K^2}{2} & SO & 0 \\
0 & i\sqrt{\frac{1}{3}}PK & -2\sqrt{2}\gamma_2\frac{K^2}{2} & 0 & 0 & SO
\end{bmatrix}
$$

where P is Kane's parameter, $LH = E_v - (\gamma_1 + 2\gamma_2)\frac{K^2}{2}$, $SO = E_v - \Delta - \gamma_1\frac{K^2}{2}$ The corresponding basis for each row of $H_{\frac{1}{2},\pm\frac{1}{2}}$ is

$$
|F, F_z, J, L\rangle = 
\begin{array}{ll}
\text{conduction band} & \begin{cases} |\frac{1}{2}, \pm\frac{1}{2}, \frac{1}{2}, 1\rangle \\ |\frac{1}{2}, \pm\frac{1}{2}, \frac{1}{2}, 0\rangle \end{cases} \\[2em]
\text{light holes} & \begin{cases} |\frac{1}{2}, \pm\frac{1}{2}, \frac{3}{2}, 1\rangle \\ |\frac{1}{2}, \pm\frac{1}{2}, \frac{3}{2}, 2\rangle \end{cases} \\[2em]
\text{spin orbit holes} & \begin{cases} |\frac{1}{2}, \pm\frac{1}{2}, \frac{1}{2}, 0\rangle \\ |\frac{1}{2}, \pm\frac{1}{2}, \frac{1}{2}, 1\rangle \end{cases}
\end{array}
$$

It can be shown that $H_{\frac{1}{2},\pm\frac{1}{2}}$ may be block diagonalized into

$$
H_{\frac{1}{2},\pm\frac{1}{2}} = 
\begin{bmatrix}
H^{(1)}_{1/2} & 0 \\
0 & H^{(2)}_{1/2}
\end{bmatrix}
$$

where (dropping the $F, F_z$ )

$$
H_{1/2}^{(1)} = \begin{array}{c} |J, L\rangle \\ |\tfrac{1}{2}, 0\rangle \\ |\tfrac{3}{2}, 1\rangle \\ |\tfrac{1}{2}, 0\rangle \end{array}
\begin{array}{ccc} |\tfrac{1}{2}, 0\rangle & |\tfrac{3}{2}, 1\rangle & |\tfrac{1}{2}, 0\rangle \end{array}
\left[ \begin{array}{ccc}
E_c + \tfrac{1}{2}K^2 & -i\sqrt{2/3}PK & -i\sqrt{1/3}PK \\
i\sqrt{2/3}PK & E_v - (\gamma_1 + 2\gamma_2)\tfrac{K^2}{2} & -2\sqrt{2}\gamma_2\tfrac{K^2}{2} \\
i\sqrt{1/3}PK & -2\sqrt{2}\gamma_2\tfrac{K^2}{2} & E_v - \Delta - \gamma_1\tfrac{K^2}{2}
\end{array} \right]
$$

and

$$
H_{1/2}^{(2)} = \begin{array}{c} |J, L\rangle \\ |\tfrac{1}{2}, 1\rangle \\ |\tfrac{3}{2}, 2\rangle \\ |\tfrac{1}{2}, 1\rangle \end{array}
\begin{array}{ccc} |\tfrac{1}{2}, 1\rangle & |\tfrac{3}{2}, 2\rangle & |\tfrac{1}{2}, 1\rangle \end{array}
\left[ \begin{array}{ccc}
E_c + \tfrac{1}{2}K^2 & -i\sqrt{2/3}PK & -i\sqrt{1/3}PK \\
i\sqrt{2/3}PK & E_v - (\gamma_1 + 2\gamma_2)\tfrac{K^2}{2} & 2\sqrt{2}\gamma_2\tfrac{K^2}{2} \\
i\sqrt{1/3}PK & -2\sqrt{2}\gamma_2\tfrac{K^2}{2} & E_v - \Delta - \gamma_1\tfrac{K^2}{2}
\end{array} \right]
$$

If the conduction and spin-orbit bands are treated as distant,

$$
H_{\tfrac{1}{2},\pm\tfrac{1}{2}} = \begin{array}{c} |\tfrac{3}{2}, 1\rangle \\ |\tfrac{3}{2}, 2\rangle \end{array}
\left[ \begin{array}{cc}
E_v - (\gamma_1 + 2\gamma_2)\tfrac{K^2}{2} & 0 \\
0 & E_v - (\gamma_1 + 2\gamma_2)\tfrac{K^2}{2}
\end{array} \right] \tag{3.6}
$$

We solve for the eigenvalues and eigenvectors of equation 3.6 using the method described in section 3.2 with $l=1$ and 2. In fact, $E_v - (\gamma_1 + 2\gamma_2)\frac{K^2}{2}$ is the light hole dispersion relation (see section 2.1.2). However, the total wave functions and their degeneracy will follow that of the coupled model. The spin-orbit band will also be treated in the same way, but we can use the uncoupled wave functions in an identical manner to the conduction band.

The $F_{3/2}$ band is more complicated, and each contains a four-fold degeneracy with respect to $F_z$. As before, the Hamiltonian can be put into a block diagonal form [12],

$$
H_{\tfrac{3}{2},\pm\tfrac{1}{2} \text{ or } \pm\tfrac{3}{2}} = \left[ \begin{array}{cc}
H_{3/2}^{(1)} & 0 \\
0 & H_{3/2}^{(2)}
\end{array} \right]
$$

where

$$
H_{3/2}^{(1)} = \begin{matrix} |\frac{1}{2},1\rangle \\ |\frac{3}{2},0\rangle \\ |\frac{3}{2},2\rangle \\ |\frac{1}{2},1\rangle \end{matrix} \begin{bmatrix} E_c + \frac{1}{2}K^2 & i\sqrt{\frac{1}{3}}PK & -i\sqrt{\frac{1}{3}}PK & -i\sqrt{\frac{1}{3}}PK \\ -i\sqrt{\frac{1}{3}}PK & E_v - \gamma_1\frac{K^2}{2} & 2\gamma_2\frac{K^2}{2} & 2\gamma_2\frac{K^2}{2} \\ i\sqrt{\frac{1}{3}}PK & 2\gamma_2\frac{K^2}{2} & E_v - \gamma_1\frac{K^2}{2} & -2\gamma_2\frac{K^2}{2} \\ i\sqrt{\frac{1}{3}}PK & 2\gamma_2\frac{K^2}{2} & -2\gamma_2\frac{K^2}{2} & E_v - \Delta - \gamma_1\frac{K^2}{2} \end{bmatrix}
$$

$$
H_{3/2}^{(2)} = \begin{matrix} |\frac{1}{2},2\rangle \\ |\frac{3}{2},1\rangle \\ |\frac{3}{2},3\rangle \\ |\frac{1}{2},1\rangle \end{matrix} \begin{bmatrix} E_c + \frac{1}{2}K^2 & i\sqrt{\frac{1}{15}}PK & -i\sqrt{\frac{3}{5}}PK & -i\sqrt{\frac{1}{3}}PK \\ -i\sqrt{\frac{1}{15}}PK & G & \frac{6}{5}\gamma_2\frac{K^2}{2} & \frac{2}{\sqrt{5}}\gamma_2\frac{K^2}{2} \\ i\sqrt{\frac{3}{5}}PK & \frac{6}{5}\gamma_2\frac{K^2}{2} & G & -\frac{6}{\sqrt{5}}\gamma_2\frac{K^2}{2} \\ i\sqrt{\frac{1}{3}}PK & \frac{2}{\sqrt{5}}\gamma_2\frac{K^2}{2} & -\frac{6}{\sqrt{5}}\gamma_2\frac{K^2}{2} & E_v - \Delta - \gamma_1\frac{K^2}{2} \end{bmatrix}
$$

where $G = E_v - \left(\gamma_1 + \frac{8}{5}\gamma_2\right)\frac{K^2}{2}$ Again we treat the conduction band and spin-orbit band as distant and $H_{\frac{3}{2},\pm\frac{1}{2}}$ or $\pm\frac{3}{2}$ becomes

$$
H_{\frac{3}{2},\pm\frac{1}{2} \text{ or } \pm\frac{3}{2}} = \begin{matrix} |\frac{3}{2},0\rangle \\ |\frac{3}{2},2\rangle \\ |\frac{3}{2},1\rangle \\ |\frac{3}{2},3\rangle \end{matrix} \begin{bmatrix} E_v - \gamma_1\frac{K^2}{2} & 2\gamma_2\frac{K^2}{2} & 0 & 0 \\ 2\gamma_2\frac{K^2}{2} & E_v - \gamma_1\frac{K^2}{2} & 0 & 0 \\ 0 & 0 & G & \frac{6}{5}\gamma_2\frac{K^2}{2} \\ 0 & 0 & \frac{6}{5}\gamma_2\frac{K^2}{2} & G \end{bmatrix}
$$

From which we can define even and odd states as

even parity states $\begin{cases} |LH\rangle_{even} = \sqrt{\frac{1}{2}}\left[|\frac{3}{2},0\rangle - |\frac{3}{2},2\rangle\right] \\ |HH\rangle_{even} = \sqrt{\frac{1}{2}}\left[|\frac{3}{2},0\rangle + |\frac{3}{2},2\rangle\right] \end{cases}$

odd parity states $\begin{cases} |LH\rangle_{odd} = \frac{1}{2}\left[|\frac{3}{2},1\rangle - 3|\frac{3}{2},3\rangle\right] \\ |HH\rangle_{odd} = \frac{1}{2}\left[3|\frac{3}{2},1\rangle + |\frac{3}{2},3\rangle\right] \end{cases}$

and obtain the heavy-hole (HH subscript) and light-hole (LH subscript) dispersion relations

$$E_{HH}(K) = E_v - (\gamma_1 - 2\gamma_2)\frac{K^2}{2} \quad \text{and} \quad E_{LH}(K) = E_v - (\gamma_1 + 2\gamma_2)\frac{K^2}{2}$$

To obtain the eigenstates, we use the position representation:

$$\langle r, \theta, \phi \,|F, F_z, L, J\rangle = R_{ln}(r) \sum_{L_z=-L}^{L} \sum_{J_z=-J}^{J} \begin{pmatrix} F & J & L \\ F_Z & J_Z & L_Z \end{pmatrix}_{cg} Y_L^{L_z}(\theta, \phi) u_{J,J_z0}(r, \theta, \phi)$$

For our purposes, we only need to solve the radial component $R_{ln}(r)$. For $\gamma_1$ and $\gamma_2$ corresponding to the inside of the dot, we have

$$\text{even states} \begin{cases} R_{n,even}^{HH}(r < r_{well}) = \sqrt{\tfrac{1}{2}} \begin{bmatrix} j_0(K_{HH}(E_n)r) \\ j_2(K_{HH}(E_n)r) \end{bmatrix} \\[3em] R_{n,even}^{LH}(r < r_{well}) = \sqrt{\tfrac{1}{2}} \begin{bmatrix} j_0(K_{LH}(E_n)r) \\ -j_2(K_{LH}(E_n)r) \end{bmatrix} \end{cases}$$

$$\text{odd states} \begin{cases} R_{n,odd}^{HH}(r < r_{well}) = \sqrt{\tfrac{1}{2}} \begin{bmatrix} 3j_1(K_{HH}(E_n)r) \\ j_3(K_{HH}(E_n)r) \end{bmatrix} \\[3em] R_{n,odd}^{LH}(r < r_{well}) = \sqrt{\tfrac{1}{2}} \begin{bmatrix} j_1(K_{LH}(E_n)r) \\ -3j_3(K_{LH}(E_n)r) \end{bmatrix} \end{cases}$$

where $j_L$ denote spherical Bessel functions Outside the dot we have

$$
\text{even states} \begin{cases} R^{HH}_{n,even}(r > r_{well}) = \sqrt{\tfrac{1}{2}} \left[ \begin{array}{c} h_0^{(1)}(\imath\lambda_{HH}(E_n)r) \\ h_2^{(1)}(\imath\lambda_{HH}(E_n)r) \end{array} \right] \\[4ex] R^{LH}_{n,even}(r > r_{well}) = \sqrt{\tfrac{1}{2}} \left[ \begin{array}{c} h_0^{(1)}(\imath\lambda_{LH}(E_n)r) \\ -h_2^{(1)}(\imath\lambda_{LH}(E_n)r) \end{array} \right] \end{cases}
$$

$$
\text{odd states} \begin{cases} R^{HH}_{n,odd}(r > r_{well}) = \sqrt{\tfrac{1}{2}} \left[ \begin{array}{c} 3h_1^{(1)}(\imath\lambda_{HH}(E_n)r) \\ h_3^{(1)}(\imath\lambda_{HH}(E_n)r) \end{array} \right] \\[4ex] R^{LH}_{n,odd}(r > r_{well}) = \sqrt{\tfrac{1}{2}} \left[ \begin{array}{c} h_1^{(1)}(\imath\lambda_{LH}(E_n)r) \\ -3h_3^{(1)}(\imath\lambda_{LH}(E_n)r) \end{array} \right] \end{cases}
$$

We can define

$$
R_n^{even}(r) = AR^{HH}_{n,even} + BR^{LH}_{n,even} \text{ and } R_n^{odd}(r) = AR^{HH}_{n,odd} + BR^{LH}_{n,odd}
$$

For even parity states, we find $E_n$ by solving

$$
\det \left| \begin{array}{cccc} j_0(K_{HH}(E_n)r) & j_0(K_{LH}(E_n)r) & h_0^{(1)}(\imath\lambda_{HH}(E_n)r) & h_0^{(1)}(\Lambda) \\ j_2(K_{HH}(E_n)r) & -j_2(K_{LH}(E_n)r) & h_2^{(1)}(\imath\lambda_{HH}(E_n)r) & -h_2^{(1)}(\Lambda) \\ j_0'(K_{HH}(E_n)r) & j_0'(K_{LH}(E_n)r) & h_0^{'(1)}(\imath\lambda_{HH}(E_n)r) & h_0^{'(1)}(\Lambda) \\ j_2'(K_{HH}(E_n)r) & -j_2'(K_{LH}(E_n)r) & h_2^{'(1)}(\imath\lambda_{HH}(E_n)r) & -h_2^{'(1)}(\Lambda) \end{array} \right|_{r=r_{well}} = 0
$$

where $\Lambda = \imath\lambda_{LH}(E_n)r$, and the prime superscript denotes a derivative. For the odd parity states we find $E_n$ by solving

$$
\det \left| \begin{array}{cccc} 3j_0(K_{HH}(E_n)r) & j_0(K_{LH}(E_n)r) & 3h_0^{(1)}(\imath\lambda_{HH}(E_n)r) & h_0^{(1)}(\Lambda) \\ j_2(K_{HH}(E_n)r & -3j_2(K_{LH}(E_n)r) & h_2^{(1)}(\imath\lambda_{HH}(E_n)r) & -3h_2^{(1)}(\Lambda) \\ 3j_0'(K_{HH}(E_n)r) & j_0'(K_{LH}(E_n)r) & 3h_0^{'(1)}(\imath\lambda_{HH}(E_n)r) & h_0^{'(1)}(\Lambda) \\ j_2'(K_{HH}(E_n)r) & -3j_2'(K_{LH}(E_n)r) & h_2^{'(1)}(\imath\lambda_{HH}(E_n)r) & -3h_2^{'(1)}(\Lambda) \end{array} \right|_{r=r_{well}} = 0
$$

Note that we use the typical boundary conditions $R_{in}(r_{well}) = R_{out}(r_{well})$ and $\nabla R_{in}(r_{well}) = \nabla R_{out}(r_{well})$.

## 3.4 Matlab Implementation

Now that we have formulated the analytical techniques needed to find the energy eigenvalues and radial eigenvectors, we must implement the calculations numerically. One challenge in doing this is obtaining the necessary band parameters. For convenience we have collected the band parameters for the 12 common III-V semiconductors and put them into table B.2. To facilitate numerical analysis, we have created a material-database-code, whose inputs are type III-V semiconductors (one for the inside material, and another for the outside material). We combined this parameter database with other codes in a convenient Graphical User Interface (GUI), shown in Figure 3.1. A flow chart for the operation of this GUI is shown in Figure 3.2.
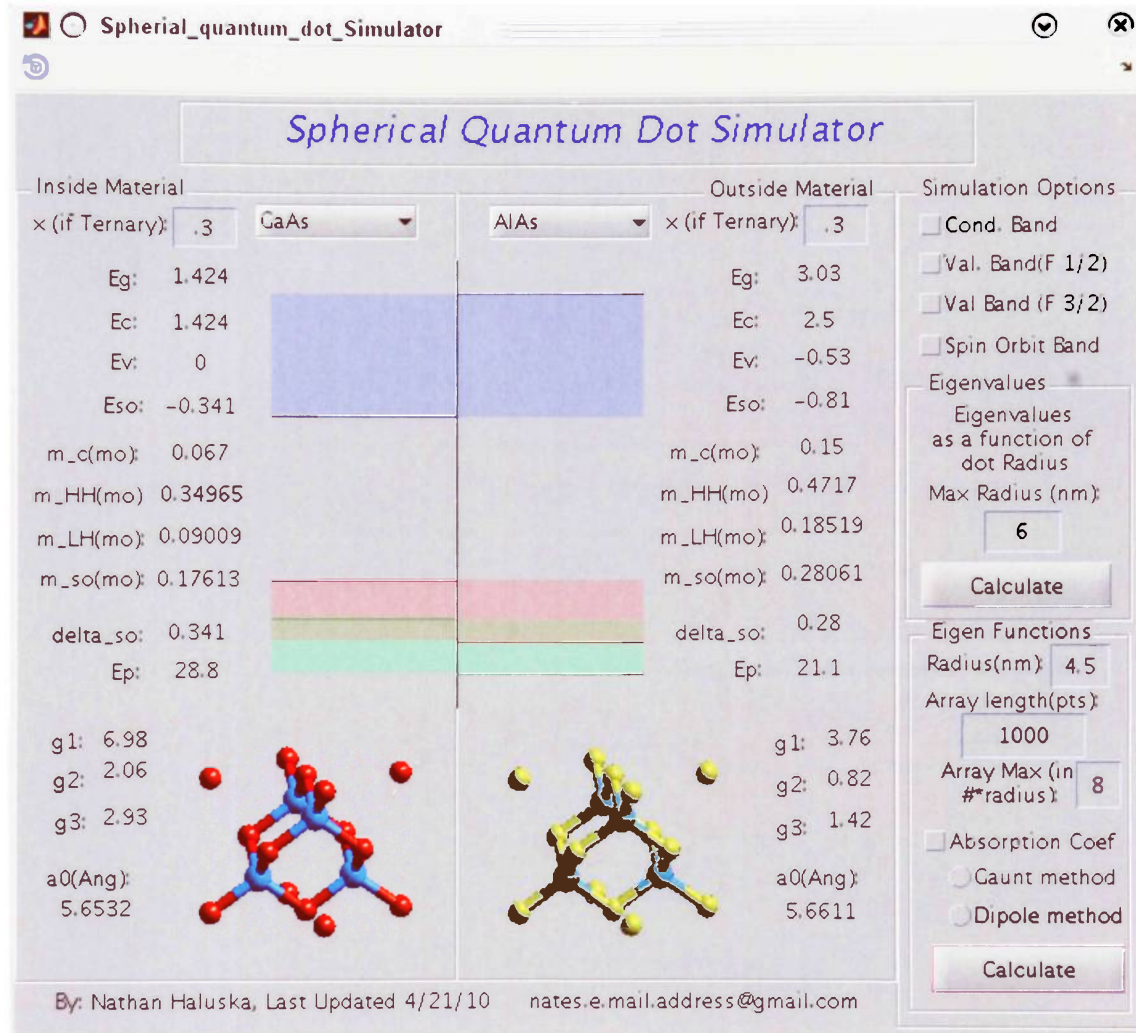
Figure 3.1: Screen shot of the Matlab GUI.
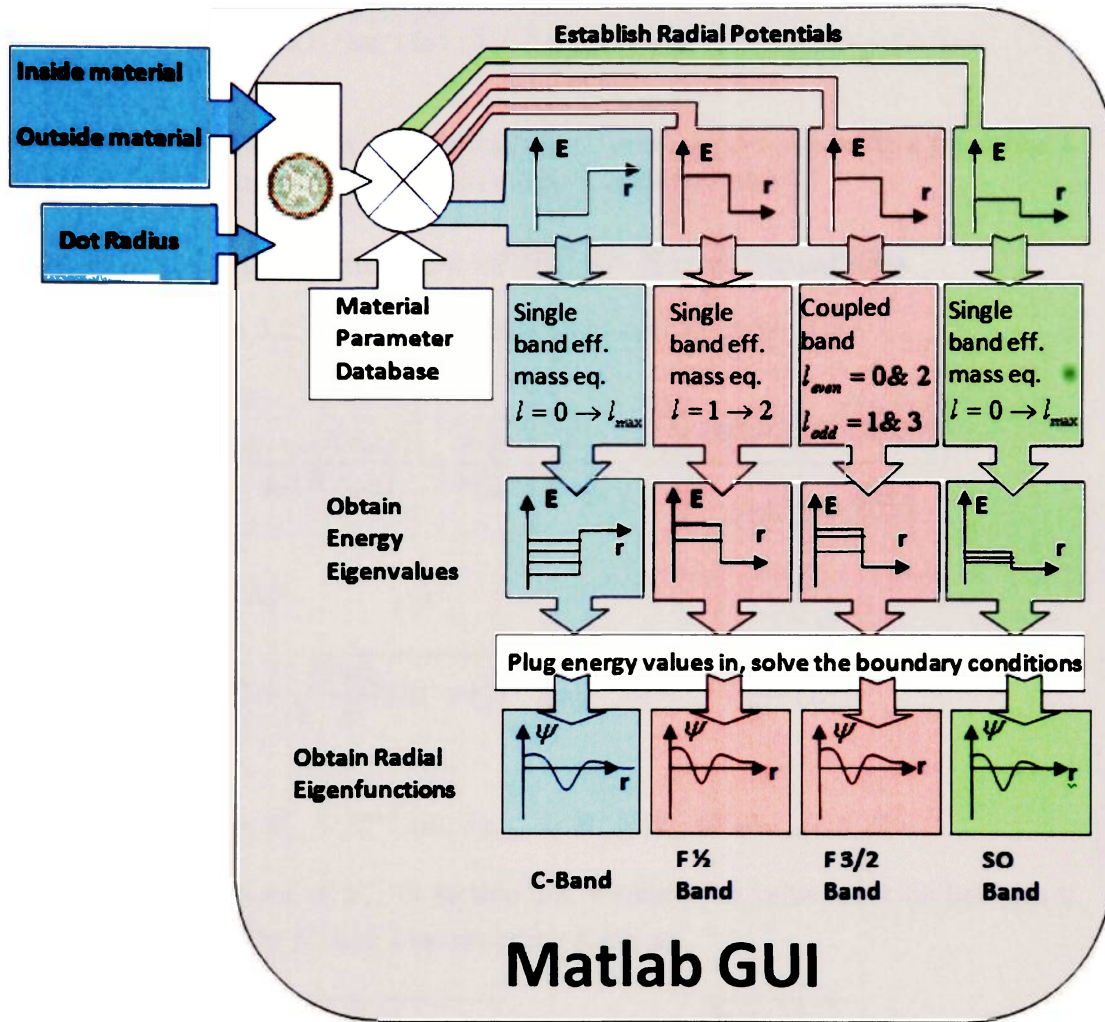
Figure 3.2: Matlab GUI flow diagram.

To further explain how to solve the single band and multiple-band equations, we elaborate on the methodology below.

```
function out=bessel_spj(n,x)
out=besselj(n+.5,x).*sqrt(pi./(2.*x));
end
```

Figure 3.3: Implementation of spherical Bessel function in Matlab Here we define a spherical Bessel function from Matlab's Bessel function "besselj."

## Numerical Implementation of Single Band Equations

Recall from section 3.2, that for the single band case we must solve

$$\frac{l}{r_{well}} - K\frac{j_{l+1,n}(Kr_{well})}{j_{ln}(Kr_{well})} = \frac{m^*_{in}}{m^*_{out}} \left[ \frac{l}{r_{well}} - \lambda \frac{\sum\limits_{m=0}^{l+1} \frac{1}{m!(2\lambda r_{well})^m} \frac{(l+m+1)!}{(l-m+1)!}}{\sum\limits_{m=0}^{l} \frac{1}{m!(2\lambda r_{well})^m} \frac{(l+m)!}{(l-m)!}} \right]$$

where $V_0 = E_c^{out} - E_c^{in}$

$$K = \sqrt{\frac{2m^*_{in}}{\hbar^2}(E'_n + V_0)} \quad \text{and} \quad i\lambda = \sqrt{\frac{2m^*_{out}}{\hbar^2}(E'_n)}$$

to obtain

$$E_{nl} = E'_{nl} + E_c^{out} \quad \text{and} \quad \psi_{Snlm} = R_{nl}(r)Y_{lm}(\theta, \phi)u_{s0}(r, \theta, \phi)$$

From the definition of $E'_n$, in section 3.2, we know its value must be between 0 and $-V_0$. We simplify $K$ and $\lambda$ by rewriting them as

$$K = \sqrt{\frac{2m^*_{in}V_0}{\hbar^2}(1 - A)} \quad \text{and} \quad \lambda = \sqrt{\frac{2m^*_{out}V_0}{\hbar^2}(A)}$$

where A is a numerical array of 10000 points from 0 to 1, and we note that $E'_{nl} = -V_0A$. Now we can express $K$ and $\lambda$ as two numerical arrays of all possible energy values. We utilize Matlab's built in Bessel function to numerically implement the relation

$$j_l(\rho) = \sqrt{\frac{\pi}{2\rho}}J_{l+\frac{1}{2}}(\rho)$$

(See appendix C.1.) Lowercase $j_l$ is the $l$th spherical Bessel function, capital J is the usual Bessel function. The code for this implementation is shown in Figure 3.3.

```matlab
function out=hankel_sp(n,p,x)
    c=0;
    if n~=0
    for m=0:n
        c=c+i^m./(factorial(m).*(2.*x).^m).*factorial(n+m)./factorial(n-m);
    end
    else
        c=1;
    end
        out=(-i).^(n+1).*exp(i.*x)./x.*c;

    if p==2
        out=conj(out);
    end
end
```

Figure 3.4: Implementation of spherical Hankel function in Matlab.

As shown in appendix C.1, the spherical Hankel function can be expressed by the recursion relation

$$h_l^{(1)}(\rho) = (-i)^{l+1} \frac{e^{i\rho}}{\rho} \sum_{m=0}^{l} \frac{i^m}{m!(2\rho)^m} \frac{(l+m)!}{(l-m)!}$$

We implement this in the function shown in Figure 3.4.

These functions allow us to express the spherical Bessel and Hankel functions as numerical arrays. Now we solve

$$\left[\frac{l}{r_{well}} - K\frac{j_{l+1,n}(Kr_{well})}{j_{ln}(Kr_{well})} - \frac{m_{in}^*}{m_{out}^*}\right] \left[\frac{l}{r_{well}} - \lambda\frac{\sum_{m=0}^{l+1} \frac{1}{m!(2\lambda r_{well})^m} \frac{(l+m+1)!}{(l-m+1)!}}{\sum_{m=0}^{l} \frac{1}{m!(2\lambda r_{well})^m} \frac{(l+m)!}{(l-m)!}}\right] = 0 \qquad (3.7)$$

We summarize this process with a portion taken from our code shown in Figure 3.5.

We also note that equation 3.7 must be solved for unknown values of $l$. Therefore we specify a value starting with zero, and we increment this process till no zero points exist. This process is shown in Figure 3.6

To numerically find each of these zero points, we loop through the "out" array–mentioned in the last line of code from Figure 3.5–and find the points where the array

```
% ra is specified in the GUI, and the materials used determine Vo
% ra is the radius of the QD
% m_in is the effective mass inside the well, specified by the chosen
% material
% m_out is the effective mass outside the well, specified by the choen
% material
Vo=Ec_out-Ec_in;
a=0:.00001:1;% define an array of 10000 points from 0 to 1;
K=sqrt(1-a);
lambda=sqrt(a);
c_in=5.1231658827147*ra*sqrt(Vo)*sqrt(m_in);
c_out=5.1231658827147*ra*sqrt(Vo)*sqrt(m_out);
z_l=c_in.*K;
z_r=lambda.*c_out;
%%%%%%%%% Break in code, this is not the actual code just a portion of it
% additional code will tak care of looping through "l" values
%starting with l=0 and incrementing till no zero solutions are found.
%%%%%%%%%%%% Break in code
LHS=AA.*(1/ra-(z_l/ra)./(bessel_spj(1,z_l)).*(bessel_spj(1+1,z_l)));
RHS=(m_in/m_out).*(1/ra-(c_out/ra).*hankel_sp_D1(1,z_r,lambda));
out=real(LHS-RHS);
% now the variable out contains the "Solution" array, that is
% the points where out=0 are solutions--the enegry eigen values
% OR it contais a values which basically says no zero was found
```

Figure 3.5: Portion of code which numerically evaluates equation 3.7 as a numerical array called "out." The code then search "out" for the points where it crosses the x axis (ignoring asymptotes).

$l = 0$, we have 2 n values ,

$l = 1$ we have 1 n value

$l = 2$, we have 1 n value ,

$l = 3$ we have no further values
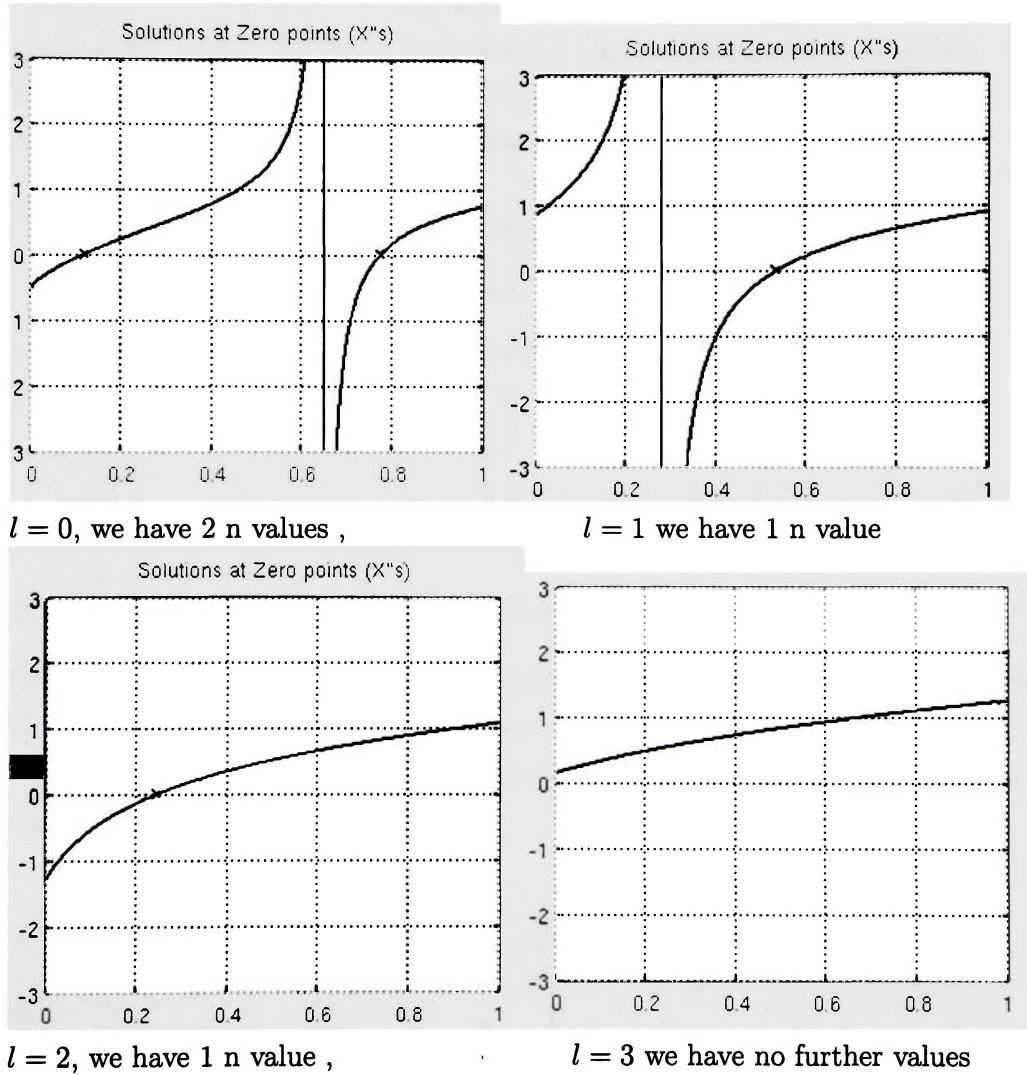
Figure 3.6: Finding the zero points of equation 3.7

crosses the x-axis (ignoring the asymptotes). We send the array "out" to the function "findzeros" which is defined in Figure 3.7.

Note that this tells us the value of "A" where the function is equal to zero, so we must input this into $E'_{nl} = -V_0 A_n$–we have added the subscript n to denote that there are multiple values of A for a particular $l$. The final energy for a particular n and $l$ is given by $E_{nl} = -V_0 A_n + E_c^{out}$ or expanded further $E_{nl} = -\left(E_c^{out} - E_c^{in}\right) A_n + E_c^{out}$. Now we numerically represent the radial functions for each value of n and l

$$R_{nl}(r) = \begin{cases} j_l(Kr) & r < r_{well} \\ B_{nl} h_l^{(1)}(i\lambda r) & r > r_{well} \end{cases}$$

and find $B_{nl}$ with the boundary condition

$$j_l(K r_{well}) = B_{nl} h_l^{(1)}(i\lambda r_{well})$$

where $K$ and $\lambda$ are evaluated at $E_{nl}$.

## Numerical Implementation of Multiple-Band Equations

To find numerical solutions for the multiple-band equations, we use the same methodology as the single band equation, except that the eigenvectors must be found with determinants and matrix inverses. For example, we find the $E_n$ values for the even states in the $F_{3/2}$ space by

$$\det \begin{vmatrix} j_0(K_{HH}(E_n)r) & j_0(K_{LH}(E_n)r) & h_0^{(1)}(i\lambda_{HH}(E_n)r) & h_0^{(1)}(i\lambda_{LH}(E_n)r) \\ j_2(K_{HH}(E_n)r) & -j_2(K_{LH}(E_n)r) & h_2^{(1)}(i\lambda_{HH}(E_n)r) & -h_2^{(1)}(i\lambda_{LH}(E_n)r) \\ j_0'(K_{HH}(E_n)r) & j_0'(K_{LH}(E_n)r) & h_0^{'(1)}(i\lambda_{HH}(E_n)r) & h_0^{'(1)}(i\lambda_{LH}(E_n)r) \\ j_2'(K_{HH}(E_n)r) & -j_2'(K_{LH}(E_n)r) & h_2^{'(1)}(i\lambda_{HH}(E_n)r) & -h_2^{'(1)}(i\lambda_{LH}(E_n)r) \end{vmatrix}_{r=r_{well}} = 0$$

$$(3.8)$$

We again implement the spherical Bessel and spherical Hankel functions as numerical arrays. Again, we solve for "A" on a interval of zero to 1. The determinant is solved for every value of "A" as shown in Figure 3.8

```matlab
function zs=findzeros(x,y,scale_size)
%*********Returns matlab value pi if NO ZEROS FOUND******
% for two numerical arrays where y=y(x)
% finds points where the function crosses the x-axis
% ignores asymiptoes
% works best if arrays are large
% scale_size is used to give limets for asymiptoes
y=real(y);
l=length(y);
index=0;
for j=1:l-1
    if(abs(y(j))<scale_size)
        if(y(j)==0)
            index=index+1;
            zs(index)=x(j);
        elseif(y(j)>0 && y(j+1)<0 )
            %locate a cross of the x axis in neg direction
            index=index+1;
            zs(index)=(x(j)+x(j+1))/2;
        elseif(y(j)<0 && y(j+1)>0 )
            %locate a cross of the x axis in pos direction
            index=index+1;
            zs(index)=(x(j)+x(j+1))/2;
        end
    end
end
if index==0
    zs=pi; %let host program know there are no zero points
end
end
```

Figure 3.7: Function findzeros.m written to find zero points. This works best for very large (10000 pt.) arrays. It searches for the two points where the function goes from negative to positive or positive to negative. If the separation between the two points is too large (specified by the variable "scale_size") it is ignored, otherwise the two points are averaged together and stored. This process is repeated for the whole array, and the output "zs" is an array all the "zero" locations along the x axis.

```
% find the value of the determinent for every value of E
% store the values to an array called even_det
for q=1:E_res
    even_d=[ j0h(q),   j0(q),    h0h(q),      h0(q);...
             j2h(q),  -j2(q),    h2h(q),     -h2(q);...
            dj0h(q),  dj0(q),   dh0h(q),      dh0(q);...
            dj2h(q), -dj2(q),   dh2h(q),     -dh2(q)];
    %dispersion relation for odd states
    even_det(q)=det(even_d);

end
% we use the findzeros function to find the zero points
```

Figure 3.8: Matlab code utilized to loop through equation 3.8 and evaluate the determinant for each "A" value.

Next, we use the "findzeros.m" function to find the "$A_n$" values and corresponding energy values. Note that the $l$ values are predetermined by the coupled-band Hamiltonian, and therefore we do not sweep over possible $l$ values. To find the eigenvectors, we plug in the energy values and solve the equation

$$
\begin{bmatrix}
j_0(K_{LH}(E_n)r) & h_0^{(1)}(i\lambda_{HH}(E_n)r) & h_0^{(1)}(i\lambda_{LH}(E_n)r) \\
-j_2(K_{LH}(E_n)r) & h_2^{(1)}(i\lambda_{HH}(E_n)r) & -h_2^{(1)}(i\lambda_{LH}(E_n)r) \\
j_0'(K_{LH}(E_n)r) & h_0'^{(1)}(i\lambda_{HH}(E_n)r) & h_0'^{(1)}(i\lambda_{LH}(E_n)r)
\end{bmatrix}
\begin{bmatrix}
C_2(r) \\
C_3(r) \\
C_4(r)
\end{bmatrix} =
$$
$$
- \begin{bmatrix}
j_0(K_{HH}(E_n)r) \\
j_2(K_{HH}(E_n)r) \\
j_0'(K_{HH}(E_n)r)
\end{bmatrix}
$$

where we have reduced equation 3.8 by arbitrarily setting the coefficient $C_1(r)$ equal to 1 for every value of r; because we can just normalize the functions later. This is solved for $\vec{C}$ with the matrix inverse "\" in Matlab, and it solved for every value of r—every value of r in our numerical array. With this we can solve the coupled radial equation

$$
R_n^{even}(r) = AR_{n,even}^{HH} + BR_{n,even}^{LH}
$$

recalling that inside the dot

$$R^{HH}_{n\;even}(r < r_{well}) = \sqrt{\frac{1}{2}} \left[ \begin{array}{c} \jmath_0(K_{HH}(E_n)r) \\ \jmath_2(K_{HH}(E_n)r) \end{array} \right],$$

$$R^{LH}_{n\;even}(r < r_{well}) = \sqrt{\frac{1}{2}} \left[ \begin{array}{c} \jmath_0(K_{LH}(E_n)r) \\ -\jmath_2(K_{LH}(E_n)r) \end{array} \right]$$

and outside the dot

$$R^{HH}_{n\;even}(r > r_{well}) = \sqrt{\frac{1}{2}} \left[ \begin{array}{c} h_0^{(1)}(\imath\lambda_{HH}(E_n)r) \\ h_2^{(1)}(\imath\lambda_{HH}(E_n)r) \end{array} \right],$$

$$R^{LH}_{n\;even}(r > r_{well}) = \sqrt{\frac{1}{2}} \left[ \begin{array}{c} h_0^{(1)}(\imath\lambda_{LH}(E_n)r) \\ -h_2^{(1)}(\imath\lambda_{LH}(E_n)r) \end{array} \right]$$

combining these together with the $\vec{C}(r)$ coefficients we have

$$R^{even}_n(r < r_{well}) = \sqrt{\frac{1}{2}} \left[ \begin{array}{c} C_1(r)\jmath_0(K_{HH}(E_n)r) + C_2(r)\jmath_0(K_{LH}(E_n)r) \\ C_1(r)\jmath_2(K_{HH}(E_n)r) - C_2(r)\jmath_2(K_{LH}(E_n)r) \end{array} \right]$$

and

$$R^{even}_n(r > r_{well}) = \sqrt{\frac{1}{2}} \left[ \begin{array}{c} C_3(r)h_0^{(1)}(\imath\lambda_{HH}(E_n)r) + C_4(r)h_0^{(1)}(\imath\lambda_{LH}(E_n)r) \\ C_3(r)h_2^{(1)}(\imath\lambda_{HH}(E_n)r) - C_4(r)h_2^{(1)}(\imath\lambda_{LH}(E_n)r) \end{array} \right]$$

This is implemented in Matlab as shown in Figure 3 9

## 3.5  Obtaining the Software

To obtain a copy of the developed Matlab code, please get the disk from the ERAU Daytona Beach library or email to author at nates e mail address@gmail com

```
for q=1:length(zs_even)
X=[ j0h(q),    j0(q),      h0h(q),      h0(q);...
        j2h(q),  -j2(q),      h2h(q),     -h2(q);...
        dj0h(q),  dj0(q), M1.*dh0h(q),  M2.*dh0(q)];
X(:,2:4);% the right portion from X ( 3x3) matrix
Q=X(:,2:4)\(-X(:,1));% calculate the matrix inverse and solve vector Q
A=1;% arbitary set =1,normalise later
B=Q(1);
C=-Q(2);
D=-Q(3);
clear R                  %create arrays for portion inside the well
R=3.62263.*r_out(1:round(fun_res/qwe));
j0z=sin(R.*kl(q))./(R.*kl(q));
j2z=-3.*cos(R.*kl(q))./(R.^2.*kl(q).^2)+(3-R.^2.*kl(q).^2)...
    .*sin(R.*kl(q))./(R.^3.*kl(q).^3);
j0hz=sin(R.*kh(q))./(R.*kh(q));
j2hz=-3.*cos(R.*kh(q))./(R.^2.*kh(q).^2)+(3-R.^2.*kh(q).^2)...
    .*sin(R.*kh(q))./(R.^3.*kh(q).^3);
clear R                  %create arrays for portion out side the well
R=3.62263.*r_out(round(fun_res/qwe)+1:fun_res);
h0z=-exp(-R.*llh(q))./(R.*llh(q));
h2z=exp(-R.*llh(q)).*(3+3.*R.*llh(q)+R.^2.*llh(q).^2)./(R.^3.*llh(q).^3);
h0hz=-exp(-R.*lhh(q))./(R.*lhh(q));
h2hz=exp(-R.*lhh(q)).*(3+3.*R.*lhh(q)+R.^2.*lhh(q).^2)./(R.^3.*lhh(q).^3);
%store functions for later use  and combine with coefficients into
even_fun1(q,1:round(fun_res/qwe))=A.*j0hz+B.*j0z;%portion < r_well
even_fun1(q,(round(fun_res/qwe)+1):fun_res)=C.*h0hz+D.*h0z;%portion >r_well
even_fun2(q,1:round(fun_res/qwe))=A.*j2hz-B.*j2z;%portion < r_well
even_fun2(q,(round(fun_res/qwe)+1):fun_res)=C.*h2hz-D.*h2z;%portion >r_well
end
```

Figure 3.9: Sample code used to find the radial eigenfunctions for the coupled $F_{3/2}$ space.

## 3.5.1 Results

Below we give results for common types of hetrojunctions. The results were obtained from our GUI. These results are very important in determining the optical properties, which we shall discuss in the next chapter.

# GaAs Embedded in AlAs

Below we have the results from a GaAs quantum dot Embedded in AlAs, plots are shown for eigenvalues then eigenvectors for dots of 4.5 and 7.5 nm in radius.



Figure 3.10: Eigenvalues as a function of dot radius for GaAs Embeded in AlAs

Figure 3.11: Conbined plot of eigenvalues as a function of dot radius for GaAs Embeded in AlAs
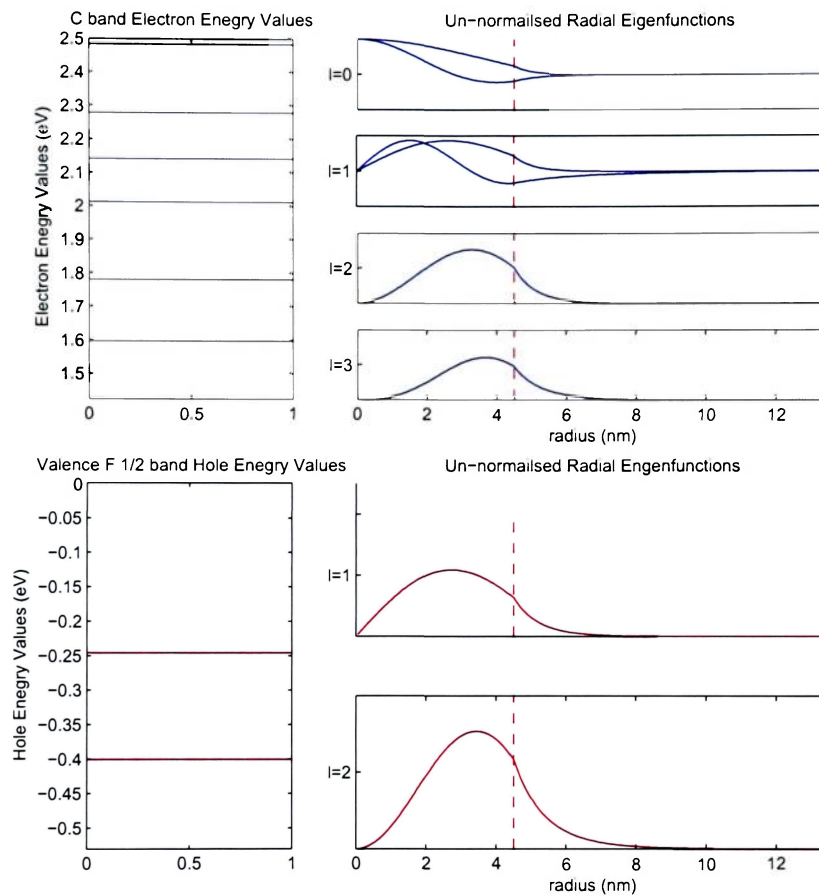
Figure 3.12: Radial eigenvectors (unnormalized) for a 4.5 nm dot of GaAs Embeded in AlAs (c band and F 1/2 band)
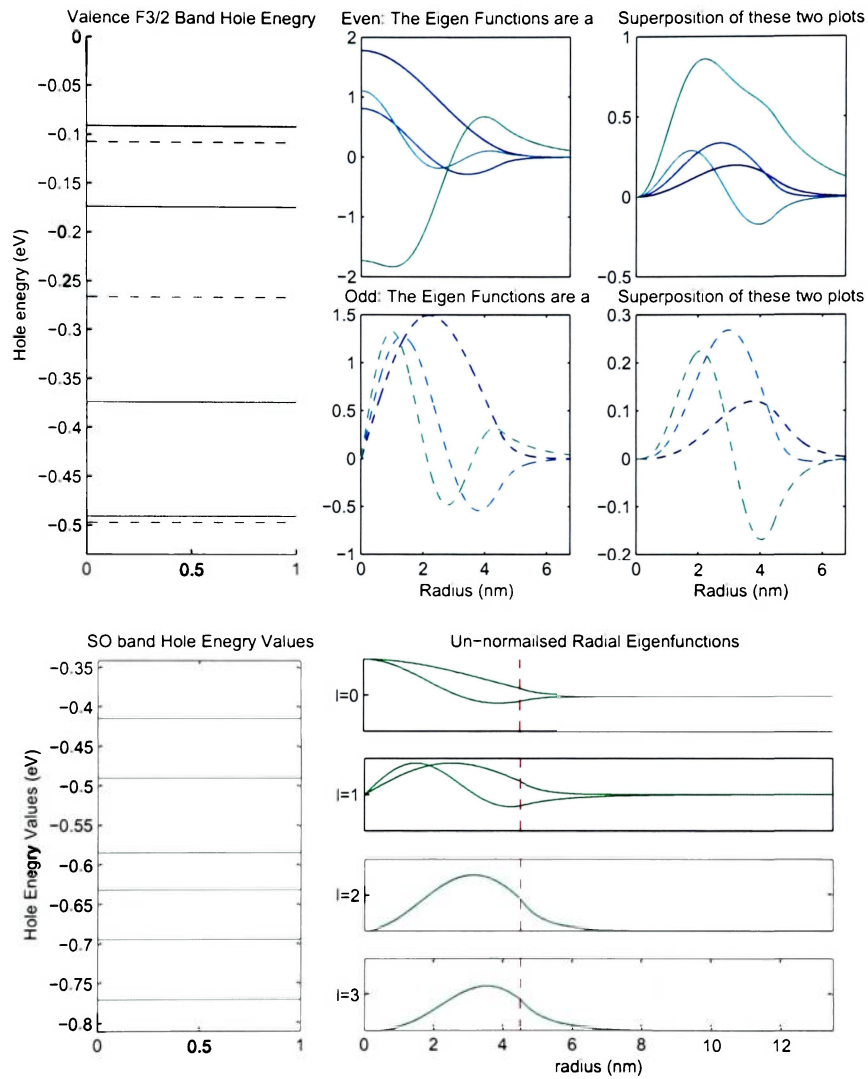
Figure 3.13: Radial eigenvectors (unnormalized) for a 4.5 nm dot of GaAs Embeded in AlAs ( F 3/2 band and SO band)
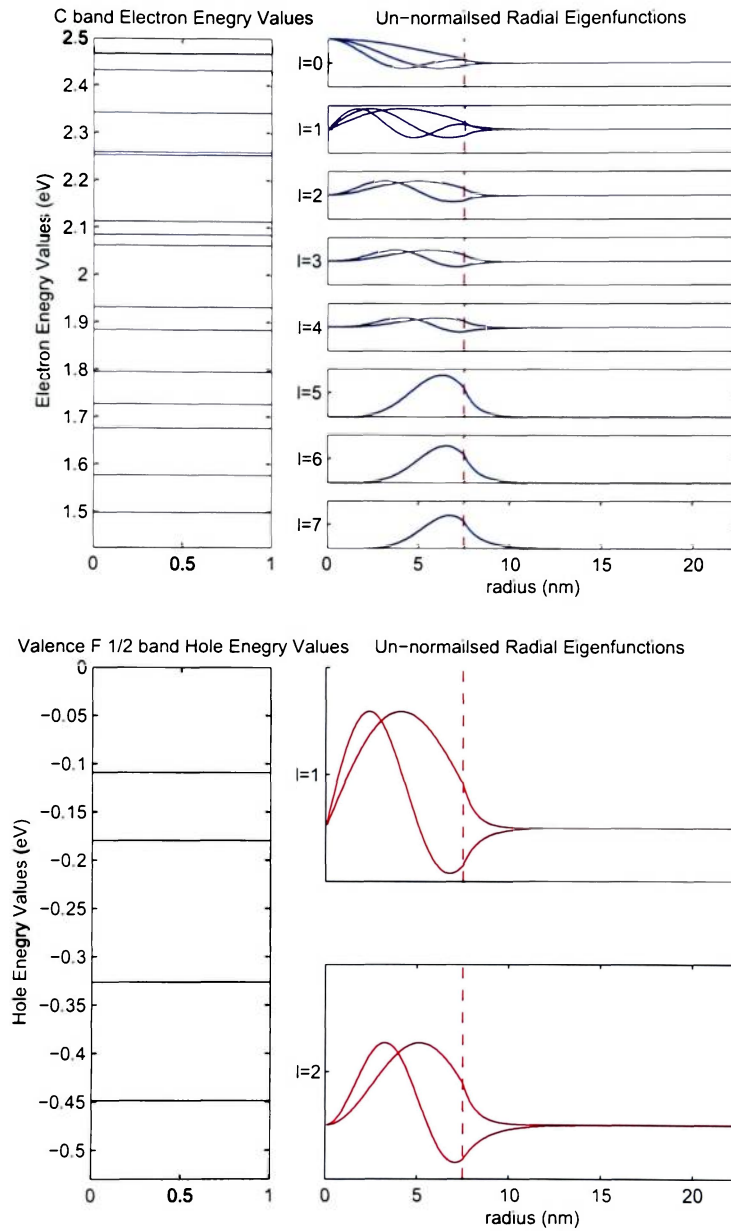
Figure 3.14: Radial eigenvectors for a 7.5 nm dot of GaAs Embeded in AlAs (c band and F 1/2 band)
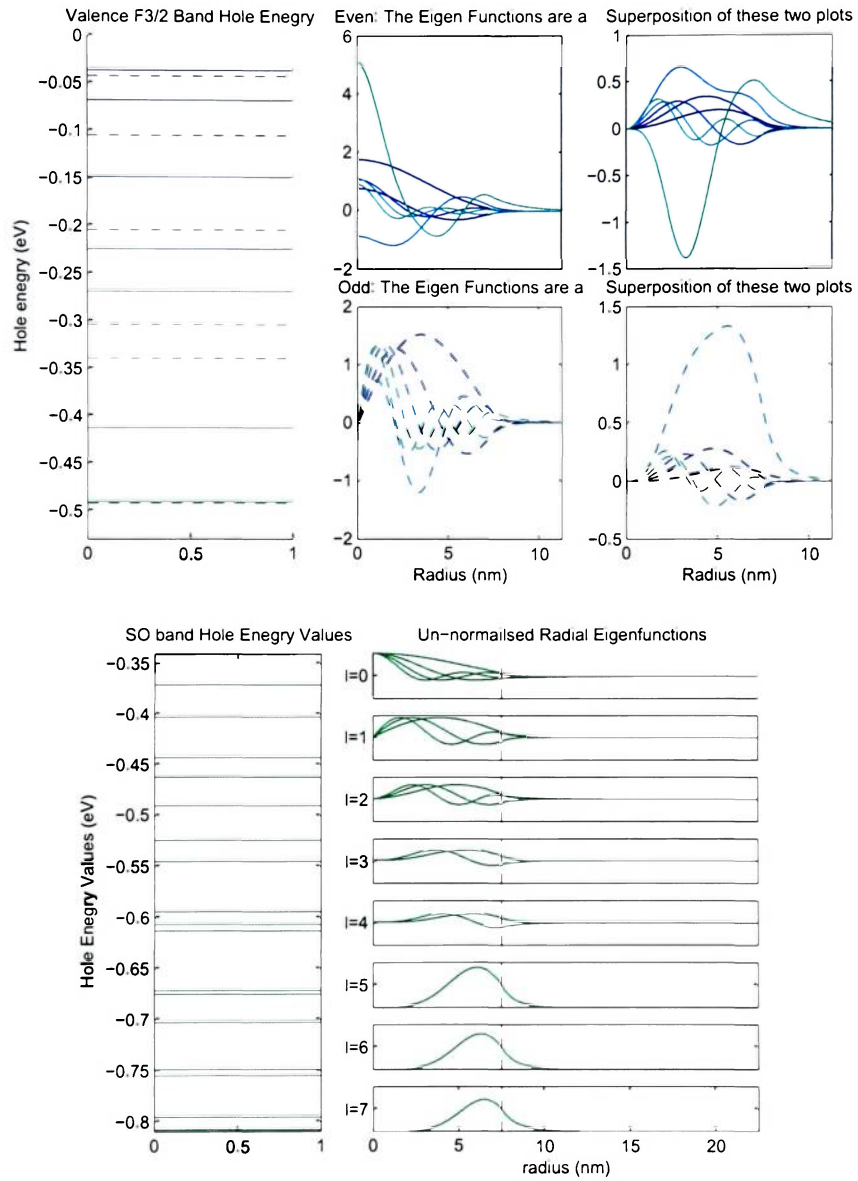
Figure 3.15: Radial eigenvectors (unnormalized) for a 7.5 nm dot of GaAs Embeded in AlAs ( F 3/2 band and SO band)

## GaAs Embedded in $Al_xGa_{1-x}As$

Below we have the results from a GaAs quantum dot Embedded in $Al_3Ga_7As$ (x =.3), plots are shown for eigenvalues then eigenvectors for dots of 4.5 and 7.5 nm in radius.
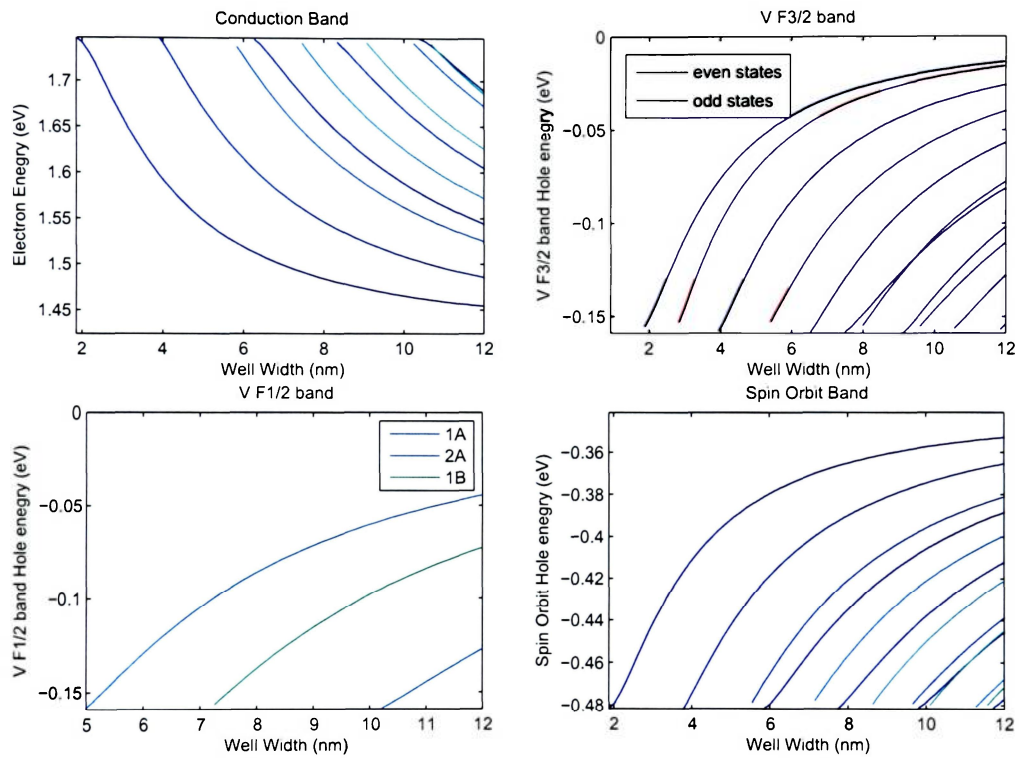


Figure 3.16: Eigenvalues as a function of dot radius for GaAs Embeded in $Al_3Ga_7As$
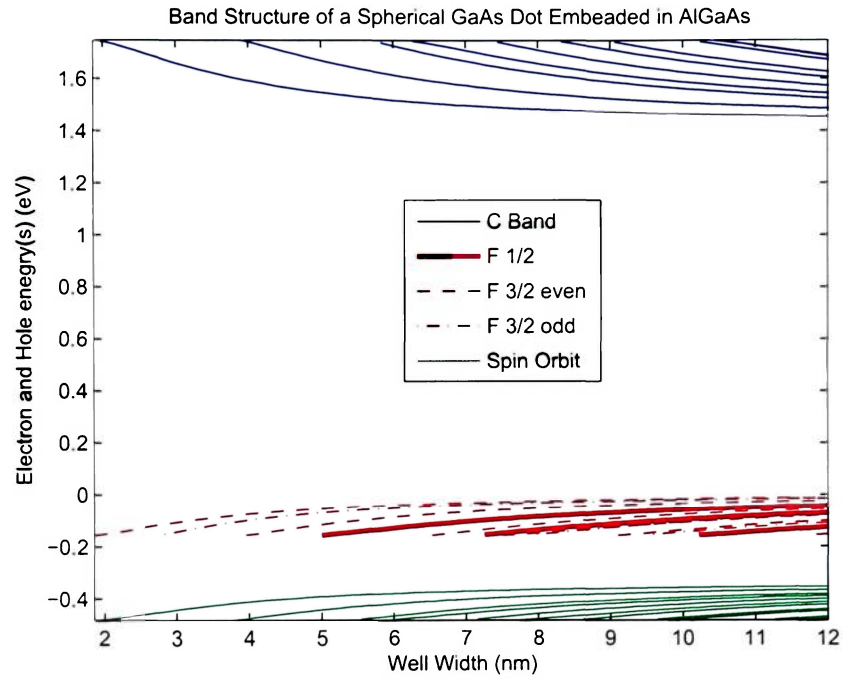
Figure 3.17: Conbined plot of eigenvalues as a function of dot radius for GaAs Embeded in $Al_{.3}Ga_{.7}As$
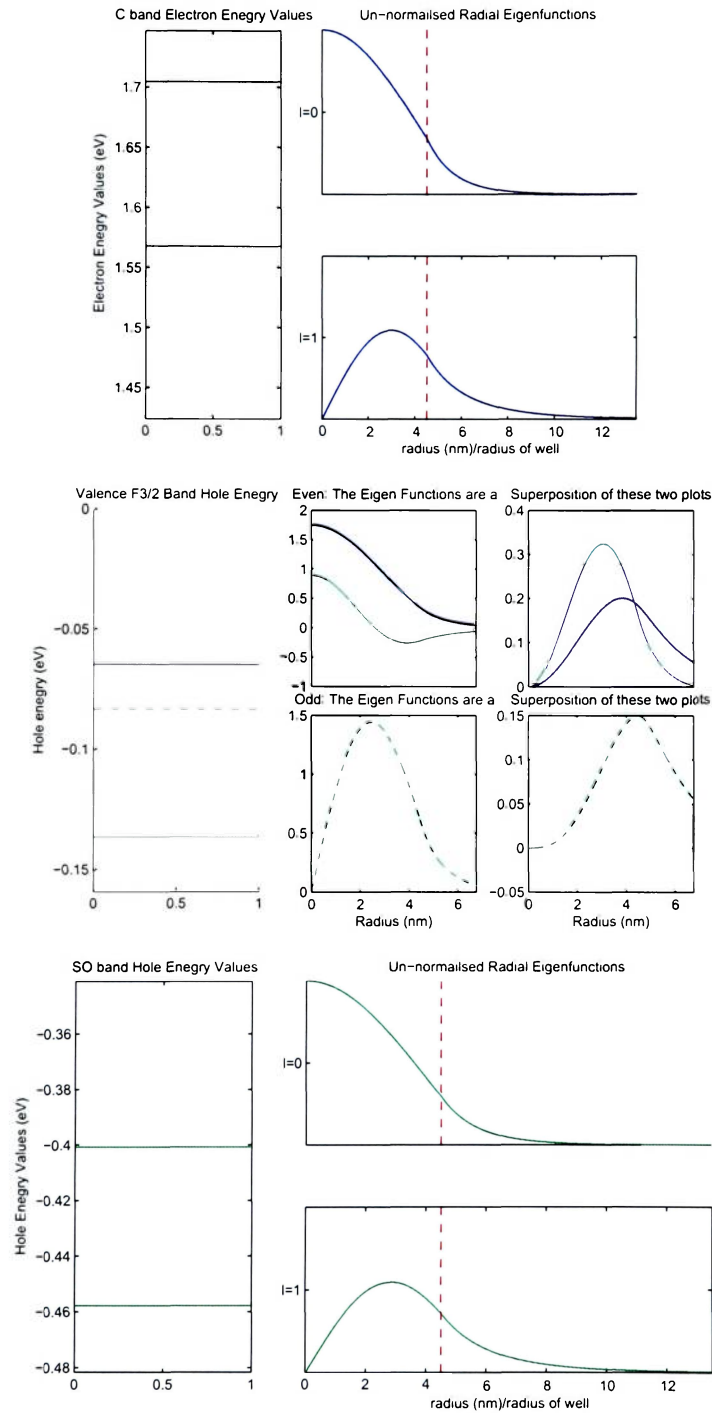
Figure 3.18: Radial eigenvectors for a 7.5 nm dot of GaAs Embeded in AlAs (c band, F 3/2 band, so band, the F 1/2 band does not exist at this dot size)
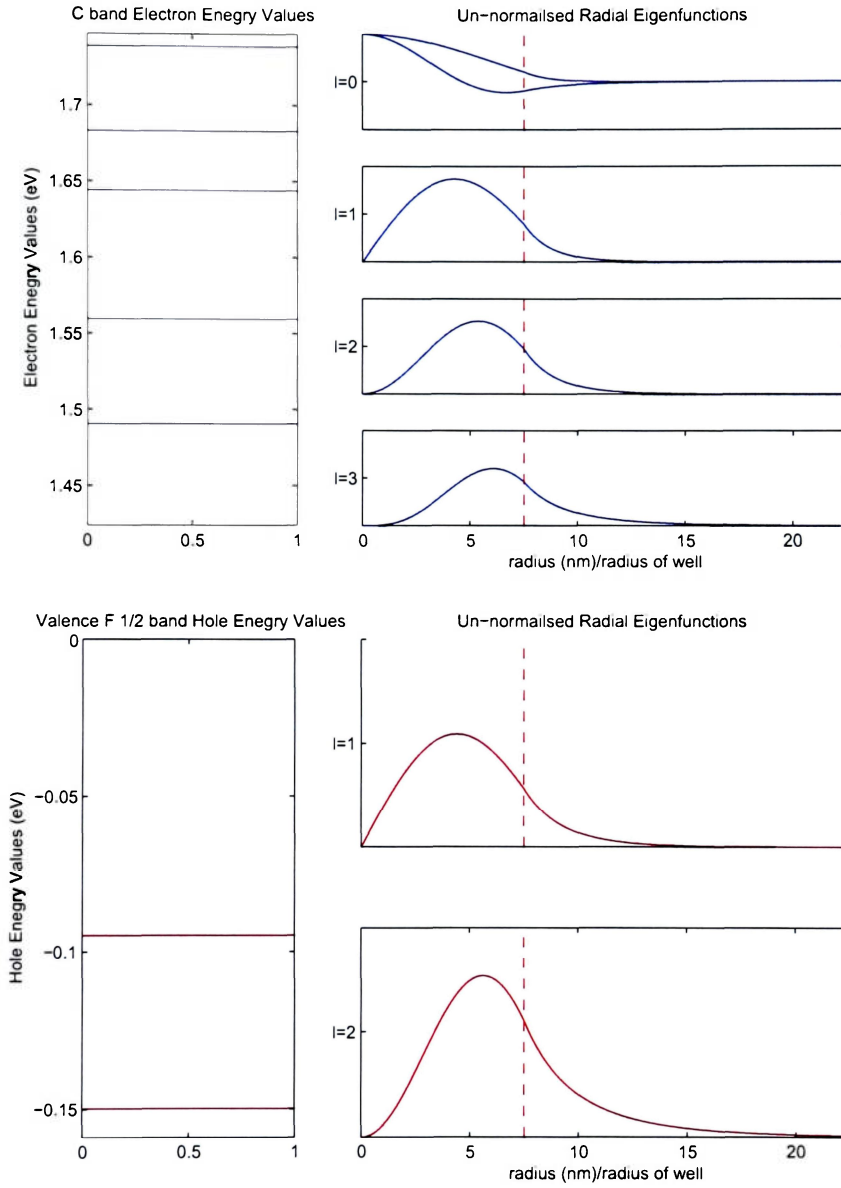
Figure 3.19: Radial eigenvectors for a 7.5 nm dot of GaAs Embeded in AlAs (c band, F 3/2 band, so band, the F 1/2 band does not exist at this dot size)
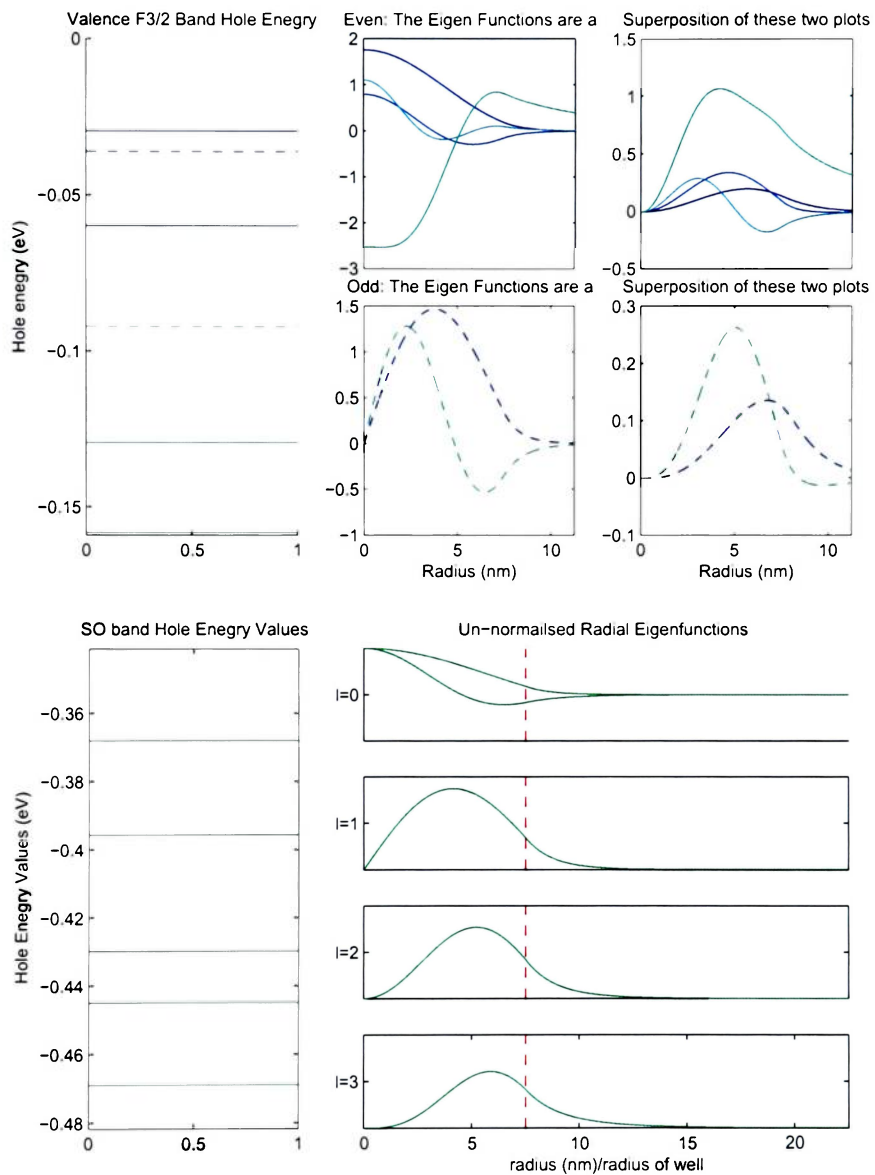
Figure 3.20: Radial eigenvectors for a 7.5 nm dot of GaAs Embeded in AlAs (c band, F 3/2 band, so band, the F 1/2 band does not exist at this dot size)

# InAs Embedded in GaAs

Below we have the results from a InAs quantum dot Embedded in GaAs, plots are shown for eigenvalues then eigenvectors for dots of 7.5 and 12 nm in radius.
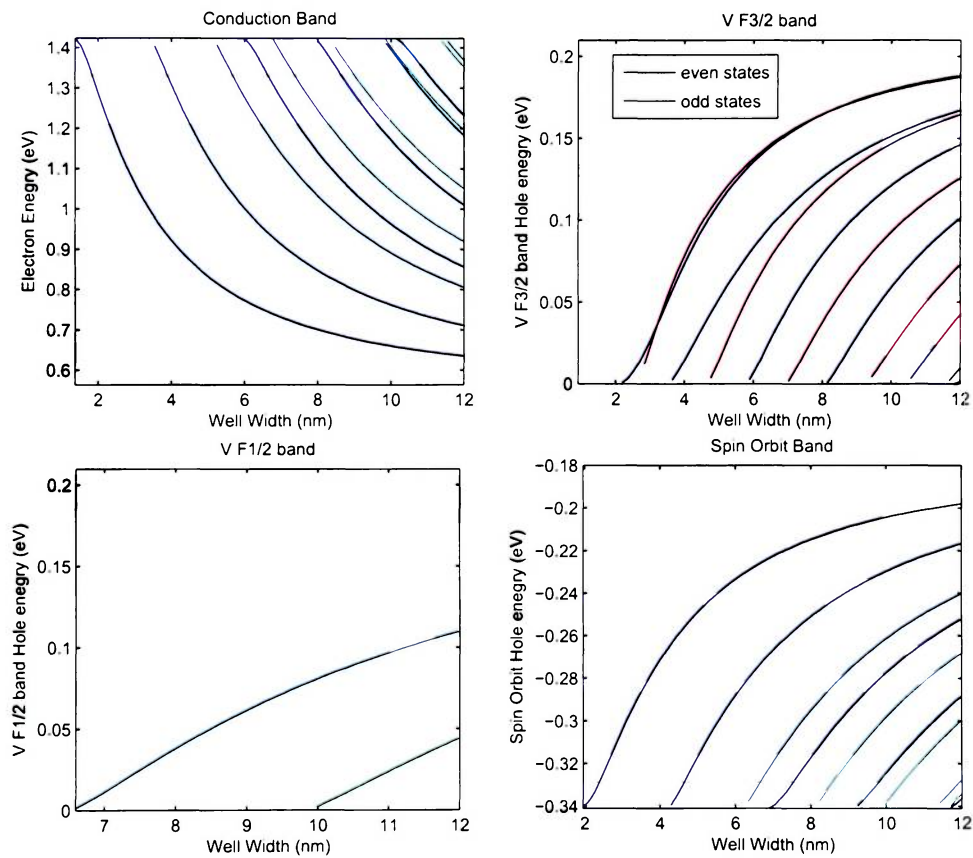
Figure 3.21: Eigenvalues as a function of dot radius for InAs Embeded in GaAs
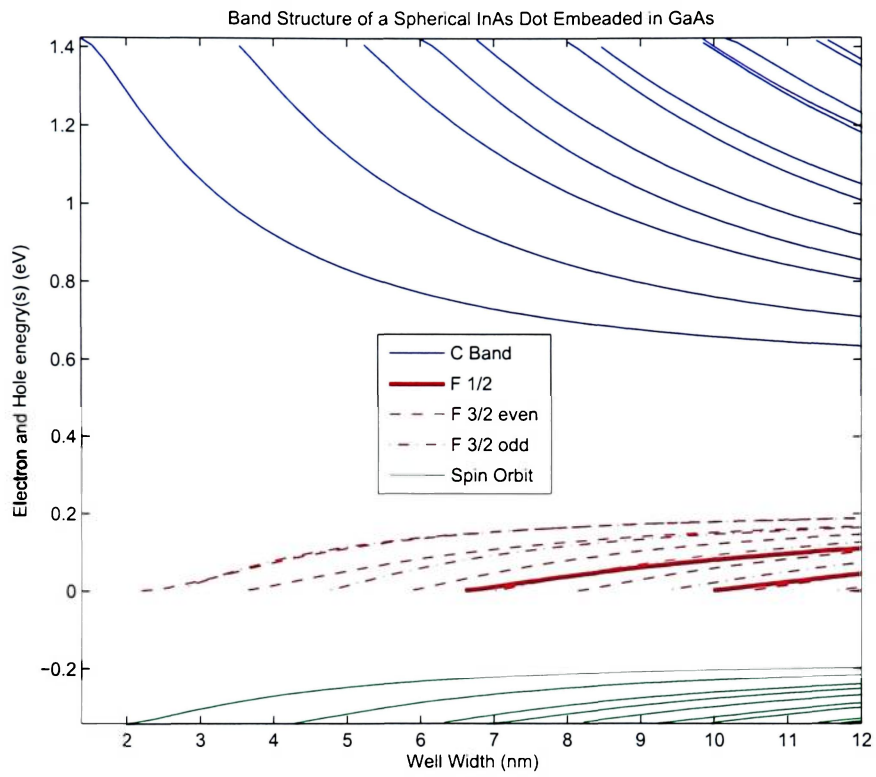
Figure 3.22: Combined plot of eigenvalues as a function of dot radius for InAs Embeded in GaAs
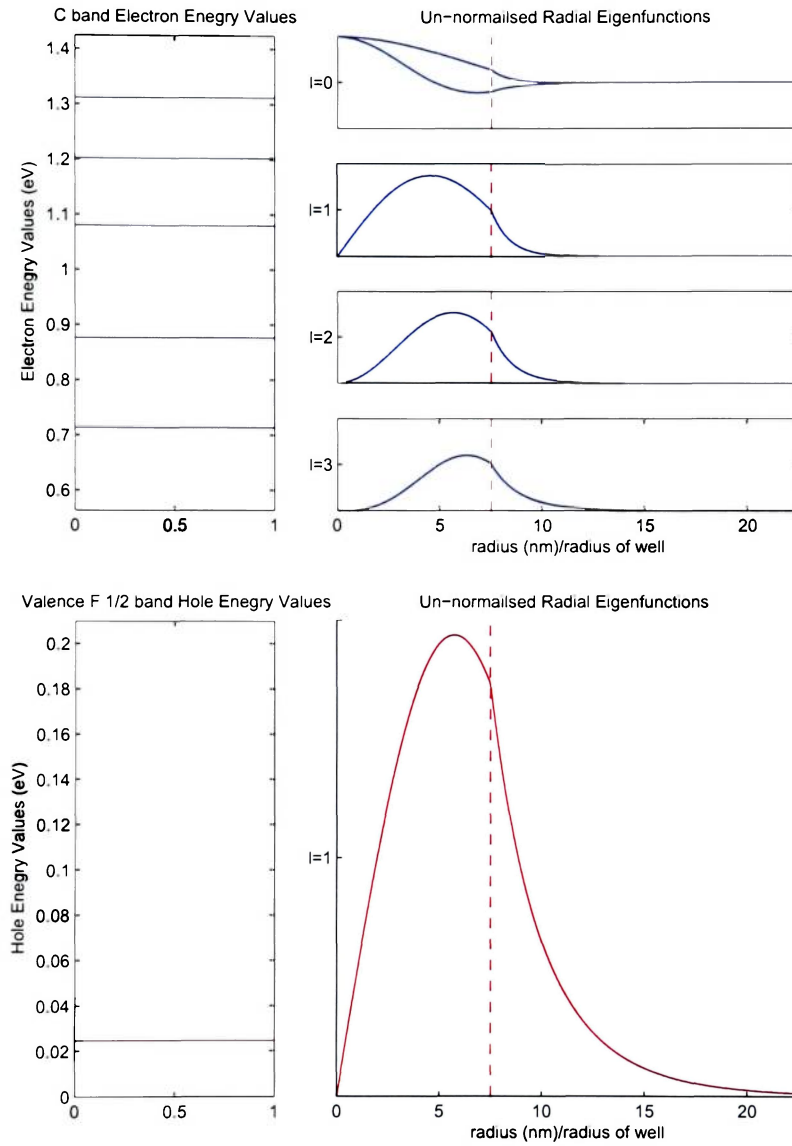
Figure 3.23: Radial eigenvectors (unnormalized)for a 7.5 nm dot of GaAs Embeded in AlAs (c band and F 1/2 band)
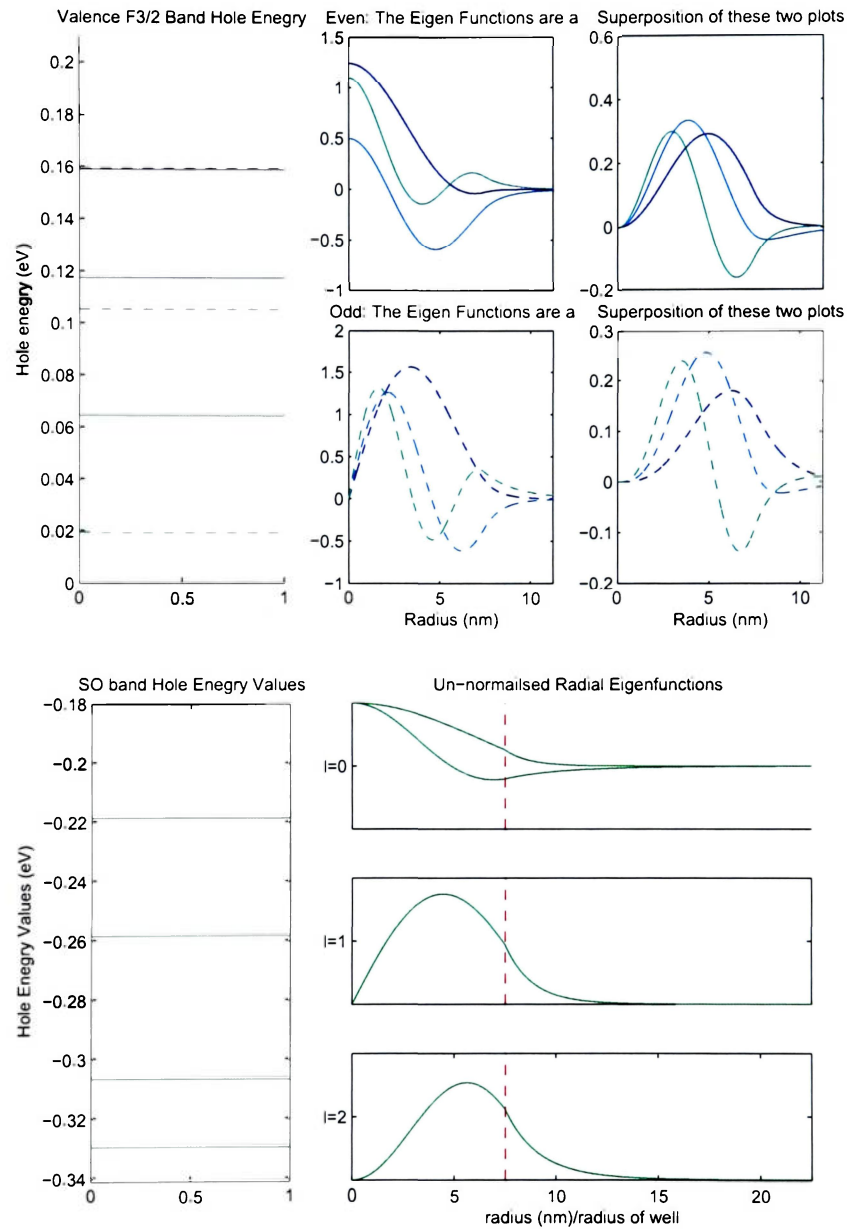
Figure 3.24: Radial eigenvectors (unnormalized) for a 7.5 nm dot of GaAs Embeded in AlAs ( F 3/2 band and SO band)
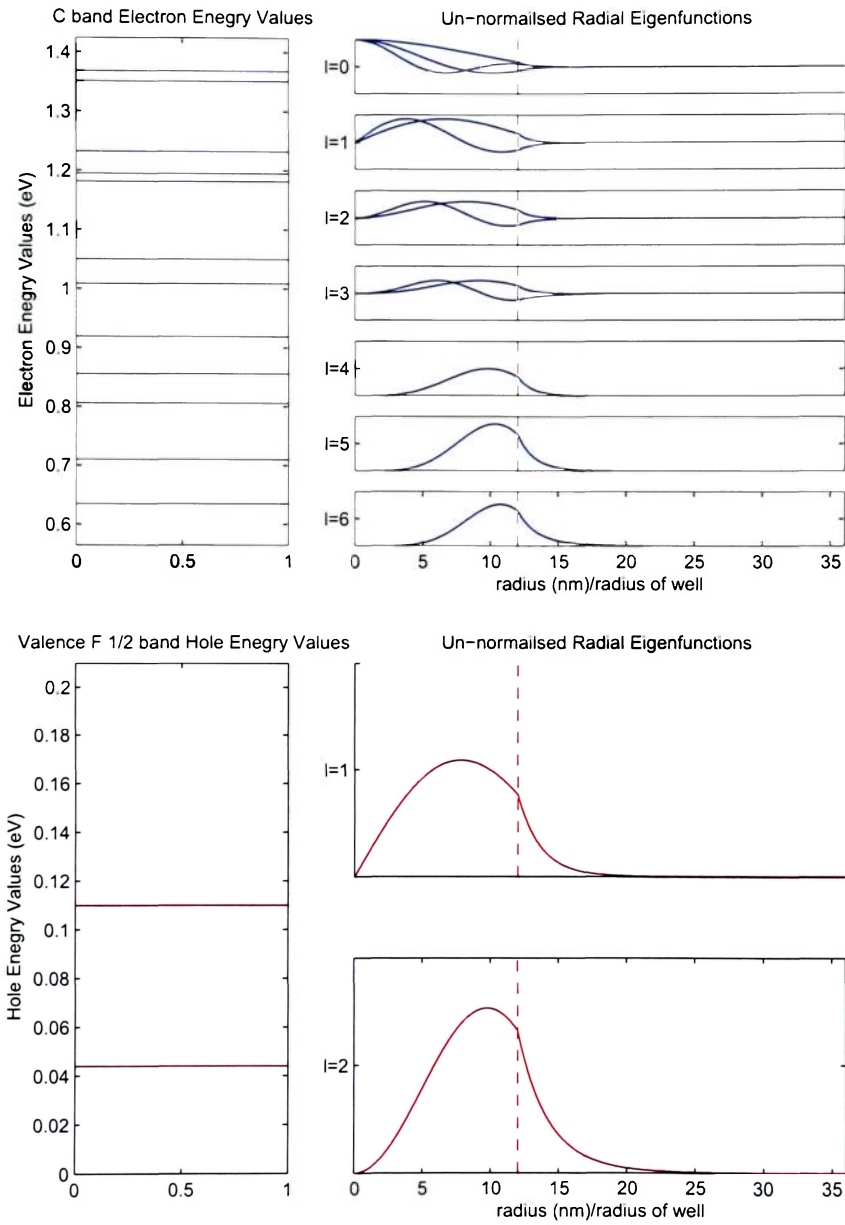
Figure 3.25: Radial eigenvectors (unnormalized) for a 12 nm dot of GaAs Embeded in AlAs (c band and F 1/2 band)
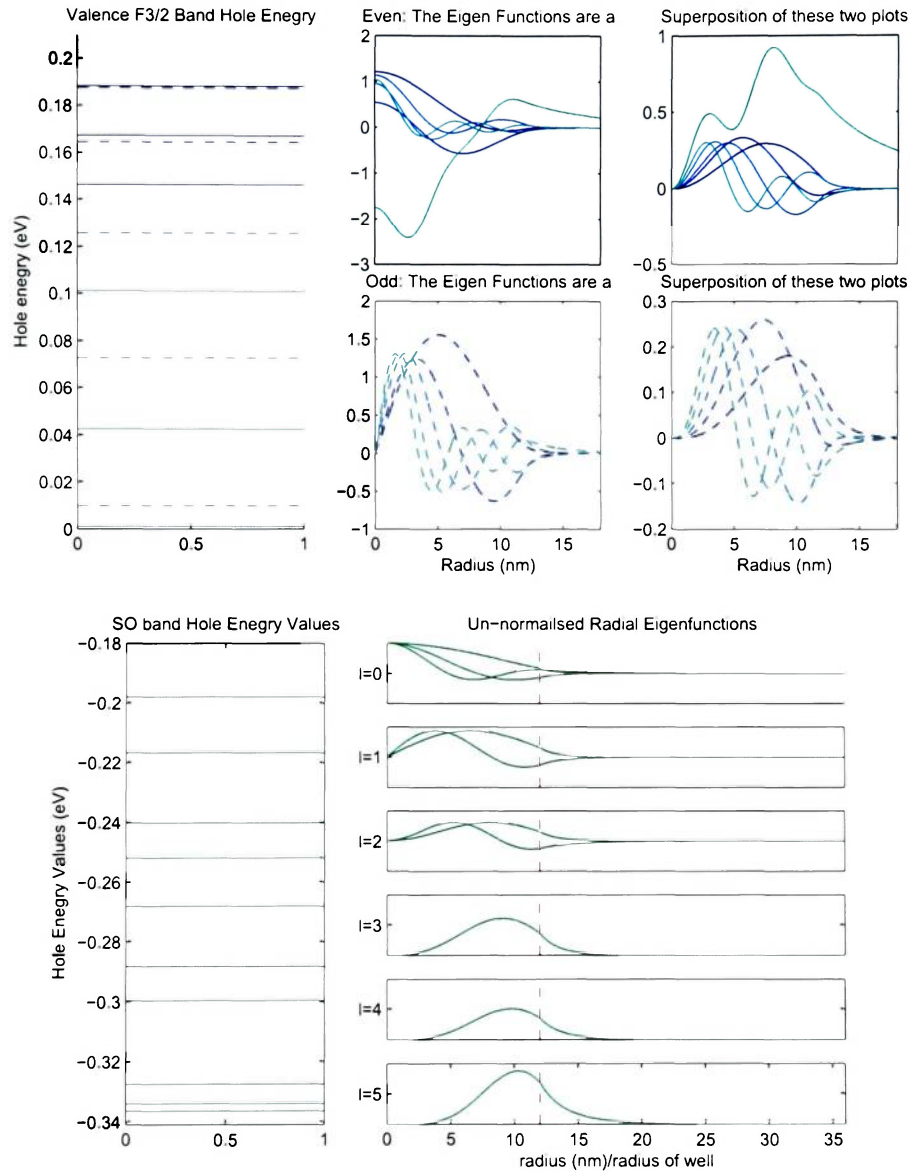
Figure 3.26: Radial eigenvectors (unnormalized) for a 12 nm dot of GaAs Embeded in AlAs ( F 3/2 band and SO band)

# GaSb Embedded in AlSb

Below we have the results from a GaSb quantum dot Embedded in AlSb, plots are shown for eigenvalues then eigenvectors for dots of 4.5 and 8 nm in radius.
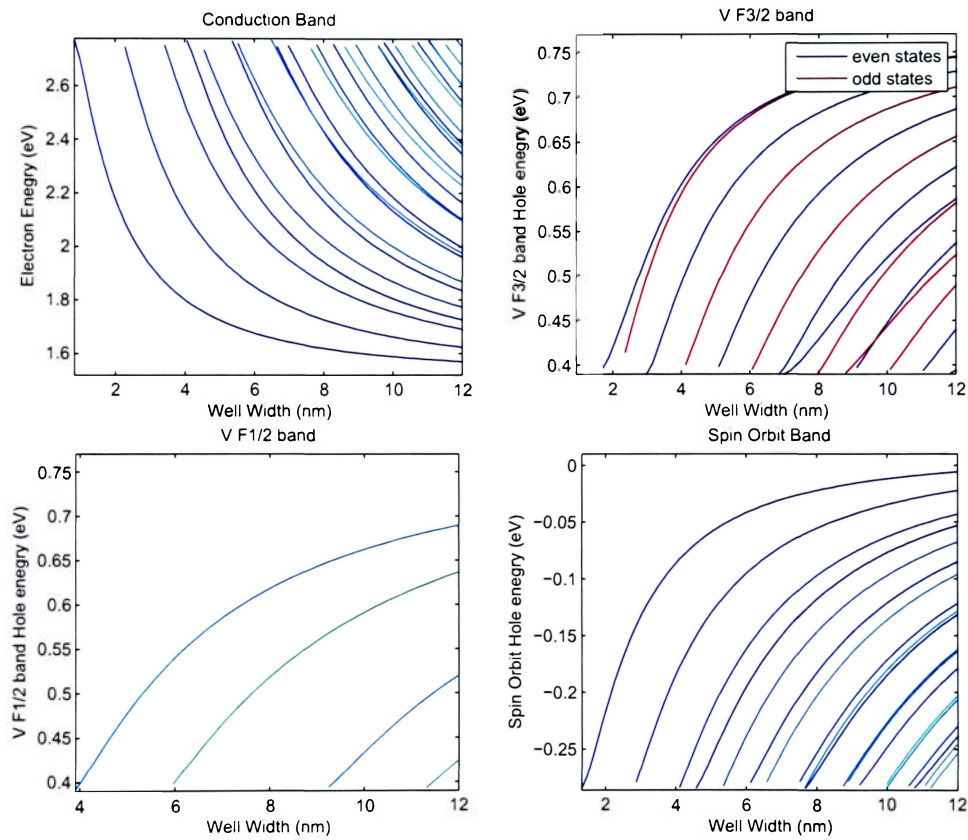


Figure 3.27: Eigenvalues as a function of dot radius for GaSb Embeded in AlSb
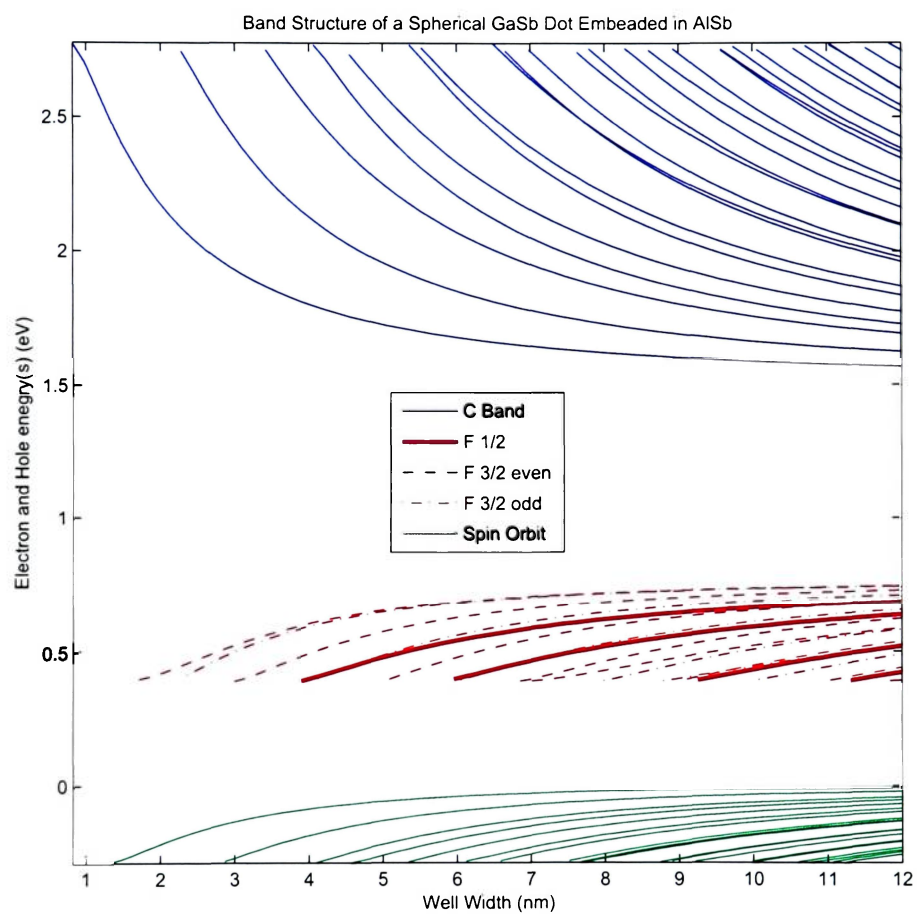
Figure 3.28: Combined plot of eigenvalues as a function of dot radius for GaSb Embeded in AlSb
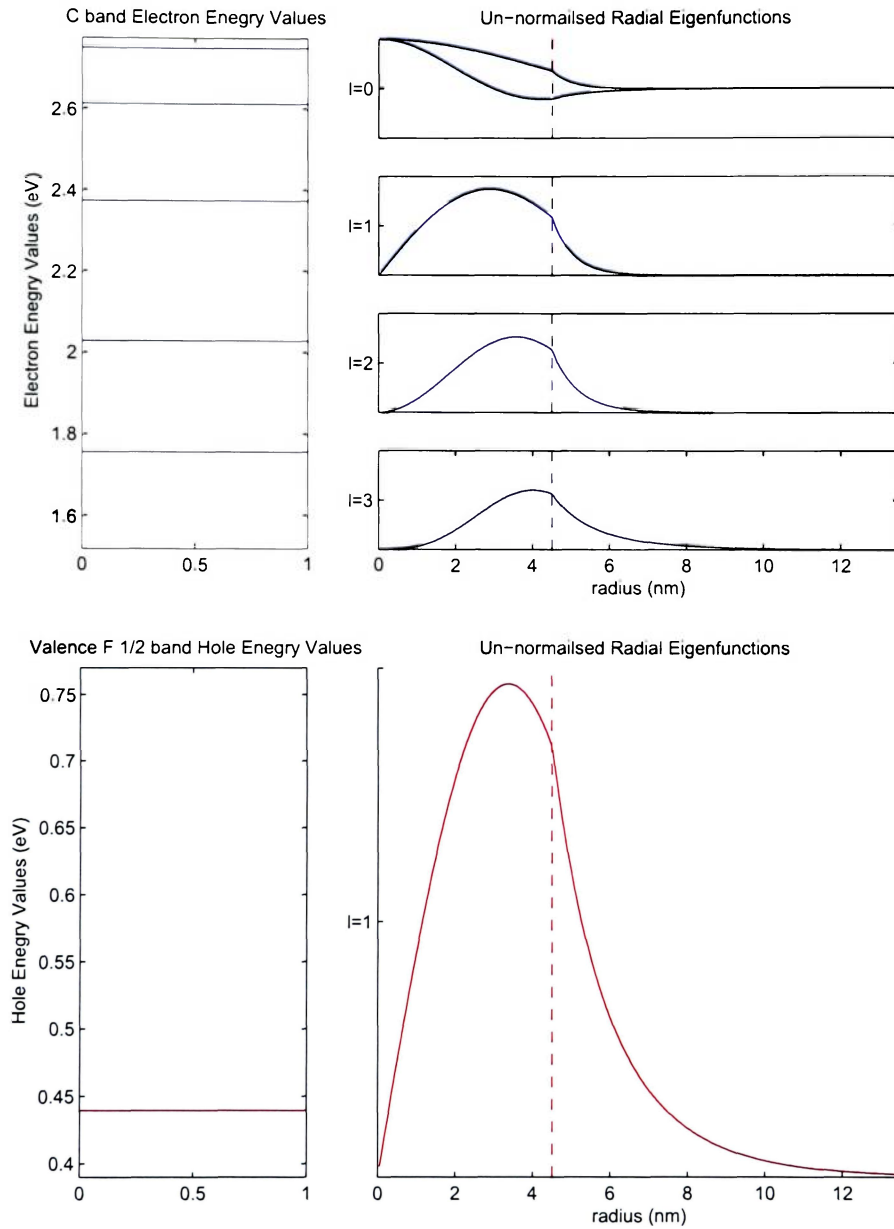
Figure 3.29: Radial eigenvectors (unnormalized) for a 4.5 nm dot of GaAs Embeded in AlAs (c band and F 1/2 band)
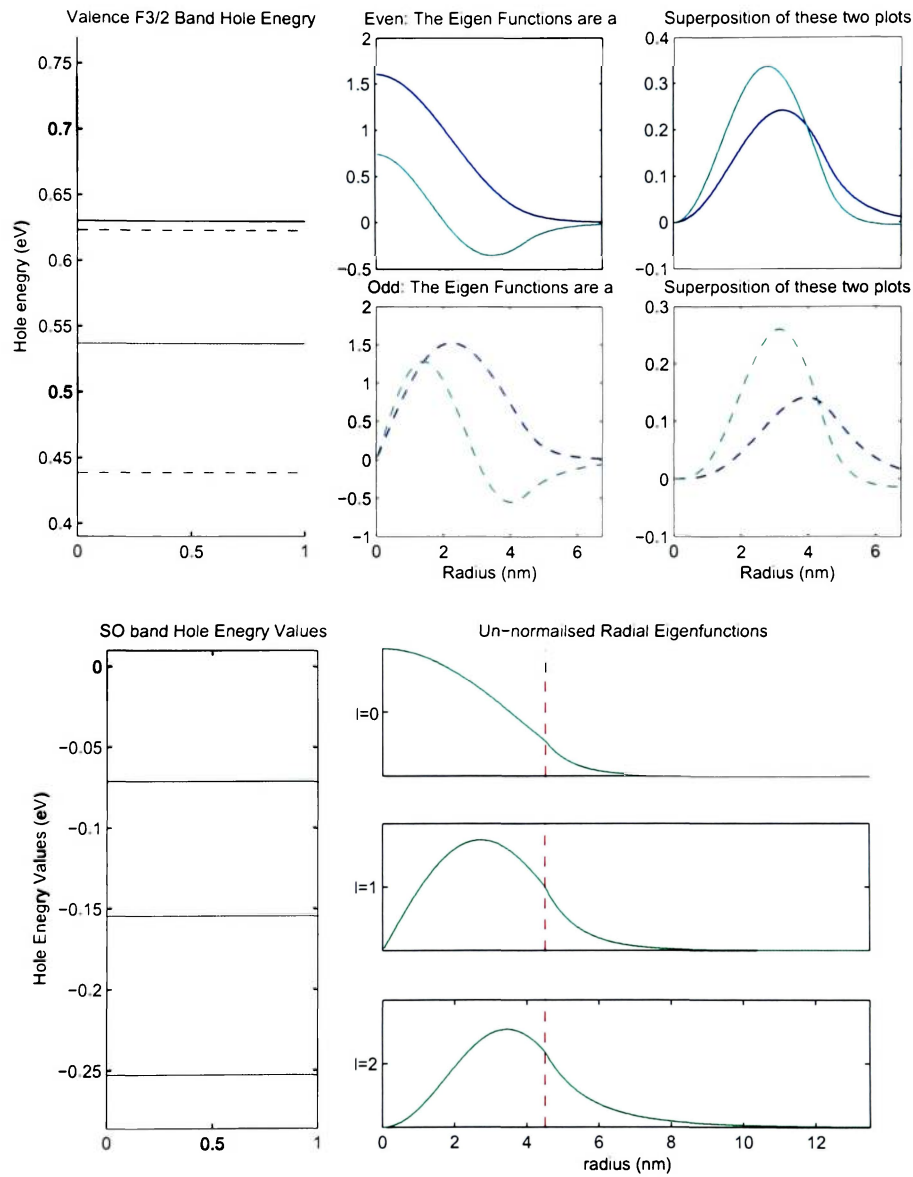
Figure 3.30: Radial eigenvectors (unnormalized) for a 4.5 nm dot of GaAs Embeded in AlAs ( F 3/2 band and SO band)
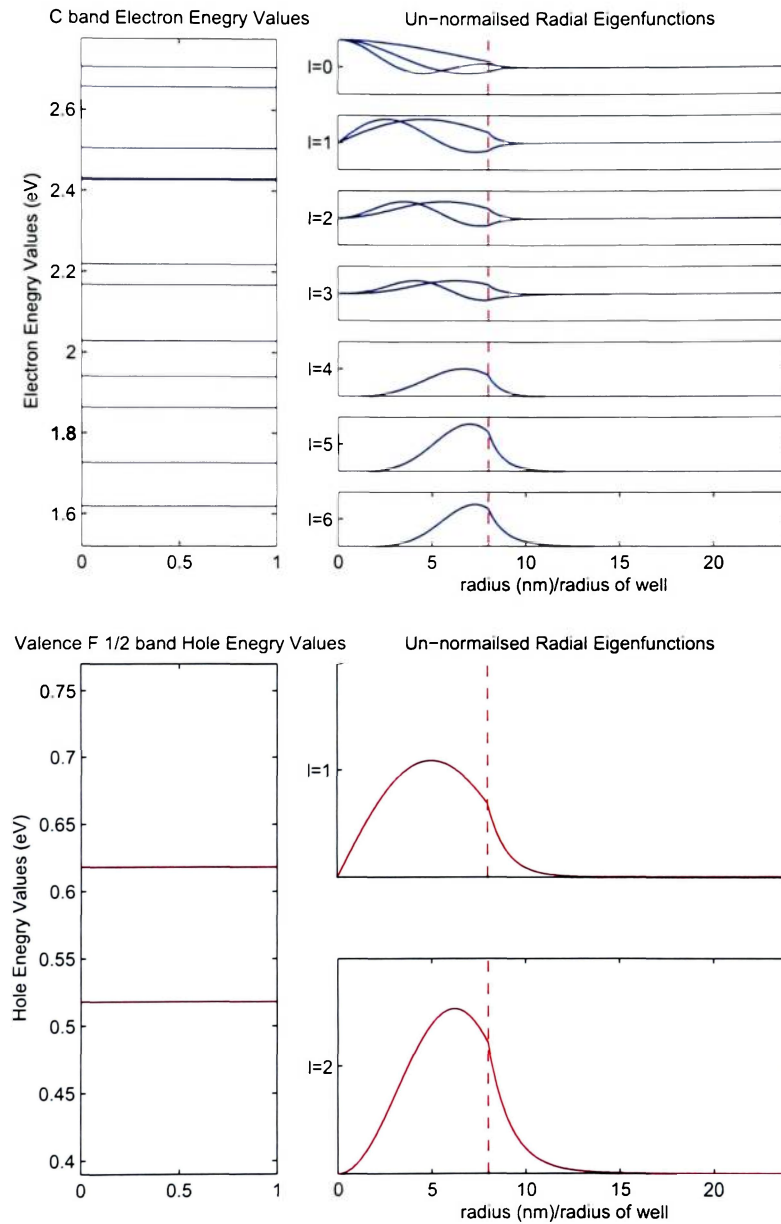
Figure 3.31: Radial eigenvectors (unnormalized) for a 4.5 nm dot of GaAs Embeded in AlAs (c band and F 1/2 band)
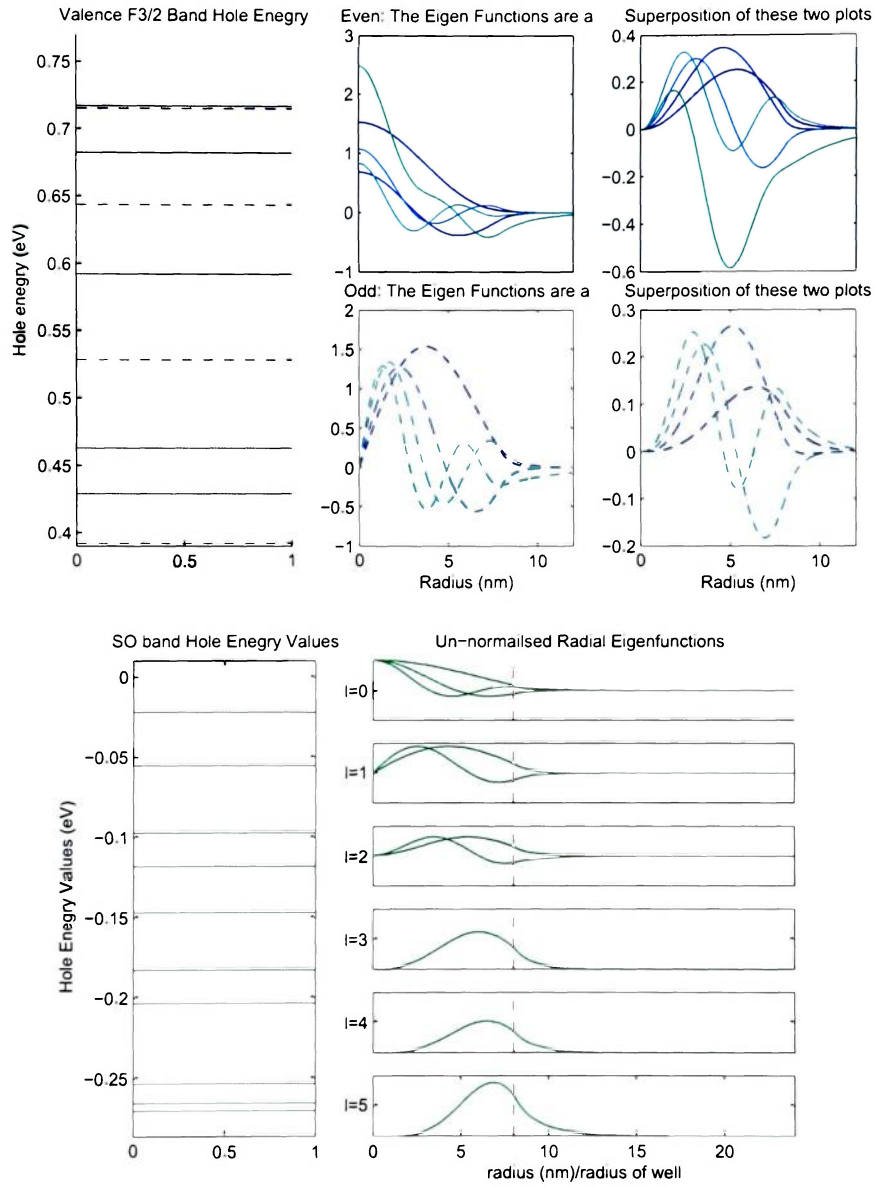
Figure 3.32: Radial eigenvectors (unnormalized) for a 4.5 nm dot of GaAs Embeded in AlAs ( F 3/2 band and SO band)

# InSb Embedded in AlSb

Below we have the results from a InSb quantum dot Embedded in AlSb, plots are shown for eigenvalues then eigenvectors for dots of 7.5 and 12 nm in radius.
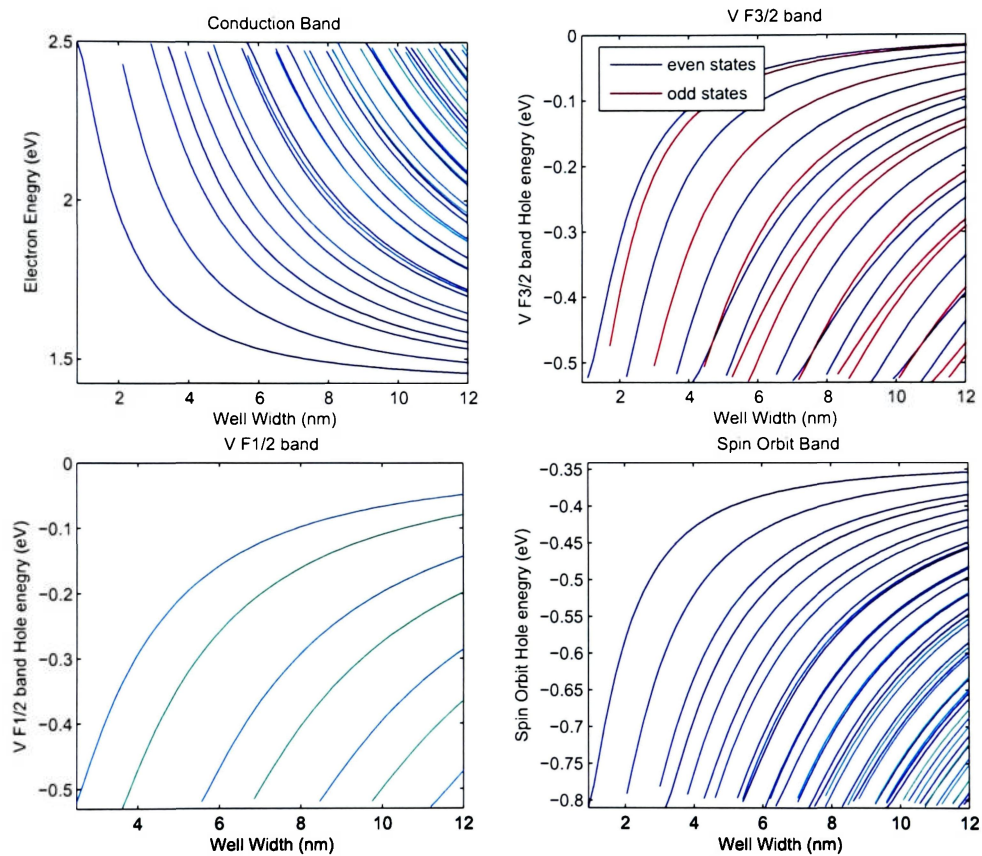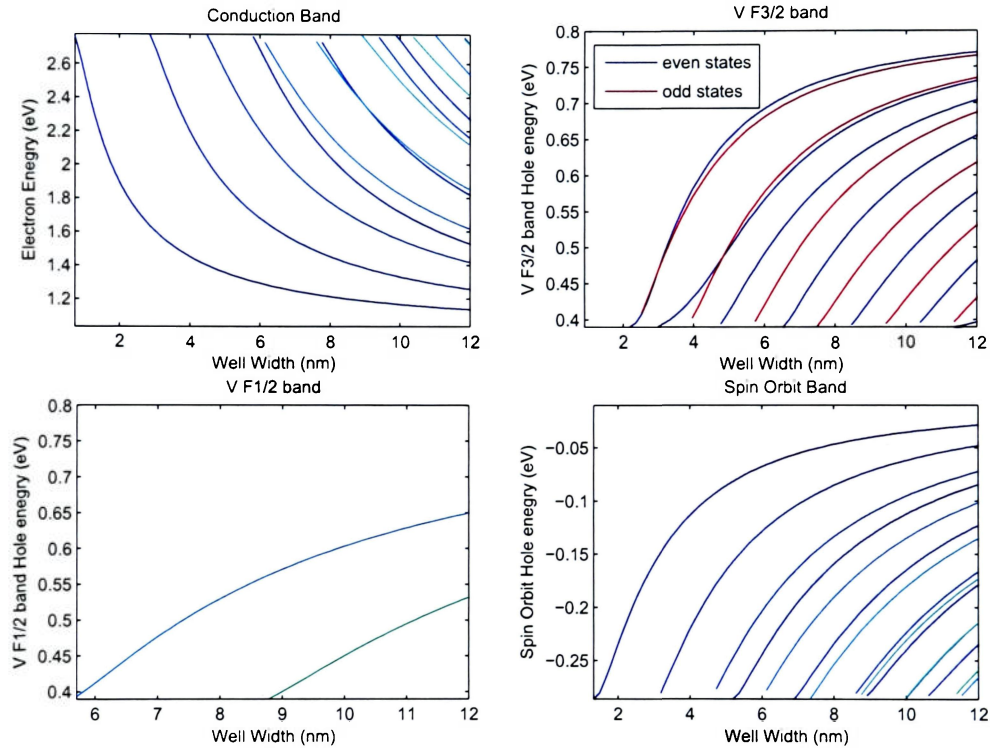


Figure 3.33: Eigenvalues as a function of dot radius for InSb Embeded in AlSb
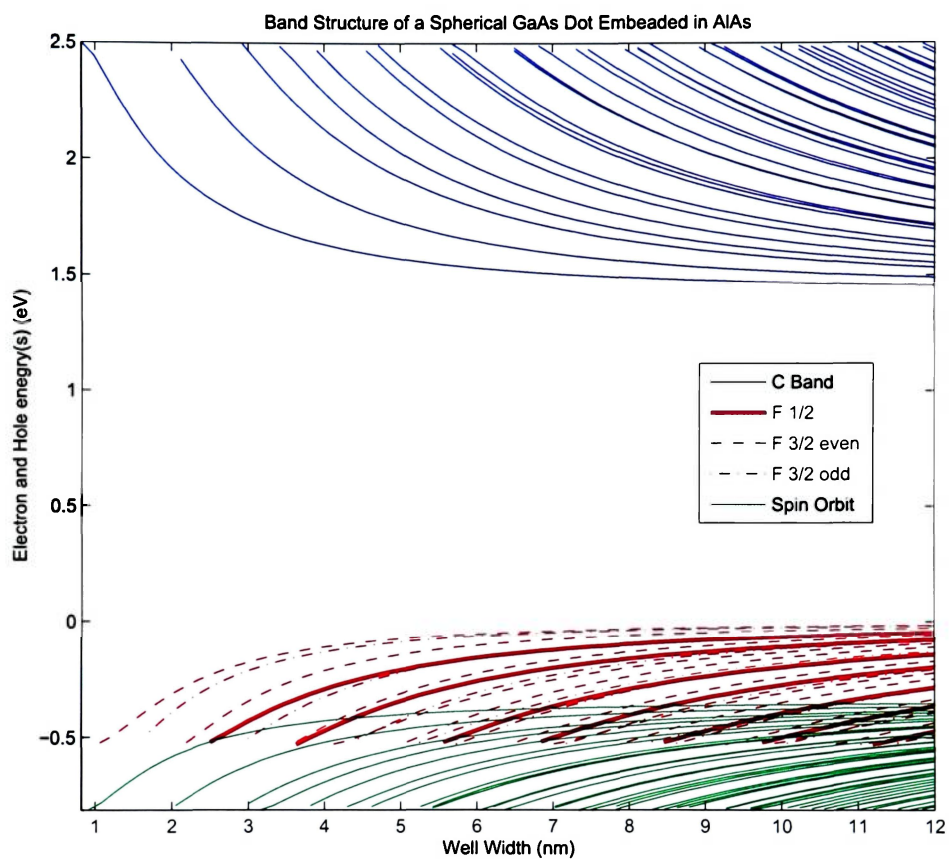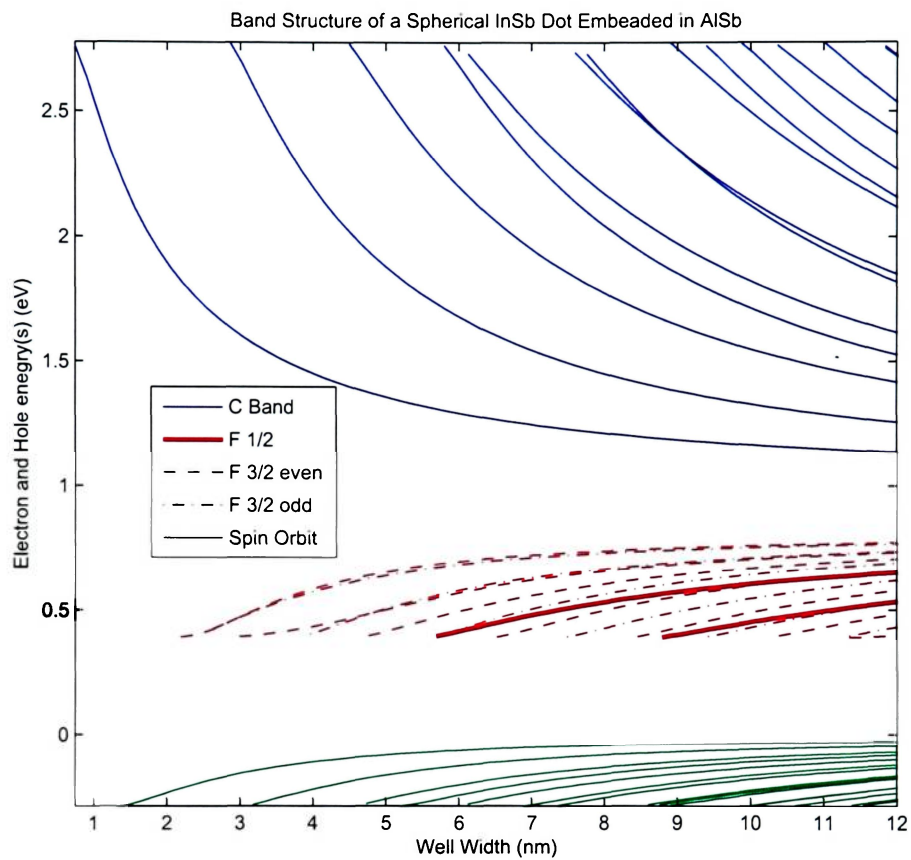
Figure 3.34: Combined plot of eigenvalues as a function of dot radius for InSb Embeded in AlSb

# Chapter 4

# Optical Properties

In the previous chapter, we developed a model for the electronic structure of a spherical quantum dot. Now we seek to further develop the Hamiltonian introduced in our model, and consider the perturbation to it caused by an external field. In particular, we will consider fields at or close to optical wavelengths, and investigate the optical transitions and absorption in quantum dots.

## 4.1 The Electron-Photon Interaction Hamiltonian

Consider a quantum dot illuminated by light. The incident photons, or oscillating electric field, will perturb the electronic states, and in some cases lead to transitions between the states [16; 10]. We include this perturbation into the model of our Hamiltonian, i.e.

$$H = H_{Model} + -\frac{e}{2m_0} \left( \vec{p} \cdot \vec{A} + \vec{A} \cdot \vec{p} \right) + \frac{e^2 A^2}{2m_0} = H_{Model} + H' \tag{4.1}$$

where $\vec{A}$ is the vector potential of the incident field. We also assume that the field is described by the Coulomb gauge condition, which means the field $\vec{A}$ has the properties

$$\nabla \cdot \vec{A} = 0 \text{ and } \vec{E} = -\frac{\partial \vec{A}}{\partial t}$$

Therefore, $\vec{A} \cdot \vec{p} = \vec{p} \cdot \vec{A}$ since $\vec{p} = -i\hbar\nabla$. If $\left|e\vec{A}\right| \ll |\vec{p}|$, which is the case for most practical optical field intensities, then $e^2 A^2/2m_0$ is negligible. With these assumptions, $H'$ becomes

$$H' \approx -\frac{e}{m_0}\vec{A} \cdot \vec{p} \tag{4.2}$$

Hence, the interaction Hamiltonian is referred to as the $A \cdot P$ *Hamiltonian*. Assuming a plain-wave magnetic field, the vector potential for the optical electric field takes the form

$$
\begin{aligned}
\vec{A} &= \hat{e} A_0 \cos\left(k_{op} \cdot r - \omega t\right) \\
&= = \hat{e}\frac{A_0}{2} e^{i k_{op} \, r} e^{-i\omega t} + \hat{e}\frac{A_0}{2} e^{-i k_{op} \, r} e^{+i\omega t}
\end{aligned}
$$

where $\vec{k}_{op}$ is the optical wave vector, which points in the propagation direction of the electromagnetic field. $\omega$ is the optical angular frequency and $\hat{e}$ is the polarization direction of the electric field. Now, the interaction Hamiltonian can be written as

$$
\begin{aligned}
H' &= -\frac{e}{m_0}\vec{A}(\vec{r}, t) \cdot \vec{p} \\
&= H'(\vec{r}) e^{-i\omega t} + H'^{\dagger}(\vec{r}) e^{+i\omega t}
\end{aligned}
$$

where

$$H'(\vec{r}) = -\frac{e A_0 e^{i k_{op} \, \vec{r}}}{2m_0}\hat{e} \cdot \vec{p} \tag{4.3}$$

## 4.1.1 Optical Transitions due to Electron-Photon Interaction

Using the perturbation Hamiltonian from equation 4.3, we now consider the transition rate of an electron in the valence band which absorbs a photon and is promoted to the conduction band. The transition rate can be found by using first order time-dependent perturbation theory [10, 25, 16, 18], described in section 1.4. Using the first half of equation 1.5–which corresponds to the absorption of a photon–the total upward transition rate is (per unit volume per second)

$$R_{v \to c} = \frac{1}{V} \sum_c \sum_v \frac{2\pi}{\hbar} \left|H'_{cv}(\vec{r})\right|^2 \delta(E_c - E_v - \hbar\omega)f_v \cdot (1 - f_c) \tag{4.4}$$

where

$$f_c = \frac{1}{1 + e^{\left(E_c - E_f\right)/k_B T}} \quad \text{and} \quad f_v = \frac{1}{1 + e^{\left(E_v - E_f\right)/k_B T}}$$

Here, we use $c$ and $v$ to indicate a summation over all conduction band states and all valence band states[1], V is the volume[2]; $f_v$ is the Fermi Dirac distribution for electrons in the valence band (section 1.2). This distribution gives the probability that an electron of a particular energy, $E_v$, exists. Similarly, $(1 - f_c)$ is the probability that a hole in the conduction band exists (see section 1.2). The matrix element $H'_{cv}$ is defined by

$$H'_{cv} \equiv \langle \psi_c | H'(\vec{r}) | \psi_v \rangle = \int \psi_c^* H'(\vec{r}) \psi_v d^3 r$$

In equation 4.4, we have used the Dirac delta function, which ignores the finite lifetime of the electronic states. A more realistic approach is to consider a Lorentizan-line-shape function which takes into account some scattering process that lead to homogeneous broadening. The line-shape function is defined as

$$\delta \left( E_c - E_v - \hbar \omega \right) \rightarrow \mathcal{L} \left( E_c - E_v - \hbar \omega \right) = \frac{\gamma / \pi}{\gamma^2 + \left( E_c - E_v - \hbar \omega \right)^2}$$

where $2\gamma$ represents the Full Width Half Maximum (FWHM or line width) of the function, in eV. Note that the line shape function has units of $1/eV$, and we have normalized it by insuring that $\int_{-\infty}^{\infty} \mathcal{L} d(\hbar \omega) = 1$. Ultimately, $\gamma$ must be found experimentally but for our purposes we take $\gamma = 15$ meV which is of the order of those used by [10, 28]. The line-shape function has an even symmetry about its maximum, therefore $\mathcal{L}(x) = \mathcal{L}(-x)$.

$R_{v \rightarrow c}$ gives the total upward transition rate; however, in the presence of the same field, there will also be a downward transition rate of

$$R_{c \rightarrow v} = \frac{1}{V} \sum_v \sum_c \frac{2\pi}{\hbar} \left| H_{vc}'^\dagger(\vec{r}) \right|^2 \mathcal{L}(E_v - E_c + \hbar \omega) f_c \cdot (1 - f_v)$$

---

[1]Not to be confused with the notation for band edges in the previous chapter.

[2]For our purposes the volume can be considered as the volume of the dot with some buffer factored in for the substrate material, or when considering an array of dots (in layers) one can consider the number of dots per unit area divided by the thickness of the layer.

The net upward transition rate per unit volume, R, is given by

$$
\begin{aligned}
R &= R_{v \to c} - R_{c \to v} \\
&= \frac{1}{V} \sum_v \sum_c \frac{2\pi}{\hbar} \left| H'_{cv}(\vec{r}) \right|^2 \mathcal{L}(E_c - E_v - \hbar\omega)(f_v - f_c)
\end{aligned}
\tag{4.5}
$$

where we have used the even property of the line-shape function $\mathcal{L}(x) = \mathcal{L}(-x)$, and the hermitian property of the Hamiltonian $\left| H'_{cv} \right| = \left| H'^{\dagger}_{vc} \right|$. If we plug in equation 4.3, we obtain:

$$
R = \frac{e^2 A_0^2}{4m_0^2} \frac{1}{V} \sum_\iota \sum_c \frac{2\pi}{\hbar} \left| \langle \psi_c | e^{\imath k_{op} \vec{r}} \hat{e} \cdot \vec{p} | \psi_v \rangle \right|^2 \mathcal{L}(E_c - E_v - \hbar\omega)(f_v - f_c)
\tag{4.6}
$$

Equation 4.6 gives the net upward transition rate. In our model, we consider three valence band manifolds. Each of the $F_{1/2}$ band, confined states, is two fold degenerate ($F_z = \pm 1/2$); the $F_{3/2}$ band states possess quadrupole degeneracy ($F_z = \pm 1/2, \pm 3/2$); and the spin-orbit band states are degenerate with respect to their two Bloch states $\left| \frac{1}{2}, \pm\frac{1}{2} \right\rangle$ and further degenerate with respect $L_z^{(s\,o)} = \{ -L^{(s\,o)}, \cdots, L^{(s\,o)} \}$. Each of these bands must be treated separately, and summed over the degenerate conduction band states which have an identical degeneracy to the spin orbit band. For clarity, we first separate equation 4.6 into separate bands

$$
\begin{aligned}
R &= \frac{\pi}{\hbar} \frac{e^2 A_0^2}{2m_0^2} \frac{1}{V} \sum_{C_{band}} \Bigg[ \sum_{F_{1/2}} \left| \langle \psi_c | e^{\imath k_{op} \vec{r}} \hat{e} \cdot \vec{p} \left| \psi_{F_{1/2}} \right\rangle \right|^2 \mathcal{L}(E_c - E_{F_{1/2}} - \hbar\omega)(f_{v_{F_{1/2}}} - f_c) \\
&+ \sum_{F_{3/2}} \left| \langle \psi_c | e^{\imath k_{op} \vec{r}} \hat{e} \cdot \vec{p} \left| \psi_{F_{3/2}} \right\rangle \right|^2 \mathcal{L}(E_c - E_{v_{F_{3/2}}} - \hbar\omega)(f_{v_{F_{3/2}}} - f_c) \\
&+ \sum_{SO_{Band}} \left| \langle \psi_c | e^{\imath k_{op} \vec{r}} \hat{e} \cdot \vec{p} | \psi_{SO} \rangle \right|^2 \mathcal{L}(E_c - E_{SO} - \hbar\omega)(f_{SO} - f_c) \Bigg]
\end{aligned}
$$

Taking into account degeneracy of the bands mentioned above

$$R(\hbar\omega) = \frac{\pi}{\hbar}\frac{e^2 A_0^2}{2m_0^2}\frac{1}{V}\sum_{L^{(c)}}\sum_{n_{c(c)}}\sum_{L_z=-L^{(c)}}^{L^{(C)}}\sum_{|iS,\uparrow\rangle,|iS,\downarrow\rangle} \tag{4.7}$$

$$\left[\sum_{F_z=-\frac{1}{2}}^{1/2}\sum_{L^{(F_{1/2})}=1}^{2}\sum_{n_{F_{1/2}}}\left[\left|\langle\psi_c|e^{ik_{op}\vec{r}}\hat{e}\cdot\vec{p}|\psi_{F_{1/2}}\rangle\right|^2\mathcal{L}(E_c-E_{F_{1/2}}-\hbar\omega)(f_{F_{1/2}}-f_c)\right]\right.$$

$$+\sum_{F_z=-\frac{3}{2}}^{3/2}\sum_{Even,Odd}\sum_{n_{F_{3/2}}}\left[\left|\langle\psi_c|e^{ik_{op}\vec{r}}\hat{e}\cdot\vec{p}|\psi_{F_{3/2}}\rangle\right|^2\mathcal{L}(E_c-E_{F_{3/2}}-\hbar\omega)(f_{F_{3/2}}-f_c)\right]$$

$$+\left.\sum_{L^{(so)}}\sum_{n_{so}}\sum_{L_z^{(so)}=-L^{(so)}}^{L^{(so)}}\sum_{|\frac{1}{2},\pm\frac{1}{2}\rangle}\left[\left|\langle\psi_c|e^{ik_{op}\vec{r}}\hat{e}\cdot\vec{p}|\psi_{SO}\rangle\right|^2\mathcal{L}(E_c-E_{SO}-\hbar\omega)(f_{SO}-f_c)\right]\right]$$

where

$$|\psi_c\rangle = \left|L^{(c)},L_z\right\rangle|J,J_z\rangle = |n_c\rangle\left|L^{(c)},L_z\right\rangle|iS,\uparrow \text{ or } \downarrow\rangle$$

$$\left|\psi_{F_{\frac{1}{2},\pm\frac{1}{2}}}\right\rangle = |F,F_z,J,L\rangle = \left|n_{F_{\frac{1}{2}}}\right\rangle\left|\frac{1}{2},\pm\frac{1}{2},\frac{3}{2},1 \text{ or } 2\right\rangle$$

$$\left|\psi^{(Even)}_{F_{\frac{3}{2},\pm\frac{1}{2}} \text{ or } \pm\frac{3}{2}}\right\rangle = |F,F_z,J,L\rangle = \left|n_{F_{\frac{3}{2}}}\right\rangle\left[\left|\frac{3}{2},\pm\frac{1}{2}\text{or}\pm\frac{3}{2},\frac{3}{2},0\right\rangle+\left|\frac{3}{2},\pm\frac{1}{2}\text{or}\pm\frac{3}{2},\frac{3}{2},2\right\rangle\right]$$

$$\left|\psi^{(odd)}_{F_{\frac{3}{2},\pm\frac{1}{2}} \text{ or } \pm\frac{3}{2}}\right\rangle = |F,F_z,J,L\rangle = \left|n_{F_{\frac{3}{2}}}\right\rangle\left[\left|\frac{3}{2},\pm\frac{1}{2}\text{or}\pm\frac{3}{2},\frac{3}{2},1\right\rangle+\left|\frac{3}{2},\pm\frac{1}{2}\text{or}\pm\frac{3}{2},\frac{3}{2},3\right\rangle\right]$$

$$|\psi_{SO}\rangle = \left|L^{(so)},L_z^{(so)}\right\rangle|J,J_z\rangle = |n_{so}\rangle\left|L^{(so)},L_z^{(so)}\right\rangle\left|\frac{1}{2},\pm\frac{1}{2}\right\rangle \tag{4.8}$$

Recall from chapter 3, each quantum-number L maybe associated with multiple energy values designated by $n_i$ below (i refers to the band). That is, for each band, we get these discrete levels which arise due to quantum confinement. The importance of the $|n_i\rangle$ quantum-number becomes clearer when we convert to position representation, where they appear in the $R_{L_n}(r)$ states

$$\langle r,\theta,\phi\,|L,L_z\rangle = R_{L_n}(r)Y_L^{L_z}(\theta,\phi) \tag{4.9}$$

The radial functions, $R_{L_n}(r)$, are addressed in chapter 3, and $Y_L^{L_z}(\theta,\phi)$ denotes the normalized spherical harmonics.

Also note that we have two distinct basis, therefore we must convert one basis to the other. That is, we have a coupled basis: $|F, F_z, J, L\rangle$, for the $\left|\psi_{F_{1/2}}\right\rangle$ and $\left|\psi_{F_{3/2}}\right\rangle$ states; and an uncoupled basis $|L, L_z\rangle |J, J_z\rangle$ (defined in section 2.1) for the $|\psi_c\rangle$ and $|\psi_{so}\rangle$ states. In the next section, we address the necessary conversions.

## 4.2 Basis Transformation

Recall from section 3.3 the definition of the coupled $F, F_z$ basis as $|F, F_z, L, J\rangle$ where $\vec{F} = \vec{J} + \vec{L}$. In the last section, we pointed out that we must express this coupled basis in terms of uncoupled basis. Using the standard angular-momentum-addition rules, [29], we get equation 4.10

$$|F, F_z, J, L\rangle = \sum_{L_z=-L}^{L} \sum_{J_z=-J}^{J} \left( \begin{array}{ccc} F & J & L \\ F_z & J_z & L_z \end{array} \right)_{cg} |L, L_z\rangle \otimes |J, J_z\rangle \qquad (4.10)$$

where the cg subscript refers to the Clebsch Gordan coefficient. For completeness, we also point out that $|L, L_z\rangle$ is short hand for $|K, L, L_z\rangle$ where K is usually left out because the Hamiltonian is diagonal with respect to K, and the calculations are done at a given K. Rather than computing the Clebsch Gordan coefficients within our Matlab program, we calculate them ahead of time in Mathematica with the command ClebschGordan[$\{J, J_z\}$,$\{L, L_z\}$,$\{F, F_z\}$]. For more details on how the Clebsch Gordan coefficients are formulated and evaluated, one should consult an advanced quantum mechanics book, such as Edmond's book [29].

### 4.2.1 $F_{1/2}$ Space

In the $F = 1/2$ space, we have two separate valence band manifolds, with $L = 1$ and $L = 2$ values. The states in each of these manifolds has a double degeneracy from $F_z = \pm 1/2$. In terms of the uncoupled basis, using equation 4.10, we have

$$\left|\frac{1}{2}, +\frac{1}{2}, \frac{3}{2}, 1\right\rangle = \frac{1}{\sqrt{2}}|1, -1\rangle\left|\frac{3}{2}, \frac{3}{2}\right\rangle - \frac{1}{\sqrt{3}}|1, 0\rangle\left|\frac{3}{2}, \frac{1}{2}\right\rangle + \frac{1}{\sqrt{6}}|1, 1\rangle\left|\frac{3}{2}, -\frac{1}{2}\right\rangle$$

$$\left|\frac{1}{2}, -\frac{1}{2}, \frac{3}{2}, 1\right\rangle = \frac{1}{\sqrt{6}}|1, -1\rangle\left|\frac{3}{2}, \frac{1}{2}\right\rangle - \frac{1}{\sqrt{3}}|1, 0\rangle\left|\frac{3}{2}, -\frac{1}{2}\right\rangle + \frac{1}{\sqrt{2}}|1, 1\rangle\left|\frac{3}{2}, -\frac{3}{2}\right\rangle$$

$$\left|\frac{1}{2}, +\frac{1}{2}, \frac{3}{2}, 2\right\rangle = -\frac{1}{\sqrt{10}}|2, -1\rangle\left|\frac{3}{2}, \frac{3}{2}\right\rangle + \frac{1}{\sqrt{5}}|2, 0\rangle\left|\frac{3}{2}, \frac{1}{2}\right\rangle - \sqrt{\frac{3}{10}}|2, 1\rangle\left|\frac{3}{2}, -\frac{1}{2}\right\rangle$$

$$+ \sqrt{\frac{2}{5}}|2, 2\rangle\left|\frac{3}{2}, -\frac{3}{2}\right\rangle \tag{4.11}$$

$$\left|\frac{1}{2}, -\frac{1}{2}, \frac{3}{2}, 2\right\rangle = -\sqrt{\frac{2}{5}}|2, -2\rangle\left|\frac{3}{2}, \frac{3}{2}\right\rangle + \sqrt{\frac{3}{10}}|2, -1\rangle\left|\frac{3}{2}, \frac{1}{2}\right\rangle - \frac{1}{\sqrt{5}}|2, 0\rangle\left|\frac{3}{2}, -\frac{1}{2}\right\rangle$$

$$+ \frac{1}{\sqrt{10}}|2, 1\rangle\left|\frac{3}{2}, -\frac{3}{2}\right\rangle$$

### 4.2.2   $F_{3/2}$ Space

The $F = 3/2$ space also has two valence band manifolds, $\left\{\left|\psi_{F_{3/2}}^{(Even)}\right\rangle\right\}$ and $\left\{\left|\psi_{F_{3/2}}^{(Odd)}\right\rangle\right\}$. The even manifold consists of a superposition of the $L = 0$ and $L = 2$ states.[3] Similarly, the odd manifold consists of a superposition of the $L = 1$ and $L = 3$ states (as defined in section 3.3 and equation 4.8). This gives 4 different sub-spaces, from the 4 possible values for L in the $F = 3/2$ space; and these four spaces have a four-fold degeneracy from $F_z$:

$$\left|\frac{3}{2}, +\frac{3}{2}, \frac{3}{2}, 0\right\rangle; \qquad \left|\frac{3}{2}, +\frac{3}{2}, \frac{3}{2}, 1\right\rangle; \qquad \left|\frac{3}{2}, +\frac{3}{2}, \frac{3}{2}, 2\right\rangle; \qquad \left|\frac{3}{2}, +\frac{3}{2}, \frac{3}{2}, 3\right\rangle$$

$$\left|\frac{3}{2}, +\frac{1}{2}, \frac{3}{2}, 0\right\rangle; \qquad \left|\frac{3}{2}, +\frac{1}{2}, \frac{3}{2}, 1\right\rangle; \qquad \left|\frac{3}{2}, +\frac{1}{2}, \frac{3}{2}, 2\right\rangle; \qquad \left|\frac{3}{2}, +\frac{1}{2}, \frac{3}{2}, 3\right\rangle$$

$$\left|\frac{3}{2}, -\frac{1}{2}, \frac{3}{2}, 0\right\rangle; \qquad \left|\frac{3}{2}, -\frac{1}{2}, \frac{3}{2}, 1\right\rangle; \qquad \left|\frac{3}{2}, -\frac{1}{2}, \frac{3}{2}, 2\right\rangle; \qquad \left|\frac{3}{2}, -\frac{1}{2}, \frac{3}{2}, 3\right\rangle$$

$$\left|\frac{3}{2}, \frac{-3}{2}, \frac{3}{2}, 0\right\rangle; \qquad \left|\frac{3}{2}, \frac{-3}{2}, \frac{3}{2}, 1\right\rangle; \qquad \left|\frac{3}{2}, \frac{-3}{2}, \frac{3}{2}, 2\right\rangle; \qquad \left|\frac{3}{2}, \frac{-3}{2}, \frac{3}{2}, 3\right\rangle$$

---

[3] Note that, due to confinement, there are potentially multiple $n$ values for the superposition states.

Using equation 4.10, for $L = 0$ we simply have

$$\left|\frac{3}{2}, +\frac{3}{2}, \frac{3}{2}, 0\right\rangle = |0,0\rangle \left|\frac{3}{2}, \frac{3}{2}\right\rangle$$

$$\left|\frac{3}{2}, +\frac{1}{2}, \frac{3}{2}, 0\right\rangle = |0,0\rangle \left|\frac{3}{2}, \frac{1}{2}\right\rangle$$

$$\left|\frac{3}{2}, -\frac{1}{2}, \frac{3}{2}, 0\right\rangle = |0,0\rangle \left|\frac{3}{2}, -\frac{1}{2}\right\rangle$$

$$\left|\frac{3}{2}, \frac{-3}{2}, \frac{3}{2}, 0\right\rangle = |0,0\rangle \left|\frac{3}{2}, -\frac{3}{2}\right\rangle$$

Next, for $L = 1$ we have

$$\left|\frac{3}{2}, +\frac{3}{2}, \frac{3}{2}, 1\right\rangle = -\sqrt{\frac{3}{5}} |1,0\rangle \left|\frac{3}{2}, \frac{3}{2}\right\rangle + \sqrt{\frac{2}{5}} |1,1\rangle \left|\frac{3}{2}, \frac{1}{2}\right\rangle$$

$$\left|\frac{3}{2}, +\frac{1}{2}, \frac{3}{2}, 1\right\rangle = -\sqrt{\frac{2}{5}} |1,-1\rangle \left|\frac{3}{2}, \frac{3}{2}\right\rangle - \sqrt{\frac{1}{15}} |1,0\rangle \left|\frac{3}{2}, \frac{1}{2}\right\rangle + 2\sqrt{\frac{2}{15}} |1,1\rangle \left|\frac{3}{2}, -\frac{1}{2}\right\rangle$$

$$\left|\frac{3}{2}, -\frac{1}{2}, \frac{3}{2}, 1\right\rangle = -2\sqrt{\frac{2}{15}} |1,-1\rangle \left|\frac{3}{2}, \frac{1}{2}\right\rangle + \sqrt{\frac{1}{15}} |1,0\rangle \left|\frac{3}{2}, -\frac{1}{2}\right\rangle + \sqrt{\frac{2}{5}} |1,1\rangle \left|\frac{3}{2}, -\frac{3}{2}\right\rangle$$

$$\left|\frac{3}{2}, \frac{-3}{2}, \frac{3}{2}, 1\right\rangle = -\sqrt{\frac{2}{5}} |1,-1\rangle \left|\frac{3}{2}, -\frac{1}{2}\right\rangle + \sqrt{\frac{3}{5}} |1,0\rangle \left|\frac{3}{2}, -\frac{3}{2}\right\rangle$$

For $L = 2$ we have

$$\left|\frac{3}{2}, +\frac{3}{2}, \frac{3}{2}, 2\right\rangle = \sqrt{\frac{1}{5}} |2,0\rangle \left|\frac{3}{2}, \frac{3}{2}\right\rangle - \sqrt{\frac{2}{5}} |2,1\rangle \left|\frac{3}{2}, \frac{1}{2}\right\rangle + \sqrt{\frac{2}{5}} |2,2\rangle \left|\frac{3}{2}, -\frac{1}{2}\right\rangle$$

$$\left|\frac{3}{2}, +\frac{1}{2}, \frac{3}{2}, 2\right\rangle = \sqrt{\frac{2}{5}} |2,-1\rangle \left|\frac{3}{2}, \frac{3}{2}\right\rangle - \sqrt{\frac{1}{5}} |2,0\rangle \left|\frac{3}{2}, \frac{1}{2}\right\rangle + \sqrt{\frac{2}{5}} |2,2\rangle \left|\frac{3}{2}, -\frac{3}{2}\right\rangle$$

$$\left|\frac{3}{2}, -\frac{1}{2}, \frac{3}{2}, 2\right\rangle = \sqrt{\frac{2}{5}} |2,-2\rangle \left|\frac{3}{2}, \frac{3}{2}\right\rangle - \sqrt{\frac{1}{5}} |2,0\rangle \left|\frac{3}{2}, -\frac{1}{2}\right\rangle + \sqrt{\frac{2}{5}} |2,1\rangle \left|\frac{3}{2}, -\frac{3}{2}\right\rangle$$

$$\left|\frac{3}{2}, \frac{-3}{2}, \frac{3}{2}, 2\right\rangle = \sqrt{\frac{2}{5}} |2,-2\rangle \left|\frac{3}{2}, \frac{1}{2}\right\rangle - \sqrt{\frac{2}{5}} |2,-1\rangle \left|\frac{3}{2}, -\frac{1}{2}\right\rangle + \sqrt{\frac{1}{5}} |2,0\rangle \left|\frac{3}{2}, -\frac{3}{2}\right\rangle$$

Finally, for $L = 3$ we have

$$\left|\frac{3}{2}, +\frac{3}{2}, \frac{3}{2}, 3\right\rangle = -\frac{1}{\sqrt{35}} |3, 0\rangle \left|\frac{3}{2}, \frac{3}{2}\right\rangle + \frac{2}{\sqrt{35}} |3, 1\rangle \left|\frac{3}{2}, \frac{1}{2}\right\rangle - \sqrt{\frac{2}{7}} |3, 2\rangle \left|\frac{3}{2}, -\frac{1}{2}\right\rangle$$
$$+ \frac{2}{\sqrt{7}} |3, 3\rangle \left|\frac{3}{2}, -\frac{3}{2}\right\rangle$$

$$\left|\frac{3}{2}, +\frac{1}{2}, \frac{3}{2}, 3\right\rangle = -\frac{2}{\sqrt{35}} |3, -1\rangle \left|\frac{3}{2}, \frac{3}{2}\right\rangle + \frac{3}{\sqrt{35}} |3, 0\rangle \left|\frac{3}{2}, \frac{1}{2}\right\rangle - 2\sqrt{\frac{3}{35}} |3, 1\rangle \left|\frac{3}{2}, -\frac{1}{2}\right\rangle$$
$$+ \sqrt{\frac{2}{7}} |3, 2\rangle \left|\frac{3}{2}, -\frac{3}{2}\right\rangle$$

$$\left|\frac{3}{2}, -\frac{1}{2}, \frac{3}{2}, 3\right\rangle = -\sqrt{\frac{2}{7}} |3, -2\rangle \left|\frac{3}{2}, \frac{3}{2}\right\rangle + 2\sqrt{\frac{3}{35}} |3, -1\rangle \left|\frac{3}{2}, \frac{1}{2}\right\rangle - \frac{3}{\sqrt{35}} |3, 0\rangle \left|\frac{3}{2}, -\frac{1}{2}\right\rangle$$
$$+ \frac{2}{\sqrt{35}} |3, 1\rangle \left|\frac{3}{2}, -\frac{3}{2}\right\rangle$$

$$\left|\frac{3}{2}, -\frac{3}{2}, \frac{3}{2}, 3\right\rangle = -\frac{2}{\sqrt{7}} |3, -3\rangle \left|\frac{3}{2}, \frac{3}{2}\right\rangle + \sqrt{\frac{2}{7}} |3, -2\rangle \left|\frac{3}{2}, \frac{1}{2}\right\rangle - \frac{2}{\sqrt{35}} |3, -1\rangle \left|\frac{3}{2}, -\frac{1}{2}\right\rangle$$
$$+ \frac{1}{\sqrt{35}} |3, 0\rangle \left|\frac{3}{2}, -\frac{3}{2}\right\rangle$$

## Example: Basis expansion of $\left|\psi_{F_{\frac{3}{2}, \frac{3}{2}}}^{(Even)}\right\rangle$

In general, the valence band state should be expressed as

$$\left|\psi_{F_{\frac{3}{2}, \frac{3}{2}}}^{(Even)}\right\rangle = A \left|\frac{3}{2}, \frac{3}{2}, \frac{3}{2}, 0\right\rangle + B \left|\frac{3}{2}, +\frac{3}{2}, \frac{3}{2}, 2\right\rangle$$

where A and B must be determined numerically. For convenience, we absorb A and B into the radial component, i.e.

$$AR_{1_n}(r) \rightarrow R_{1_n} \text{ and } BR_{2_n}(r) \rightarrow R_{2_n}$$

Therefore, the expansion of the states takes the form

$$\left|\psi_{F_{\frac{3}{2},\frac{3}{2}}}^{(Even)}\right\rangle = \left|\frac{3}{2},\frac{3}{2},\frac{3}{2},0\right\rangle + \left|\frac{3}{2},+\frac{3}{2},\frac{3}{2},2\right\rangle$$

$$= |0,0\rangle\left|\frac{3}{2},\frac{3}{2}\right\rangle + \sqrt{\frac{1}{5}}|2,0\rangle\left|\frac{3}{2},\frac{3}{2}\right\rangle - \sqrt{\frac{2}{5}}|2,1\rangle\left|\frac{3}{2},\frac{1}{2}\right\rangle + \sqrt{\frac{2}{5}}|2,2\rangle\left|\frac{3}{2},-\frac{1}{2}\right\rangle$$

It is more convenient to convert to position representation, with $\langle r,\theta,\phi\,|L,L_z\rangle = R_{L_n}(r)Y_L^{L_z}(\theta,\phi)$:

$$\left|\psi_{F_{\frac{3}{2},\frac{3}{2}}}^{(Even)}\right\rangle = R_{0_n}(r)Y_0^0(\theta,\phi)\left|\frac{3}{2},\frac{3}{2}\right\rangle + \sqrt{\frac{1}{5}}R_{2_n}(r)Y_2^0(\theta,\phi)\left|\frac{3}{2},\frac{3}{2}\right\rangle$$

$$- \sqrt{\frac{2}{5}}R_{2_n}(r)Y_2^1(\theta,\phi)\left|\frac{3}{2},\frac{1}{2}\right\rangle + \sqrt{\frac{2}{5}}R_{2_n}(r)Y_2^2(\theta,\phi)\left|\frac{3}{2},-\frac{1}{2}\right\rangle \quad (4.12)$$

With the above expansions, we can now consider how to calculate the integral

$$\left\langle\psi_c\middle|e^{\imath k_{op}\cdot r}\hat{e}\cdot\vec{p}\middle|\psi_v\right\rangle$$

These integrals are usually referred to as the momentum matrix elements or optical-momentum matrix elements.

## 4.3   Momentum Matrix Elements

We now address how to compute a single matrix element[4] $\left\langle \psi_c | e^{\imath k_{op} \vec{r}} \hat{e} \ \vec{p} | \psi_v \right\rangle$  Our goal here is to separate out all the components of the integral into one of the following

$$\left\langle \psi_c | e^{\imath k_{op} \vec{r}} \hat{e} \ \vec{p} | \psi_{F_{1/2} F_z} \right\rangle = \sum_{L_z^{(v)}} \sum_{J_z^{(v)}} \begin{pmatrix} \frac{1}{2} & \frac{3}{2} & L^{(v)} \\ F_z & J_Z^{(v)} & L_Z^{(v)} \end{pmatrix}_{cg}$$

$$\left\langle L^{(c)}, L_z^{(c)} | e^{\imath k_{op} \vec{r}} | L^{(v)}, L_z^{(v)} \right\rangle \left\langle J^{(c)}, J_z^{(c)} | \hat{e} \ \vec{p} | J^{(v)}, J_z^{(v)} \right\rangle$$

$$\left\langle \psi_c | e^{\imath k_{op} \vec{r}} \hat{e} \ \vec{p} | \psi_{F_{3/2}, F_z} \right\rangle = \sum_{L_{even,odd}^{(v)}} \sum_{L_z^{(v)}} \sum_{J_z^{(v)}} \begin{pmatrix} \frac{3}{2} & \frac{3}{2} & L^{(v)} \\ F_z & J_Z^{(v)} & L_Z^{(v)} \end{pmatrix}_{cg}$$

$$\left\langle L^{(c)}, L_z^{(c)} | e^{\imath k_{op} \vec{r}} | L^{(v)}, L_z^{(v)} \right\rangle \left\langle J^{(c)}, J_z^{(c)} | \hat{e} \ \vec{p} | J^{(v)}, J_z^{(v)} \right\rangle$$

$$\left\langle \psi_c | e^{\imath k_{op} \vec{r}} \hat{e} \ \vec{p} | \psi_{so} \right\rangle = \left\langle L^{(c)}, L_z^{(c)} | e^{\imath k_{op} \vec{r}} | L^{(\imath)}, L_z^{(v)} \right\rangle \left\langle J^{(c)}, J_z^{(c)} | \hat{e} \ \vec{p} | J^{(v)}, J_z^{(v)} \right\rangle$$

(4 13)

The summations result from the expansion of a coupled basis into a superposition of the uncoupled basis states   To evaluate equation 4 13, we utilize the $\left\langle \psi_c | e^{\imath k_{op} \vec{r}} \hat{e} \ \vec{p} | \psi_{so} \right\rangle$ integral, we first expand the expression

$$\left\langle \psi_c | e^{\imath k_{op} \vec{r}} \hat{e} \ \vec{p} | \psi_{so} \right\rangle = \left\langle L^{(c)}, L_z^{(c)} \right| \left\langle J^{(c)}, J_z^{(c)} \right| e^{\imath k_{op} \vec{r}} \hat{e} \ \vec{p} \left| L^{(v)}, L_z^{(v)} \right\rangle \left| J^{(v)}, J_z^{(v)} \right\rangle \quad (4\ 14)$$

and we represent it in integral notation using

$$\left\langle L^{(c)}, L_z^{(c)} \right| \left\langle L^{(c)}, L_z^{(c)} \right| \ \rightarrow \ \phi_c^*(L^{(c)}, L_z^{(c)}) u_c^*(J^{(c)}, J_z^{(c)}) = \phi_c^*(\vec{r}) u_c^*$$

$$\left| L^{(v)}, L_z^{(v)} \right\rangle \left| J^{(v)}, J_z^{(v)} \right\rangle \ \rightarrow \ \phi_v(L^{(v)}, L_z^{(v)}) u_v(J^{(v)}, J_z^{(v)}) = \phi_v(\vec{r}) u_v$$

Next we expand the integral with the chain rule, since $\vec{p} = -\imath \hbar \nabla$   Therefore equation 4 14 becomes

---

[4]A single but complete conduction band state in terms of $n, L, L_z, J, J_z$ to a single valence band state in terms of n and summed over $L, L_z, J, J_z$ because the F=1/2 and F=3/2 states may have multiple of these due to the expansion of basis, but this is still a single valence band state  Also the F=1/2 or 3/2 states have a c g  coefficient in the expression, inside both summations

$$\langle \psi_c | e^{ik_{op} \vec{r}} \hat{e} \cdot \vec{p} | \psi_v \rangle = \int \phi_c^* u_c^* e^{ik_{op} \vec{r}} \hat{e} \cdot \vec{p} \phi_v u_v d^3\vec{r}$$

$$= \int e^{ik_{op} \vec{r}} \phi_c^* u_c^* \phi_v \hat{e} \cdot \vec{p} u_v d^3\vec{r} + \int e^{ik_{op} \vec{r}} \phi_c^* u_c^* u_v \hat{e} \cdot \vec{p} \phi_v d^3\vec{r}$$

Next we must make an important approximation: *the variation of the Bloch function, $u_{n\vec{k}}(\vec{r})$, is on the order of the unit cell, and the variation of the envelope function is on the order of the quantum dot.* As we note in section 2.1, the Bloch function is highly oscillatory on the order of the unit cell. A typical unit cell is about .5 nm, which means the Bloch function will vary on a size of about 1/2 or 1/4 of .5 nm (or smaller) The dots we consider are about 3 nm to 10 nm in radius which means a variation over the diameter of 6 nm to 20 nm. To help us understand this method of approximation, in chapter 1 we illustrated the structure of a zine blende type quantum dot. For example, in Figure 1 7 we see a quantum dot of 13 unit cells in radius. Here, we can visualize how the variation of the Bloch function, on the size of the atoms and unit cells, is much smaller than the envelope functions, which vary at about the size of the quantum dot. We illustrate this in Figure 4.1. Therefore, we consider this approximation to be acceptable. This allows us to break the integral into a summation over the unit cells, much like a Riemann sum; and we can therefore integrate the Bloch component separately along a slice of constant envelope function.

$$\langle \psi_c | e^{ik_{op} \vec{r}} \hat{e} \cdot \vec{p} | \psi_v \rangle = \sum_i \left[ \Omega e^{ik_{op} \vec{r}} \phi_c^*(\vec{r}_i) \hat{e} \cdot \vec{p} \phi_v(\vec{r}_i) \left( \frac{1}{\Omega} \int_{\Omega_i} u_c^* u_v d^3\vec{r} \right) \right]$$

$$+ \sum_i \left[ \Omega e^{ik_{op} \vec{r}} \phi_c^*(\vec{r}_i) \phi_v(\vec{r}_i) \left( \frac{1}{\Omega} \int_{\Omega_i} u_c^* \hat{e} \cdot \vec{p} u_v d^3\vec{r} \right) \right]$$
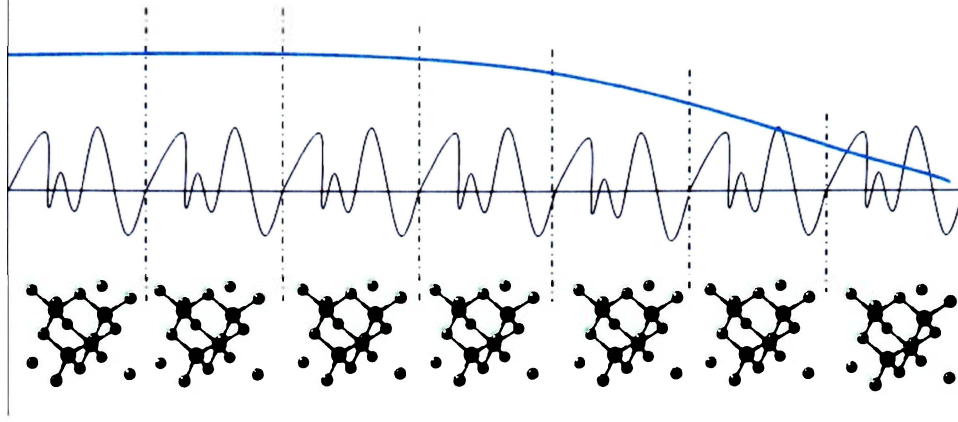
Figure 4.1: Approximating the optical momentum matrix element into a summation over all unit cells. The thick blue line represents the envelope function $F(r, \theta, \phi) = |L, L_z\rangle$, and the thin black line represents the Bloch function

where $\Omega$ is the unit cell volume. In section 2.1, we noted that the Bloch states are orthonormal. Therefore[5]

$$\int_{\Omega_i} u_c^* u_v d^3 \vec{r} = 0$$

Next, as we sum over all unit cells, the summation can be converted back to an integral and we have

$$\left\langle \psi_c | e^{ik_{op}\cdot\vec{r}} \hat{e} \cdot \vec{p} | \psi_v \right\rangle = P_{cv} \int e^{ik_{op}\cdot\vec{r}} \phi_c^* \phi_v d^3\vec{r} = P_{cv} \left\langle L^{(c)}, L_z^{(c)} | e^{ik_{op}\cdot\vec{r}} | L^{(v)}, L_z^{(v)} \right\rangle \quad (4.15)$$

where

$$P_{cv} = \int u_c^* \hat{e} \cdot \vec{p} u_v d^3\vec{r} = \left\langle J^{(c)}, J_z^{(c)} | \hat{e} \cdot \vec{p} | J^{(v)}, J_z^{(v)} \right\rangle \quad (4.16)$$

For further discussion of $P_{cv}$, see appendix section A.3. The possible values of $P_{cv}$ are summarized in table A.1.

---

[5]This is because there is no conduction valence band mixing in our model, (distant conduction band). Otherwise the integral would equal the Kronecker delta function $\delta_{cv}$

## Example: Calculation of $P_{cv}$ with $|iS, \uparrow\rangle$, $|\frac{3}{2}, \frac{3}{2}\rangle$, and $\hat{e} = \hat{e}_x$ for an InAs dot Embeded in GaAs

In this case, the incident electric field is polarized in the $\hat{e}_x$ direction We will take the electric field propagation direction to be in the $\hat{e}_z$ direction We have

$$P_{cv} = \left\langle iS, \uparrow | \hat{e}_x \ \vec{p} | \frac{3}{2}, \frac{3}{2} \right\rangle$$

using table A 1

$$P_{cv} = \hat{e}_x \ \left( -\frac{\sqrt{E_p m_0}}{2} (\hat{e}_x + i\hat{e}_y) \right) = -\frac{\sqrt{E_p m_0}}{2}$$

The parameter $E_p$ is an experimentally determined parameter, and varies for each material It is often referred to as the optical-matrix-element-parameter[6] Values for $E_p$ are given in table B 2 In the case of a quantum confined structure, we use $E_p$ values of the inside material of the quantum dot, because the contribution to the integral comes predominantly from the inside of the dot For InAs we have[7]

$$P_{cv} = -\frac{\sqrt{21\,5eV}}{2} \sqrt{m_0}$$

Some approximations ignore the $\left\langle L^{(c)}, L_z^{(c)} | e^{ik_{op} \ \vec{r}} | L^{(v)}, L_z^{(v)} \right\rangle$ component of the integral (i e $\left\langle \psi_c | e^{ik_{op} \ \vec{r}} \hat{e} \ \vec{p} | \psi_v \right\rangle = P_{cv}$ ), because the Dirac-delta approximations would make that portion of the integral unimportant, however, we include it

### 4.3.1 The Dipole Approximation

In order to numerically evaluate $\left\langle L^{(c)}, L_z^{(c)} | e^{ik_{op} \ \vec{r}} | L^{(v)}, L_z^{(v)} \right\rangle$, we can use the Gaunt method–discussed in the next section–or make the dipole approximation Due to the

---

[6]Note that if we look over our derivation, we may conclude that the optical matrix element should be independent of material This is true, but experimentally, it still varies slightly from material to material, which is why the factor (or correction) $E_p$ is utilized

[7]Note that we have left the $\sqrt{m_0}$ intact because, in our calculations this term becomes squared, factored out, and re included at the end, which makes it easier for numerical calculations

spherical symmetry of the quantum dot, we can arbitrarily assume that the incident light propagates in the z direction. Therefore,

$$\vec{k}_{op} = k_z \rightarrow e^{ik_{op}\cdot\vec{r}} = e^{ik_z r\cos(\theta)} = e^{i2\pi\frac{r}{\lambda}\cos(\theta)}$$

In integral form, we have

$$\left\langle L^{(c)}, L_z^{(c)} | e^{ik_{op}\cdot\vec{r}} | L^{(v)}, L_z^{(v)} \right\rangle = \int \left( R_{L,n}^{(c)} Y_L^{L_z} \right)^* R_{L'n'}^{(v)} Y_{L'}^{L'_z} e^{i2\pi\frac{r}{\lambda}\cos(\theta)} r^2 \sin(\theta) dr d\theta d\phi$$

$$(4.17)$$

The integral in equation 4.17 is difficult to evaluate because of the $e^{i2\pi\frac{r}{\lambda}\cos(\theta)}$ term. However, we can make the dipole approximation–that is we set $e^{i2\pi\frac{r}{\lambda}\cos(\theta)} = 1$ by assuming that $\lambda \gg r$.

$$\left\langle L^{(c)}, L_z^{(c)} | e^{ik_{op}\cdot\vec{r}} | L^{(v)}, L_z^{(v)} \right\rangle = \int \left( R_{L,n}^{(c)} Y_L^{L_z} \right)^* R_{L'n'}^{(v)} Y_{L'}^{L'_z} r^2 \sin(\theta) dr d\theta d\phi$$

$$= \int_0^\infty R_{L,n}^{(c)} R_{L'n'}^{(v)} r^2 dr \int_0^\pi \int_0^{2\pi} \left( Y_L^{L_z} \right)^* Y_{L'}^{L'_z} d\Omega$$

where $(R_{L,n}^{(c)})^* = R_{L,n}^{(c)}$ because it is known to be real, and the prime notation is used to denote the $L$ of the valence band. Using the definitions of the normalized spherical harmonic functions, $Y_L^M$, the integration over the angular components is easily done as follows:

$$\int_0^\pi \int_0^{2\pi} \left( Y_L^{L_z} \right)^* Y_{L'}^{L'_z} d\Omega = \delta_{LL'} \delta_{L_z L'_z}$$

where $\delta_{ab}$ is the Kronecker delta function, $\delta_{ab} = 0$ if $a \neq b$ and $\delta_{ab} = 1$ if $a = b$. Now, we express equation 4.17 as

$$\left\langle L^{(c)}, L_z^{(c)} | e^{ik_{op}\cdot\vec{r}} | L^{(v)}, L_z^{(v)} \right\rangle = \delta_{LL'} \delta_{L_z L'_z} \int_0^\infty R_{L,n}^{(c)} R_{L'n'}^{(v)} r^2 dr \qquad (4.18)$$

Thus, we write the optical momentum matrix element as

$$\left\langle \psi_c | e^{\imath k_{op} \cdot \vec{r}} \hat{e} \cdot \vec{p} | \psi_v \right\rangle = P_{cv} \delta_{LL'} \delta_{L_z L_z'} \int_0^\infty R_{L,n} R_{L'n'}' r^2 dr \qquad (4.19)$$

Recall that we have only considered a transition from the spin orbit band to the conduction band. However, this must be done for each term in the coupled $F_{1/2}$ and $F_{3/2}$ manifolds as in the following example.

**Example:**   Let us expand the integral $\left\langle \psi_c | e^{\imath k_{op} \cdot \vec{r}} \hat{e} \cdot \vec{p} | \psi_{F_{\frac{3}{2},\frac{3}{2}}}^{(Even)} \right\rangle$ for $|\psi_c\rangle =$ $|2,1\rangle |iS, \downarrow\rangle$ , with the dipole approximation, equation 4.19, and an electric field described by $\vec{k_{op}} = k\hat{e}_z$ and $\hat{e} = \hat{e}_x$

As in the previous example, we can represent the valence band state using equation 4.12. Expanding the integral, we obtain

$$
\begin{aligned}
\left\langle \psi_c | e^{\imath k_{op} \vec{r}} \hat{e} \cdot \vec{p} | \psi_{F_{\frac{3}{2},\frac{3}{2}}}^{(Even)} \right\rangle &= \left\langle R_{2_n}^{(c)} \left(Y_2^1\right) \right| \langle iS, \downarrow | \hat{e}_x \cdot \vec{p} | \\
&\qquad \left[ \left| R_{0_n}^{(v)} Y_0^0 \right\rangle \left|\frac{3}{2},\frac{3}{2}\right\rangle + \left| \sqrt{\frac{1}{5}} R_{2_n}^{(v)} Y_2^0 \right\rangle \left|\frac{3}{2},\frac{3}{2}\right\rangle \right. \\
&\qquad \left. - \left| \sqrt{\frac{2}{5}} R_{2_n}^{(v)} Y_2^1 \right\rangle \left|\frac{3}{2},\frac{1}{2}\right\rangle + \left| \sqrt{\frac{2}{5}} R_{2_n} Y_2^2 \right\rangle \left|\frac{3}{2},-\frac{1}{2}\right\rangle \right]
\end{aligned}
$$

Applying the dipole selection rules $L = L'$ and $L_z = L_z'$ (see equation 4.18)

$$\left\langle \psi_c | e^{\imath k_{op}\,\vec{r}}\hat{e} \;\; \vec{p} | \psi_{F_{\frac{3}{2}\,\frac{3}{2}}}^{(Even)} \right\rangle = -\left\langle R_{2n}^{(c)}\left(Y_2^1\right) \middle| \langle \imath S, \downarrow | \hat{e}_x \;\; \vec{p} \middle| \sqrt{\frac{2}{5}}R_{2n}^{(v)}Y_2^1 \right\rangle \left| \frac{3}{2},\frac{1}{2} \right\rangle$$

$$= \left\langle -R_{2n}^{(c)} \middle| \sqrt{\frac{2}{5}}R_{2n}^{(v)} \right\rangle \langle \imath S, \downarrow | \hat{e} \;\; \vec{p} \left| \frac{3}{2},\frac{1}{2} \right\rangle$$

$$= -\sqrt{\frac{2}{5}}\int_0^\infty R_{2n}^{(c)} R_{2n}^{(v)} r^2 dr \;\; \hat{e}_x \left[ -\sqrt{\frac{E_p m_0}{12}}(\hat{e}_x + \imath \hat{e}_y) \right]$$

$$= \sqrt{\frac{E_p m_0}{30}}\int_0^\infty R_{2n}^{(c)} R_{2n}^{(v)} r^2 dr$$

We have used equation 4 15 to separate the integral components, and table A 1 to evaluate $P_{cv}$  Note that the combination of dipole selection rules and expansion of the $F_{3/2}$ state with the C G  coefficients ensures that only one term of the coupled expansion remains  Thus, the dipole selection rules eliminate the need to evaluate many integrals, which is very important when we numerically implement the transitions over all states as in equation 4 7

### 4.3.2  Plain-Wave Expansion and Gaunt Coefficients

In the previous section, we made the approximation that $e^{\imath 2\pi \frac{r}{\lambda}\cos(\theta)} = 1$ by assuming that $\lambda \gg r$  However, for some of the dots we want to address–like a GaAs dot embedded in AlAs–may have excitations that correspond to visible photons[8]  Using the extreme case of $\lambda_{min} = 300 nm$ and a 15 nm dot, we get

$$\frac{2\pi r}{\lambda} \approx 3$$

---

[8]We know this from looking at the possible energies in the conduction and valence band wells $\Delta E_{min} = 1\,424 eV \Rightarrow \lambda_{max} = 870 nm$ , we can also see that $\Delta E_{max} \Rightarrow \lambda_{min} = 300 nm$

Thus, if $e^{i2\pi r \cos\theta/\lambda} \neq 1$, we must perform the angular integral numerically, and the dipole selection rules will not necessarily hold. To simplify the process, we start with the plain-wave expansion [30]

$$e^{i\vec{k}\cdot\vec{r}} = \sum_{L=0}^{\infty}\sum_{m=-L}^{L} 4\pi i^L Y_{Lm}^*(\theta_k, \phi_k) Y_{Lm}(\theta, \phi) j_L(kr)$$

where $j_l$ are spherical Bessel functions, and $\vec{k}$ is in the $\theta_k, \phi_k$ direction. Therefore,

$$\left\langle L^{(c)}, L_z^{(c)} | e^{ik_{op}\vec{r}} | L^{(v)}, L_z^{(v)} \right\rangle = \int dr d\theta d\phi \left( R_{L^{(c)},n}^{(c)} Y_{L^{(c)}}^{L_z^{(c)}} \right)^* R_{L^{(v)},n'}^{(v)} Y_{L^{(v)}}^{L_z^{(v)}} r^2 \sin(\theta)$$

$$\cdot \left( \sum_{L=0}^{\infty}\sum_{m=-L}^{L} 4\pi i^L Y_{Lm}^*(\theta_k, \phi_k) Y_{Lm}(\theta, \phi) j_L(kr) \right)$$

Combining this with the Gaunt Coefficients, we obtain

$$\left\langle L^{(c)}, L_z^{(c)} | e^{ik_{op}\cdot\vec{r}} | L^{(v)}, L_z^{(v)} \right\rangle =$$

$$\delta_{L_z^{(c)}, L_z^{(v)}} \sum_{L=|L^{(c)}-L^{(v)}|}^{L^{(c)}+L^{(v)}} \left[ (2L+1)\sqrt{(2L^{(c)}+1)(2L^{(v)}+1)} i^L \right.$$

$$\cdot (-1)^{L_z^{(c)}} \cdot \begin{pmatrix} L & L^{(c)} & L^{(v)} \\ 0 & 0 & 0 \end{pmatrix} \begin{pmatrix} L & L^{(c)} & L^{(v)} \\ 0 & -L_z^{(c)} & L_z^{(c)} \end{pmatrix}$$

$$\left. \cdot \int_0^{\infty} R_{L^{(c)},n}^{(c)} R_{L^{(v)}n'}^{(v)} j_L\left(\frac{2\pi}{\lambda}r\right) r^2 dr \right] \tag{4.20}$$

Where $\begin{pmatrix} L & L' & L'' \\ m & m' & m'' \end{pmatrix}$ is the Wigner 3-j symbol. For further discusion, see appendix section A.4. For this expression to be non zero, $L_z^{(c)} = L_z^{(v)}$, and $L + L^{(c)} + L^{(v)}$ must be an even number.[9]

---

[9]These come from properties of the Wigner 3-j symbol

The most important impact of this expansion is that we now have coupling between $L^{(c)}$ and $L^{(v)}$ states, even when $L^{(c)} \neq L^{(v)}$  Also note that $\left\langle L^{(c)}, L_z^{(c)} | e^{\imath k_{op}\ \vec{r}} | L^{(v)}, L_z^{(v)} \right\rangle$ is now $\lambda$ dependent, which is also another numerical complication  Under the dipole approximation, we essentially only have one integral when calculating the transition rate as a function $\lambda$ for a single state to another single state  However, in the more accurate solution, we see coupling which introduces more integrals, and we also see a $\lambda$ dependence, therefore we must integrate for each value of $\lambda$

## 4.4  Optical Absorption Coefficient

Now that we have discussed the calculations for the transition rate $R(\lambda)$ or $R(\hbar\omega)$, we can consider a more relevant parameter–the optical absorption coefficient  The optical absorption coefficient is the fraction of photons absorbed per unit distance into a crystal structure,

$$\alpha = \frac{\text{Number of photons absorbed per second per unit volume}}{\text{Number of photons injected per second per unit area}} \qquad (4\ 21)$$

In other words, if we have light incident on an area of a material with intensity $I$, then for a photon energy $\hbar\omega$, we have

$$\alpha(\hbar\omega) = \frac{R(\hbar\omega)}{I/\hbar\omega} \qquad (4\ 22)$$

where the transition rate, in a compact form is given by[10]

$$R(\hbar\omega) = \frac{e^2 A_0^2}{4m_0^2} \frac{2}{V} \sum_{\psi_c} \sum_{\psi_v} \frac{2\pi}{\hbar} \left| \langle \psi_c | e^{\imath k_{op}\ \vec{r}} \hat{e}\ \vec{p} | \psi_v \rangle \right|^2 \mathcal{L}(E_c - E_v - \hbar\omega)(f_v - f_c)$$

Recall that the interaction Hamiltonian, from equation 4 3, uses the vector potential

$$\vec{A} = \hat{e} A_0 \cos\left(k_{op}\ r - \omega t\right)$$

---

[10]As opposed to the expanded expression from equation 4 7

The vector potential is in Coulomb gauge; therefore, the electric and magnetic fields can be written as

$$\vec{E}(\vec{r}, t) = -\frac{\partial \vec{A}}{\partial t} = -\hat{e}A_0 \sin(k_{op} \cdot \vec{r} - \omega t)$$

$$\vec{H}(\vec{r}, t) = \frac{1}{\mu}\nabla \times \vec{A} = -\frac{1}{\mu}k_{op} \times \hat{e}A_0 \sin(k_{op} \cdot \vec{r} - \omega t)$$

From these, we can compute the Poynting vector in $W/m^2$

$$\vec{P}(\vec{r}, t) = \vec{E}(\vec{r}, t) \times \vec{H}(\vec{r}, t) = \hat{k}_{op}k\frac{\omega A_0^2}{\mu}\sin^2(k_{op} \cdot \vec{r} - \omega t)$$

Because light oscillates on the order of $10^{14}$ Hz, we can take the time average of the Poynting vector to obtain the optical intensity $I$

$$I = \left|\left\langle \vec{P}(\vec{r}, t)\right\rangle\right| = k\frac{\omega A_0^2}{2\mu} = \frac{n_r c\epsilon_0 \omega^2 A_0^2}{2}$$

Here, $n_r$ is the refractive index of the material. Therefore,

$$\alpha(\hbar\omega) = \frac{\pi e^2}{n_r c\epsilon_0 m_0^2 \omega}\frac{2}{V}\sum_{\psi_c}\sum_{\psi_v}\left|\langle\psi_c|\, e^{ik_{op}\cdot\vec{r}}\hat{e}\cdot\vec{p}\,|\psi_v\rangle\right|^2 L(E_c - E_v - \hbar\omega)(f_v - f_c) \quad (4.23)$$

We can see that the factors of $A_0$, from $R$ and $I$, cancel; therefore, under our current assumptions, the optical absorption coefficient is independent of the optical intensity (that is, we don't consider non-linear optics).

For our quantum dot model, we convert the volume V to the number of quantum dots per unit area $N_{dot}^{2D}$, for a layer with thickness $T_h$ (in meters) ($V = \frac{N_{dot}^{2D}}{T_h}$). This allows us to expand our model to an array of quantum dots (provided that we assume

no interaction between them).

$$\alpha(\hbar\omega) =$$

$$\frac{\pi e^2}{n_r c\epsilon_0 m_0^2 \omega} \frac{2N_{dot}^{2D}}{T_h} \sum_{L^{(c)}} \sum_{n_c} \sum_{L_z=-L^{(c)}}^{L^{(C)}} \sum_{|\imath S,\uparrow\rangle,|\imath S,\downarrow\rangle}$$

$$\left[ \sum_{F_z=-1/2}^{1/2} \sum_{L^{(F_{1/2})}=1}^{2} \sum_{n_{F_{1/2}}} \left[ \left| \langle \psi_c | Q | \psi_{F_{1/2}} \rangle \right|^2 \mathcal{L}(E_c - E_{F_{1/2}} - \hbar\omega)(f_{F_{1/2}} - f_c) \right] \right.$$

$$+ \sum_{F_z=-3/2}^{3/2} \sum_{Even,Odd} \sum_{n_{F_{3/2}}} \left[ \left| \langle \psi_c | Q | \psi_{F_{3/2}} \rangle \right|^2 \mathcal{L}(E_c - E_{F_{3/2}} - \hbar\omega)(f_{F_{3/2}} - f_c) \right]$$

$$+ \sum_{L^{(so)}} \sum_{n_{so}} \sum_{L_z^{(so)}=-L^{(so)}}^{L^{(so)}} \sum_{|\frac{1}{2},-\frac{1}{2}\rangle,|\frac{1}{2},\frac{1}{2}\rangle} \left[ |\langle \psi_c | Q | \psi_{SO} \rangle|^2 \mathcal{L}(E_c - E_{SO} - \hbar\omega)(f_{SO} - f_c) \right] \Bigg]$$

where $Q = e^{\imath k_{op} \vec{r}} \hat{e} \cdot \vec{p}$. To review how we would evaluate this, we first obtain the radial functions, $R_{L_N}$, from our model and then evaluate the momentum matrix elements by expanding the $F_{1/2}$ and $F_{3/2}$ coupled basis in terms of the uncoupled basis. Next, we approximate $\left\langle L^{(c)}, L_z^{(c)} \right| \left\langle J^{(c)}, J_z^{(c)} \right| e^{\imath k_{op} \vec{r}} \hat{e} \cdot \vec{p} \left| L^{(v)}, L_z^{(v)} \right\rangle \left| J^{(v)}, J_z^{(v)} \right\rangle$ as

$$\left\langle L^{(c)}, L_z^{(c)} | e^{\imath k_{op} \vec{r}} | L^{(v)}, L_z^{(v)} \right\rangle \left\langle J^{(c)}, J_z^{(c)} | \hat{e} \cdot \vec{p} | J^{(v)}, J_z^{(v)} \right\rangle = P_{cv} \left\langle L^{(c)}, L_z^{(c)} | e^{\imath k_{op} \vec{r}} | L^{(v)}, L_z^{(v)} \right\rangle$$

and evaluate each $\left\langle L^{(c)}, L_z^{(c)} | e^{\imath k_{op} \vec{r}} | L^{(v)}, L_z^{(v)} \right\rangle$ using either the dipole approximation method, or the plain-wave expansion with Gaunt coefficients method.

# 4.5 Other Considerations

We have ignored inhomogeneous broadening. When fabricating an array of quantum dots, one of the problems that arises is the dots will vary in size. Since the energy eigenvalues depend on the radius, if some of the dots in an array are smaller than the average, then a particular transition will occur at a higher energy (shorter
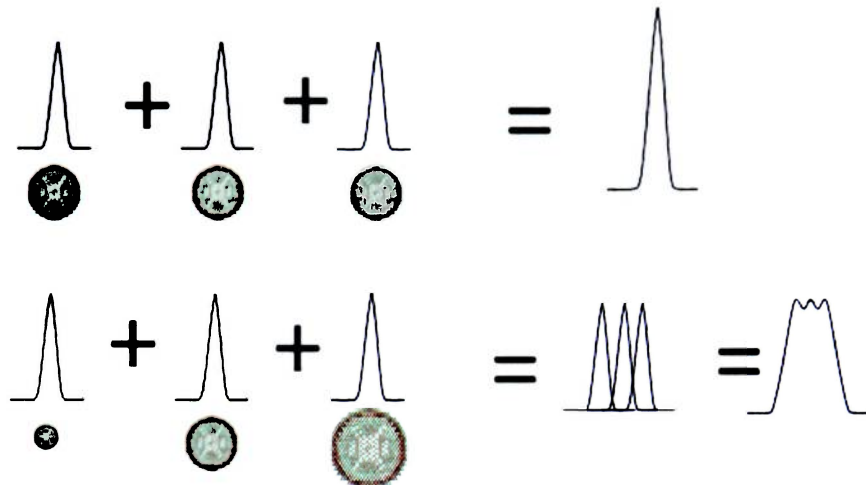
Figure 4.2: Inhomogeneous broadening example. In the first row, we have an array of three quantum dots with the exactly the same size. Thus, there is only homogeneous broadening and no inhomogeneous broadening. The second row shows the case where the three dots vary in size and therefore the absorption peaks for a given transition will vary slightly, which results in a total absorption with a shorter and wider peak.

wavelength). On the other hand. the larger than average dots would have the corresponding transition at a lower energy. Therefore, the average stays the same but the transition amplitude becomes shorter and wider. An example of this is shown in Figure 4.2.

We have also neglected some lesser effects in our discussion, such as spontaneous emission, bi-exciton effects, and intersubband transitions/absorption. Spontaneous emission would cause a slight decrease in the net upward transition rate. Intersubband means transitions that occur within the same band–a conduction band to conduction band transition or a valence band to valence band transition.

Figure 4.3: Absorption section of Matlab GUI.

# 4.6  Absorption Coefficient Results

In section 3.4, we introduced a tool to calculate energy eigenvalues and eigenvectors. We now add an additional component to the GUI to calculate the absorption coefficient using either the dipole or Gaunt methods (or both). This is shown in Figure 4.3. We normalize each of the radial eigenfunctions using Riemann sums:

$$\int_0^\infty (C_0\psi)^* C_0\psi r^2 dr \xrightarrow{\text{numerical sum}} C_0^* C_0 \sum_{i=0}^{i_{max}} (\psi(i))^* \psi(i) r(i)^2 \Delta r = 1$$

$$\Rightarrow \qquad \psi_{norm} = \frac{\psi}{\sqrt{|C_0|}}$$

where $C_0$ is a normalization constant, $i_{max}$ is the array length used (1000 to 10000 points), and $\Delta r = r_{max}/(i_{max})$ (usually 9 to 12 times the well radius). The factor of $r^2$ is required with spherical coordinates. We mention the detail of the arrays because the same summation technique is used to evaluate all integrals.

Table 4.1: Comparison of Gaunt and dipole methods using 1000 point arrays from $r = 0$ to $r = 8r_{well}$ on a 2.01 GHz processor

| Dot Radius($r_{well}$) | Run Time | | Max Residual | Corresponding Peak Level | Relative Residual |
|---|---|---|---|---|---|
| | Dipole | Gaunt | | | |
| 3nm | t<1sec | $t \approx 8$ min | ~$8 \cdot 10^{-3}$ | 9 | $8.89 \cdot 10^{-4}$ |
| 10nm | t<1min | $t \approx 20$ hr | ~.25 | 10 | .025 |

## 4.6.1 Comparison of Absorption Coefficient using the Dipole Approximation and Gaunt Coefficients

In this section, we shall compare the two methods proposed for calculating the optical absorption coefficient. Using the GUI-tool developed, we simulate GaAs dots embedded in AlAs with two different radii–10 nm and 3nm. Figure 4.5 shows the comparison for the 10 nm case. Figure 4.4. The results are summarized in table 4.1
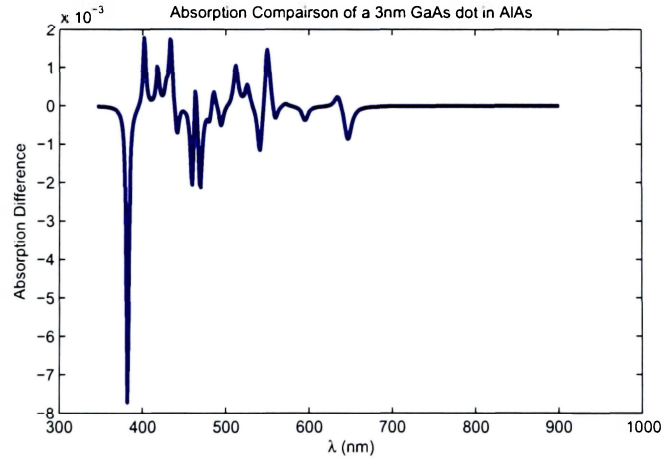


Figure 4.4: Absorption comparison of Gaunt and dipole methods for a 3nm radius GaAs dot in AlAs.
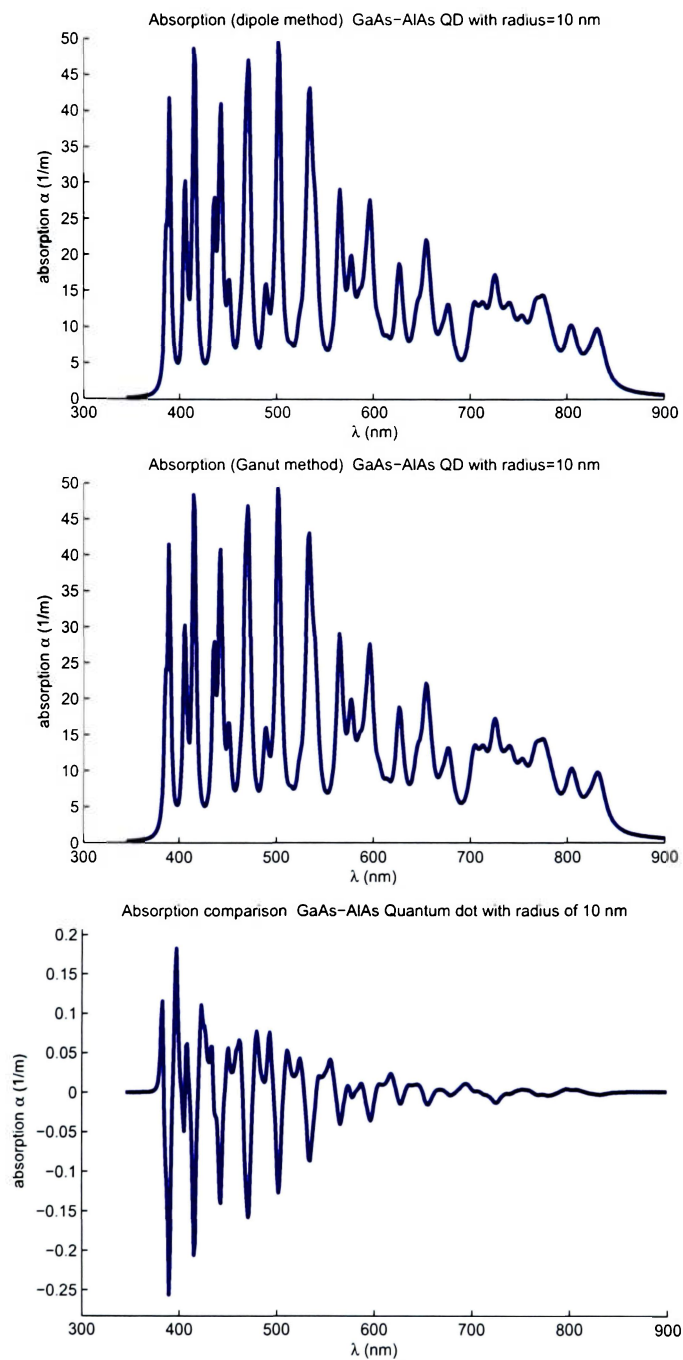
Figure 4.5: Absorption comparison of Gaunt and dipole methods for a 10nm radius GaAs dot in AlAs. The third plot shows the Gaunt method minus the dipole method

### 4.6.2 Absorption Coefficients

## GaAs Embeded in AlAs

Figure 4.6 shows the results for a GaAs quantum dot Embeded in AlAs, for radii of 4.5, 6, 7.5, 9 nm.
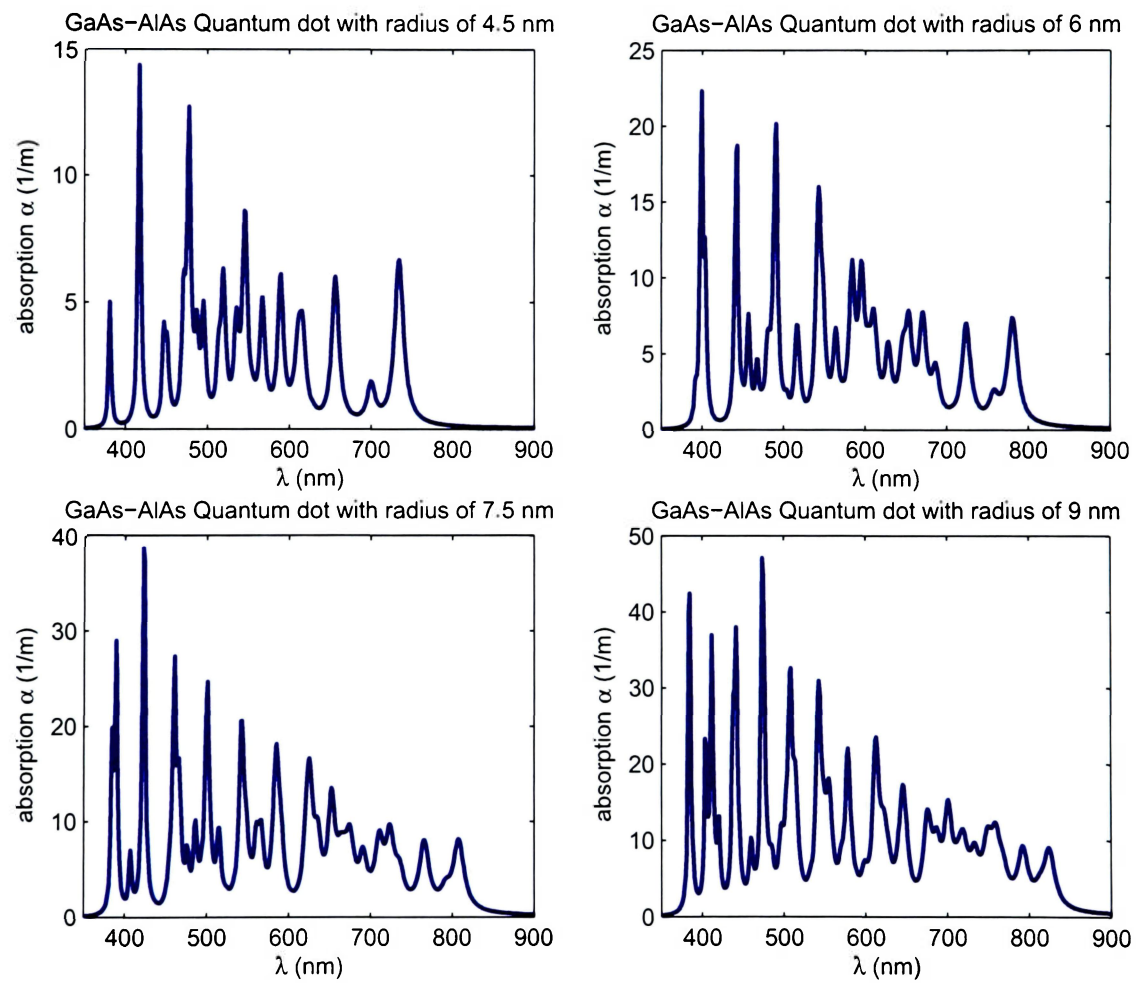


Figure 4.6: Absorption Coefficient plots

# GaAs Embeded in Al$_x$Ga$_{1-x}$As

Figure 4.7 shows the results for a GaAs quantum dot Embeded in Al$_3$Ga$_7$As (x =.3), for radii of 4.5, 6, 7.5, 9 nm.
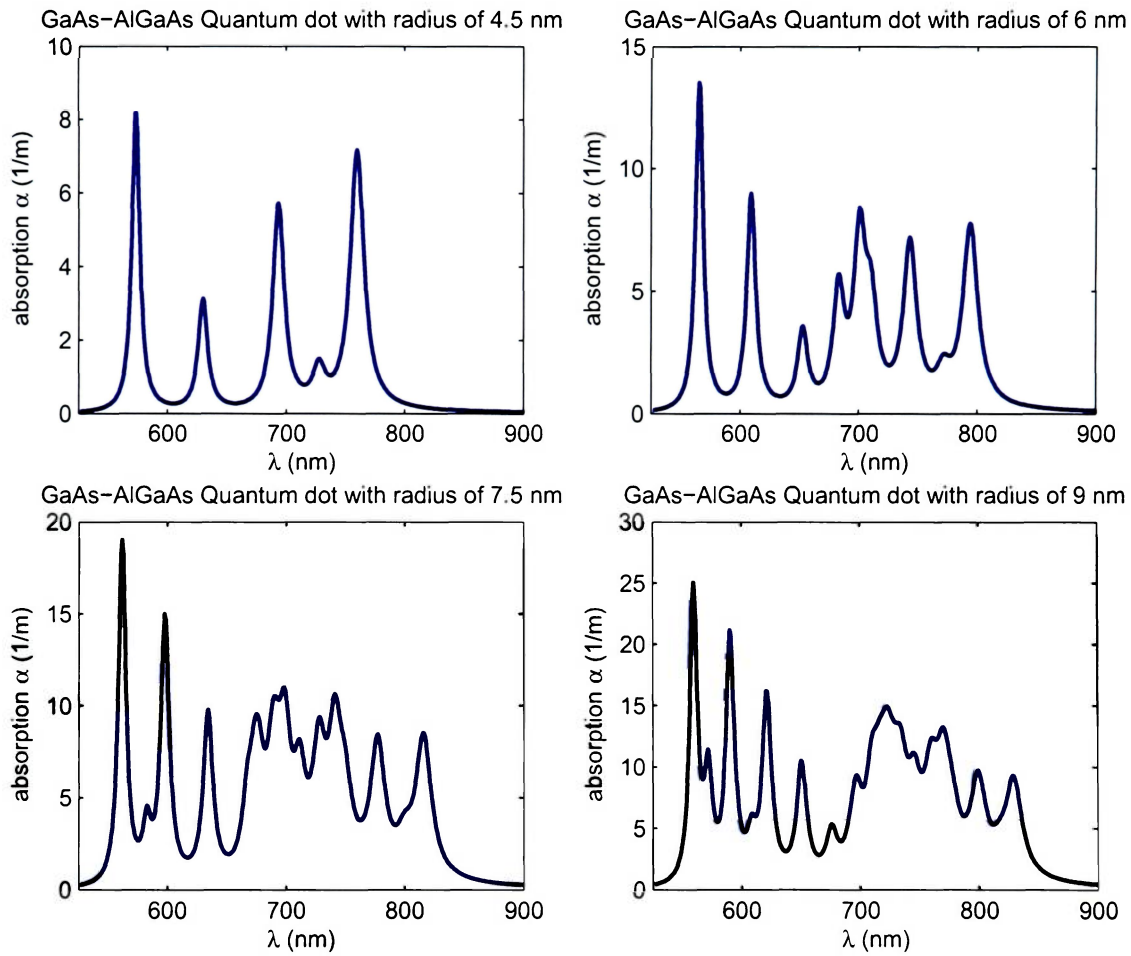


Figure 4.7: Absorption Coefficient plots

# InAs Embeded in GaAs

Figure 4.8 shows the results for an InAs quantum dot Embeded in GaAs, for radii of 4.5, 6, 7.5, 9 nm.
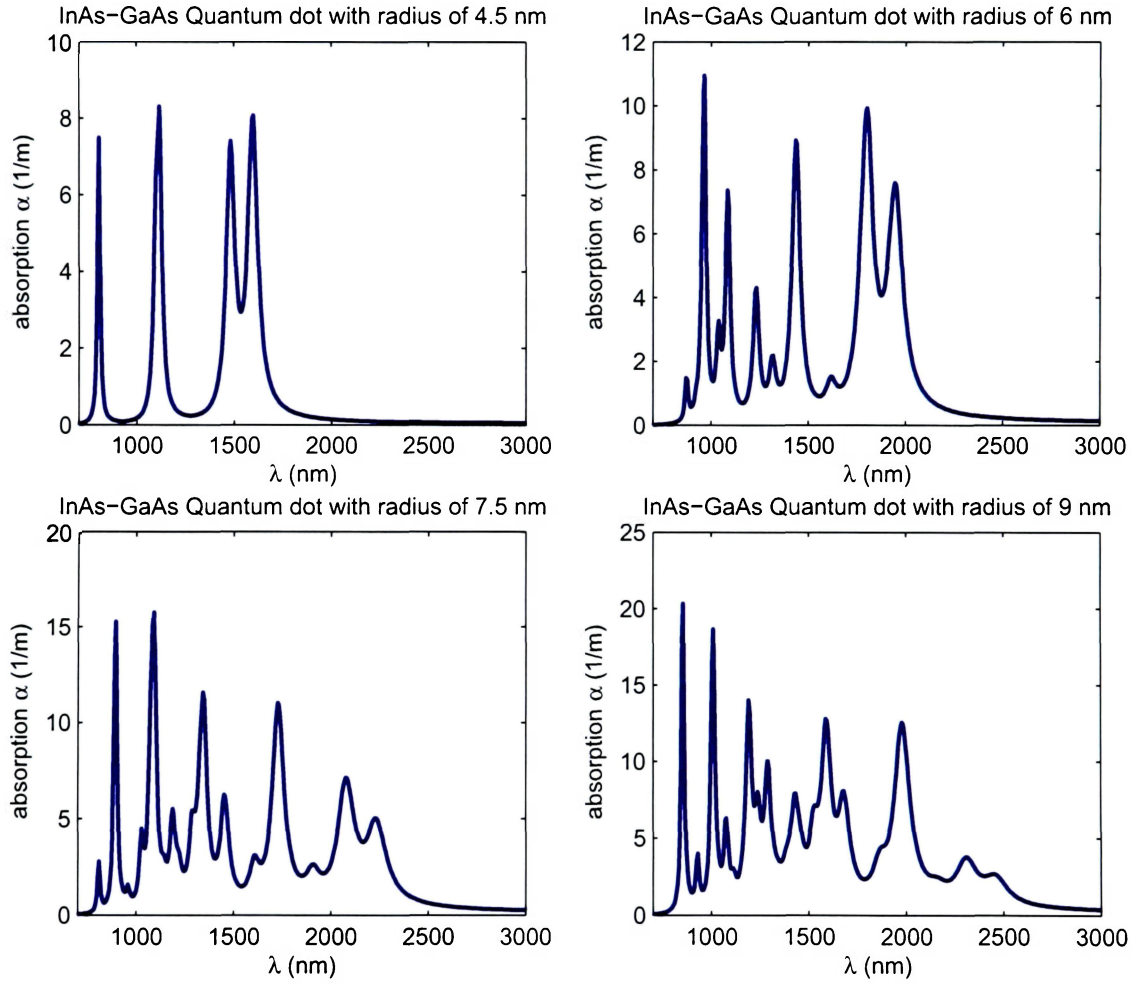


Figure 4.8: Absorption Coefficient plots

# GaSb Embeded in AlSb

Figure 4.9 shows the results for a GaSb quantum dot Embeded in AlSb, for radii of 4.5, 6, 7.5, 9 nm.
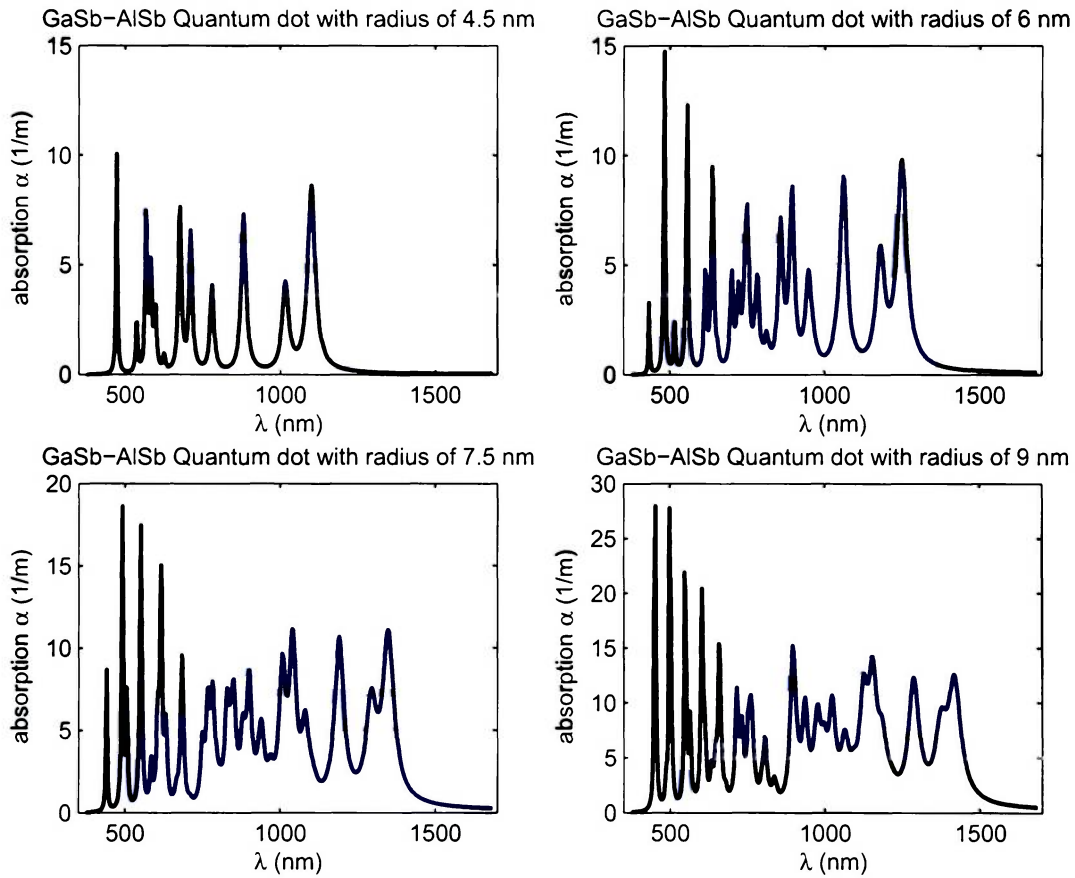


Figure 4.9: Absorption Coefficient plots

# InSb Embeded in AlSb

Figure 4.10 shows the results for an InSb quantum dot Embeded in AlSb, for radii of 4.5, 6, 7.5, 9 nm.
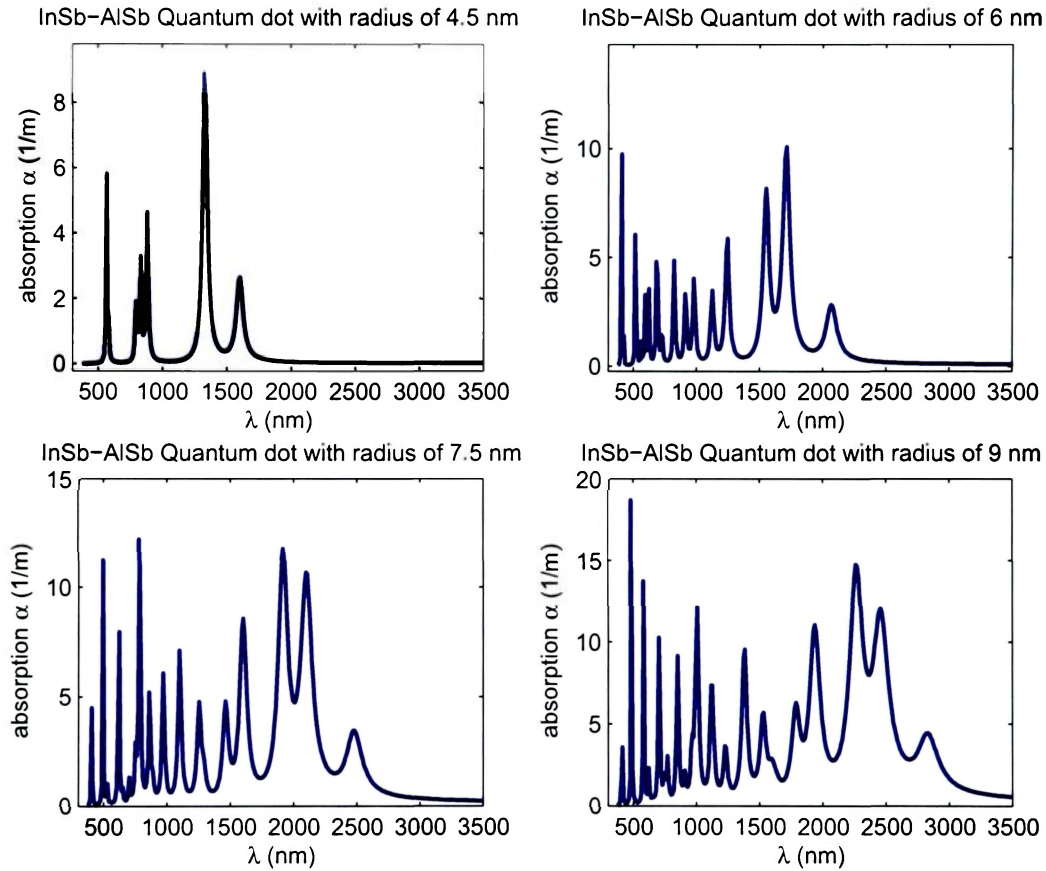


Figure 4.10: Absorption Coefficient plots

# Chapter 5

# Applications to Solar Cells

## 5.1 Quantum Dot Solar Cells

There is ever increasing demand for clean alternative energy sources, and naturally, solar cells come to mind. However, it was pointed out by Shockley and Queisser in 1961 [6] that the maximum theoretical efficiency of a solar cell, using a single p-n junction to collect power from the cell, is about 31%. In their analysis, a major factor limiting the efficiency to 31% is that the absorbed photon energy above the band gap is lost as heat. One method to increase efficiency above this limit is the use of a stack of p-n junctions; each with band-gaps better matched to the Air Mass (AM) 1.5 solar spectrum. The AM 1.5 spectrum[1] is the generally accepted input spectrum used to obtain solar cell efficiency[7]; this is shown in Figure 5.1–note that this spectrum is normalized with respect to photon enegry [7]. For an infinite stack of PN junctions the theoretical efficiency has been shown to be about 66% for the AM 1.5 spectrum. Due to practical reasons, these stacks have been limited to about three PN junctions, and efficiencies of about 32% [8].

However, in recent years it has been proposed [31, 32, 7, 33, 9], and in some cases experimentally verified [34, 35], that quantization effects (e.g. a quantum dot)

---

[1]The air mass 1.5 spectrum is used for terrestrial efficiencies, the AM 0 spectrum is used for space applications.
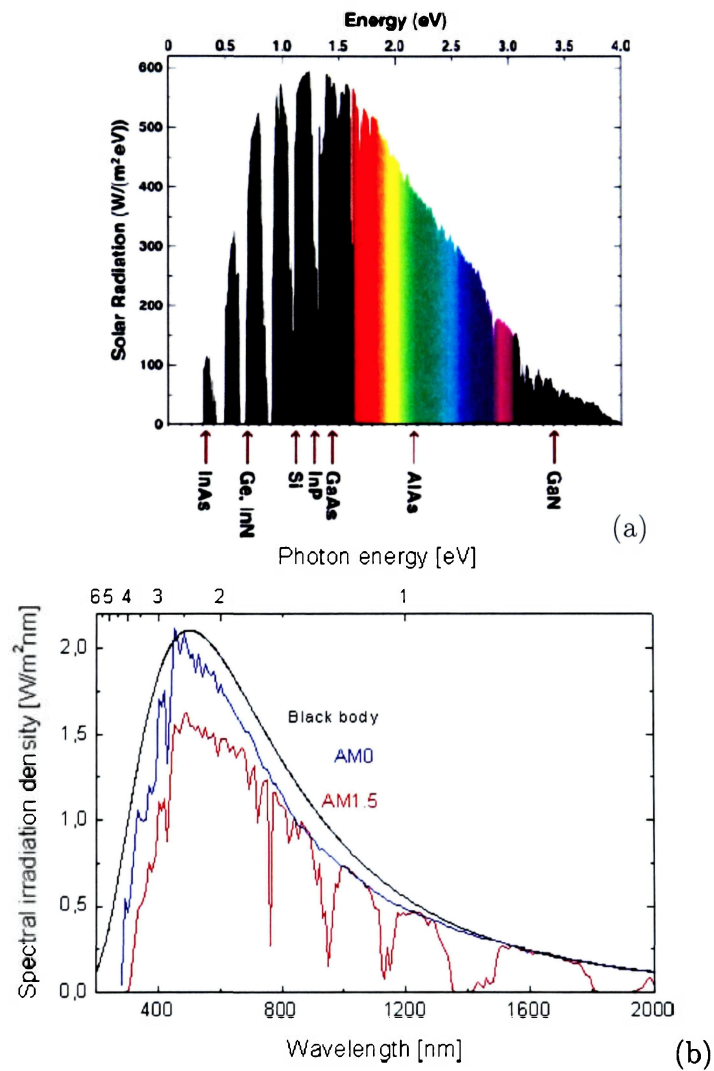
Figure 5.1: (a)The Air Mass (AM) 1.5 spectrum, shown with a normalized power density. Some bulk semiconductor band-gaps are also given. (b) The AM0 and AM1.5, and black body spectrum, shown with a linear wavelength scale.
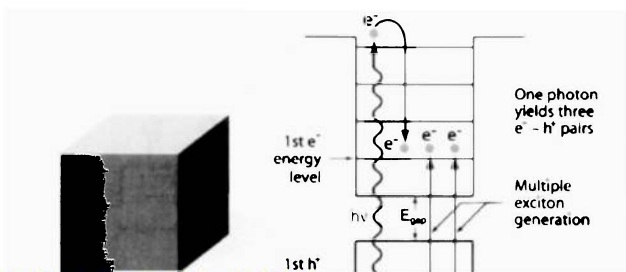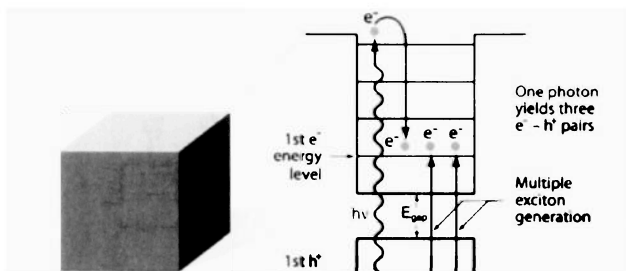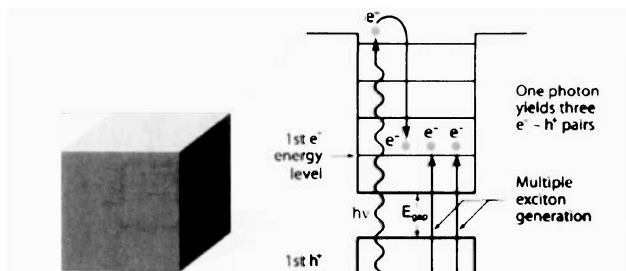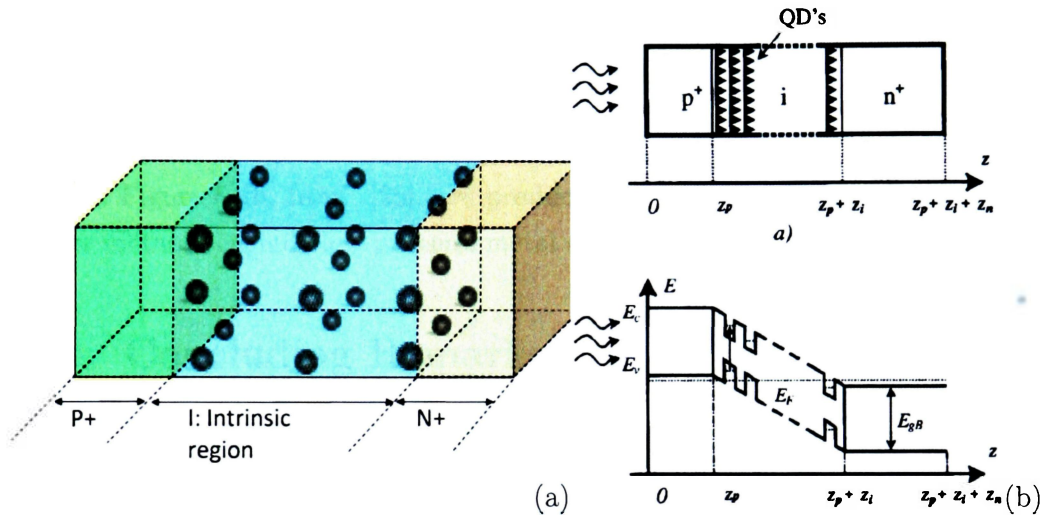
Figure 5.3: (a) The PIN junction with quantum dots in the intrinsic region (the p+ should be p-). (b) A suggested implementation of a PIN junction.

from the excited quantum dots in the intrinsic region. It has been suggested that a single PIN junction with quantum dots in the intrinsic region, could increase the efficiency to >63%[5]. Practical implementations to date have shown increases of ⌐6% for the type of solar cell shown in Figure 5.3b [36]. Also note from Figure 5.3b, from [36], that the p and n material alter the carrier densities because they induce carrier injection. Such effects alter the Fermi-Dirac statistics, and influence the confining potential, which could be difficult to account for under spherical symmetry. Thus, many transport effects would need to be considered to go from our absorption results to an actual solar cell; but we have shown the importance of such results and where our work fits into some intriguing modern research. Finally, we consider some examples of quantum dots produced today.

## 5.2 Modern Fabrication of Quantum Dot Arrays

There are currently many groups working on the fabrication of quantum dots[28; 37; 38]. The most popular types produced are pyramid shaped dots (for example [37]) and cylindrical shaped dots (28).

The pyramidal quantum dots Figure 5.4a, from [37], and cylindrical quantum dots in Figure 5.4b, from [28], are produced by molecular beam epitaxy [37, 28]. Other methods include low-pressure metal organic chemical vapor deposition.

## 5.3 Concluding Remarks

In conclusion, we have utilized a Hamiltonian with spin-orbit coupling; and, using perturbation theory and $\vec{k} \cdot \vec{p}$ theory, we obtained the necessary single and coupled band effective mass equations. Through spherical symmetry and sophisticated analytical methods, we simplified the problem and used additional analytical methods to make the problem numerically efficient to solve. We assumed quasi-equilibrium conditions, well matched unit cell sizes, and distant conduction and spin-orbit bands. A tool was developed, with a convenient user interface, to obtain the eigenenergies and eigenfunctions for arbitrary type III-V semiconductor materials and dot sizes. We further expanded this tool to implement the absorption coefficient for both the dipole and Gaunt calculation methods. Our results verified that the dipole approximation holds for the quantum dot sizes we considered.

In addition, we have also pointed out the relevance of these methods to quantum dot solar cells. However, if we which to consider a PIN junction, spherical coordinates present a complication. It is also possible to model the transport effects needed to analyze a theoretical photocurrent. This would change the Fermi-Dirac statistics from the equilibrium case, to one with charge carriers, which will influence the Fermi energy level. Also, we implicitly included scattering processes through the line-shape function (homogeneous broadening), however these scattering processes could be analyzed theoretically in more detail. We could also expand the proposed model further
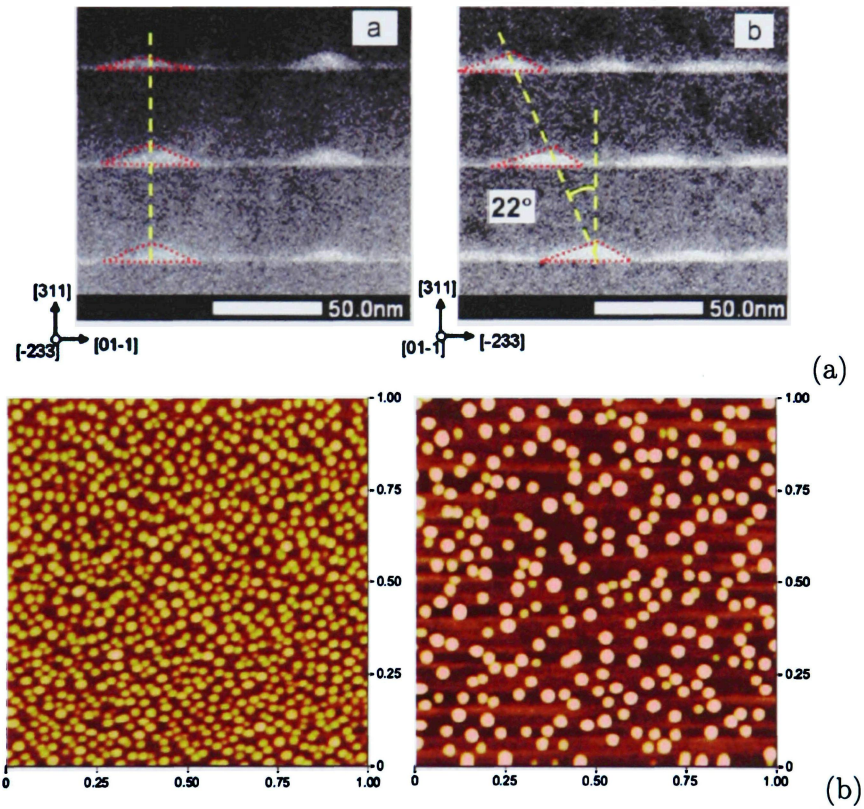
Figure 5.4: (a) Pyramid shaped Quantum dots. (b) InGaAs quantum dots in GaAs grown at 480°C and 510°C, line-widths of 36 meV were observed for the 480°C case. The scale is $1\mu m$. the densities observed were $\approx 6 \cdot 10^8 cm^{-2}$ for the 480°C case and $\approx 1 \cdot 10^8 cm^{-2}$ for 510°C. These quantum dots are cylindrical with a height (into page) of 1.4nm.

by including inhomogeneous broadening, and higher order blocks of the block diagonalized Hamiltonian (i.e. the F=5/2 space). It is also possible to reconsider the distant band approximations, and analyze their impact on the band structure.

Finally, we believe the methods discussed and GUI developed will be of practical use to those designing quantum dot photovoltaic cells, quantum dot lasers, and any quantum dot based optoelectronic devices.

# Appendix A

# First Appendix

## A.1 Spherical Harmonics

The normalised Spherical Harmonics are defined as

$$Y_{lm} = Y_l^m = Y_l^m(\theta, \phi) = \sqrt{\frac{(2l+1)}{4\pi}\frac{(l-m)!}{(l+m)!}} P_l^m(\cos\theta)e^{im\phi}$$

Where $P_L^M$ are the associated Legendre functions. Because the functions are normalized they have the property

$$\int_0^\pi \int_0^{2\pi} \left(Y_L^M\right)^* Y_{L'}^{M'} d\Omega = \delta_{LL'}\delta_{L_z L_z'}$$

where $\delta_{ab}$ is the Kronecker delta function, $\delta_{ab} = 0$ if $a \neq b$ and $\delta_{ab} = 1$ if $a = b$.

For more details on spherical harmonics consult an undergraduate physics text such as Griffiths book[18]. A few normalized spherical harmonics are given below.

$$Y_0^0 = \frac{1}{2}\sqrt{\frac{1}{\pi}} \qquad\qquad Y_2^{-1} = \frac{1}{2}\sqrt{\frac{15}{2\pi}}\sin\theta\cos\theta e^{-\imath\phi}$$

$$Y_1^{-1} = \frac{1}{2}\sqrt{\frac{3}{2\pi}}\sin\theta e^{-\imath\phi} \quad Y_2^0 = \frac{1}{2}\sqrt{\frac{15}{2\pi}}(3\cos^2\theta - 1)$$

$$Y_1^0 = \frac{1}{2}\sqrt{\frac{3}{\pi}}\cos\theta \qquad\qquad Y_2^1 = \frac{1}{4}\sqrt{\frac{5}{\pi}}\sin\theta\cos\theta e^{\imath\phi}$$

$$Y_1^1 = \frac{-1}{2}\sqrt{\frac{3}{2\pi}}\sin\theta e^{\imath\phi} \quad Y_2^{-2} = \frac{1}{4}\sqrt{\frac{15}{2\pi}}\sin^2\theta e^{\imath 2\phi}$$

$$Y_2^{-2} = \frac{1}{4}\sqrt{\frac{15}{2\pi}}\sin^2\theta e^{-\imath 2\phi}$$

## A.2   Bloch Function's Relation to $Y_L^M$

The names and formulation of the block-function-definitions can be traced back to the naming scheme used for the hydrogen atom; that is the s-p-d-f states. The nature of the Bloch functions for the conduction band have s-state like properties ($\ell=0$) and

$$Y_{00} = \frac{1}{\sqrt{4\pi}}$$

The 6 valence band states have "p" ($\ell=1$) like properties. The Z states:

$$Y_{10} = \sqrt{\frac{3}{4\pi}}\cos\theta$$
$$z = r \cdot \cos\theta$$
$$Y_{10} = \sqrt{\frac{3}{4\pi}}\frac{z}{r} \equiv |Z\rangle$$

and the X and Y states:

$$
\begin{aligned}
Y_{1\pm 1} &= \mp \sqrt{\frac{3}{8\pi}} \sin\theta \, e^{\pm i\phi} \\
x &= r \cdot \cos\phi \sin\theta \\
y &= r \cdot \sin\phi \sin\theta \\
Y_{1\pm 1} &= \mp \sqrt{\frac{3}{8\pi}} \frac{x \pm y}{r} \equiv \mp \frac{1}{\sqrt{2}} \, |X \pm iY\rangle
\end{aligned}
$$

Bloch functions for valence band states can be represented by a superposition of these $\ell=1$ states. The Bloch functions are given again in equation A.1below. It is in fact the spin-orbit interaction which couples these $|X\rangle, |Y\rangle, |Z\rangle$ states into those in A.1, otherwise the 6 valence band states would be

$$|X, \uparrow\rangle \quad |Y, \uparrow\rangle \quad |Z, \uparrow\rangle$$

$$|X, \downarrow\rangle \quad |Y, \downarrow\rangle \quad |Z, \downarrow\rangle$$

# A.3   Momentum Matrix Elements

As noted in chapter 2, the Bloch functions $u_{n\vec{k}}(\vec{r})$ for the light-hole, heavy-hole, and spin-orbit holes can be represented by:

$$\text{heavy hole 1: } u_{10}(\vec{r}) \;=\; \left|\frac{3}{2},\frac{3}{2}\right\rangle = \frac{-1}{\sqrt{2}}|X+iY,\uparrow\rangle$$

$$\text{light hole 1: } u_{20}(\vec{r}) \;=\; \left|\frac{3}{2},\frac{1}{2}\right\rangle = \frac{-1}{\sqrt{6}}|X+iY,\downarrow\rangle + \sqrt{\frac{2}{3}}|Z,\uparrow\rangle$$

$$\text{light hole 2: } u_{30}(\vec{r}) \;=\; \left|\frac{3}{2},\frac{-1}{2}\right\rangle = \frac{-1}{\sqrt{6}}|X-iY,\uparrow\rangle + \sqrt{\frac{2}{3}}|Z,\downarrow\rangle \qquad (A.1)$$

$$\text{heavy hole 2: } u_{40}(\vec{r}) \;=\; \left|\frac{3}{2},\frac{-3}{2}\right\rangle = \frac{1}{\sqrt{2}}|X-iY,\downarrow\rangle$$

$$\text{Spin-orbit 1: } u_{50}(\vec{r}) \;=\; \left|\frac{1}{2},\frac{1}{2}\right\rangle = \frac{1}{\sqrt{3}}|X+iY,\downarrow\rangle + \sqrt{\frac{1}{3}}|Z,\uparrow\rangle$$

$$\text{Spin-orbit 2: } u_{60}(\vec{r}) \;=\; \left|\frac{1}{2},\frac{-1}{2}\right\rangle = \frac{1}{\sqrt{3}}|X-iY,\uparrow\rangle - \sqrt{\frac{1}{3}}|Z,\downarrow\rangle$$

The conduction band states can be expressed as

$$|iS,\uparrow\rangle \text{ and } |iS,\downarrow\rangle$$

When calculating the Momentum matrix element $\langle \psi_c \,|\vec{p}|\, \psi_v\rangle$ a useful portion of the integral is

$$P_{cv} = \langle \vec{u}_{cb,0} \,|\vec{p}|\, \vec{u}_{vb,0}\rangle$$

The spin basis is factored out and simply integrated by orthogonality (it is unaffected by the momentum operator)

$$\langle \uparrow \,|\, \uparrow \rangle = \langle \downarrow \,|\, \downarrow \rangle = 1$$

$$\langle \downarrow \,|\, \uparrow \rangle = \langle \uparrow \,|\, \downarrow \rangle = 0$$

It can be shown [25] that

$$\left\langle S \left| -i\hbar\frac{\partial}{\partial x} \right| X \right\rangle = \left\langle S \left| -i\hbar\frac{\partial}{\partial y} \right| Y \right\rangle = \left\langle S \left| -i\hbar\frac{\partial}{\partial z} \right| Z \right\rangle = P_0$$

other integrals such as

$$\left\langle \mathbf{S} \,\middle|\, -i\hbar\frac{\partial}{\partial \mathbf{x}} \,\middle|\, \mathbf{Z} \right\rangle = \mathbf{0}$$

Note that a lot of confusion can result from the multiple ways people define these integrals. Chuang [10], for example, uses Kane's parameter $P$

$$P = \frac{\hbar}{m_0} \left\langle iS \,\middle|\, -i\hbar\frac{\partial}{\partial x} \,\middle|\, X \right\rangle$$

and

$$\left\langle iS \,\middle|\, -i\hbar\frac{\partial}{\partial x} \,\middle|\, X \right\rangle = \left\langle iS \,\middle|\, -i\hbar\frac{\partial}{\partial y} \,\middle|\, Y \right\rangle = \left\langle iS \,\middle|\, -i\hbar\frac{\partial}{\partial z} \,\middle|\, Z \right\rangle = P_x$$

The advantage of this variant is that it matches basis we use for the conduction band, and it is related to the experimentally known parameter $E_p$, which is defined by

$$E_p = \frac{2m_0}{\hbar^2} P^2$$

Values for $E_p$ are found experimentally and are given in table B.2. This parameter is often refered to as the optical matrix parameter We want to summarize these integrals so that they will benumerically useful. From the above expressions we can see that

$$P_x = \sqrt{\frac{E_p m_0}{2}}$$

Next we put the results for light incident from one direction into the following table (h1 is heavy-hole 1 from equaiton A.1):

Table A.1: Optical Momentum Matrix Elements for Bloch Functions in Terms of Known Parameters

|       | $\langle iS, \uparrow \vert$ | $\langle iS, \downarrow \vert$ |
|-------|------------------------------|-------------------------------|
| **hh1** | $-\frac{\sqrt{E_p m_0}}{2}(\hat{e}_x + i\hat{e}_y)$ | **0** |
| **hh2** | **0** | $\frac{\sqrt{E_p m_0}}{2}(\hat{e}_x - i\hat{e}_y)$ |
| **ℓh1** | $\sqrt{\frac{E_p m_0}{3}}\hat{e}_z$ | $-\sqrt{\frac{E_p m_0}{12}}(\hat{e}_x + i\hat{e}_y)$ |
| **ℓh2** | $\sqrt{\frac{E_p m_0}{12}}(\hat{e}_x - i\hat{e}_y)$ | $\sqrt{\frac{E_p m_0}{3}}\hat{e}_z$ |
| **so1** | $\sqrt{\frac{E_p m_0}{6}}\hat{e}_z$ | $\sqrt{\frac{E_p m_0}{6}}(\hat{e}_x + i\hat{e}_y)$ |
| **so2** | $\sqrt{\frac{E_p m_0}{6}}(\hat{e}_x - i\hat{e}_y)$ | $-\sqrt{\frac{E_p m_0}{6}}\hat{e}_z$ |

# A.4  Plane-Wave Expansion and Gaunt Coefficients

We wish to evaluate the integral

$$\langle L^{(c)}, L_z^{(c)} \vert e^{ik_{op}\vec{r}} \vert L^{(v)}, L_z^{(v)} \rangle = \int \left( R_{L^{(c)},n}^{(c)} Y_{L^{(c)}}^{L_z^{(c)}} \right)^* R_{L^{(v)},n'}^{(v)} Y_{L^{(v)}}^{L_z^{(v)}} e^{i\vec{k}\cdot\vec{r}} r^2 \sin(\theta)drd\theta d\phi$$

Which is required in section 4.3.2. We start with the plain-wave expansion into spherical components[30]

$$e^{i\vec{k}\vec{r}} = \sum_{L=0}^{\infty} \sum_{m=-L}^{L} 4\pi i^L Y_{Lm}^*(\theta_k, \phi_k)Y_{Lm}(\theta, \phi)j_L(kr)$$

Where $j_l$ are spherical Bessel functions, and $\vec{k}$ is in the $\theta_k, \phi_k$ direction. Therefore

$$\langle L^{(c)}, L_z^{(c)} \vert e^{ik_{op}\cdot\vec{r}} \vert L^{(v)}, L_z^{(v)} \rangle = \int \left( R_{L^{(c)},n}^{(c)} Y_{L^{(c)}}^{L_z^{(c)}} \right)^* R_{L^{(v)},n'}^{(v)} Y_{L^{(v)}}^{L_z^{(v)}}$$

$$\left( \sum_{L=0}^{\infty} \sum_{m=-L}^{L} 4\pi i^L Y_{Lm}^*(\theta_k, \phi_k)Y_{Lm}(\theta, \phi)j_L(kr) \right) r^2 \sin(\theta)drd\theta d\phi \qquad (A.2)$$

We can put the summation outside the integral because it is mathematically the same

$$\left\langle L^{(c)}, L_z^{(c)}|e^{ik_{op}\,\vec{r}}|L^{(v)}, L_z^{(v)}\right\rangle = \sum_{L=0}^{\infty}\sum_{m=-L}^{L}\int \left(R_{L^{(c)},n}^{(c)}Y_{L^{(c)}}^{L_z^{(c)}}\right)^* R_{L^{(v)}n'}^{(v)}Y_{L^{(v)}}^{L_z^{(v)}}$$

$$\left(4\pi i^L Y_{Lm}^*(\theta_k,\phi_k)Y_{Lm}(\theta,\phi)j_L(kr)\right)r^2\sin(\theta)drd\theta d\phi$$

A major simplification can be achieved from the term $Y_{Lm}^*(\theta_k,\phi_k)$ where we use $k_{op} = k\hat{e}_z$, therefore $\theta_k = \phi_k = 0$ and

$$Y_{Lm}^*(\theta_k,\phi_k) = Y_{Lm}^*(0,0) = \frac{0^{-m/2}}{\Gamma(1-m)}\sqrt{\frac{2L+1}{4\pi}\frac{(L-m)!}{(L+m)!}}$$

where $\Gamma$ is the gamma function. Because we are working with integers, $0^{-0/2}/\Gamma(1 - 0) = 1$ and from the limit of $0^{-m/2}$, we can see that

$$Y_{Lm}^*(0,0) = \begin{cases} \sqrt{\frac{2L+1}{4\pi}} & m = 0 \\ 0 & m \neq 0 \end{cases} \tag{A.3}$$

For completeness, we can verify this by looking

$$Y_{Lm}^*(0,0) = \sqrt{\frac{2L+1}{4\pi}\frac{(L-m)!}{(L+m)!}}P_l^m(\cos 0)e^{im\,0}$$

$$= \sqrt{\frac{2L+1}{4\pi}\frac{(L-m)!}{(L+m)!}}P_l^m(1)$$

The Associated Legendre functions with integer indexes can be written as (equation 8.810 from [39])

$$P_l^m(x) = (-1)^m(1-x^2)^{\frac{m}{2}}\frac{d^m}{dx^m}P_n(x)$$

with $x = 1$

$$
\begin{aligned}
P_l^m(1) &= (-1)^m (1-1)^{\frac{m}{2}} \frac{d^m}{dx^m} P_l(1) \\
&= (-1)^m (0)^{m/2} \frac{d^m}{dx^m} P_l(1) \\
&= (-1)^m (0)^{m/2} \\
&= \begin{cases} 1 & m = 0 \\ 0 & m \neq 0 \end{cases}
\end{aligned}
$$

Because[1] $P_l(1) = 1$ is a constant we have again verified equation A 3  Therefore the $\sum_{m=-L}^{L}$ disappears in equation A 2 because all none zero values for m result in a zero  Now we only need to sum over L, all m's are replaced with $m = 0$, and plug in equation A 3

$$
\begin{aligned}
\langle L^{(c)}, L_z^{(c)} | e^{ik_{op} \vec{r}} | L^{(v)}, L_z^{(v)} \rangle &= \sum_{L=0}^{\infty} \int \left( R_{L^{(c)} n}^{(c)} Y_{L^{(c)}}^{L_z^{(c)}} \right)^* R_{L^{(v)} n'}^{(v)} Y_{L^{(v)}}^{L_z^{(v)}} \\
&\quad \left( 4\pi i^L \sqrt{\frac{2L+1}{4\pi}} Y_{L\,0}(\theta, \phi) j_L(kr) \right) r^2 \sin(\theta) dr d\theta d\phi
\end{aligned}
$$

Now we separate the integral into angular and radial integrals

$$
\begin{aligned}
\langle L^{(c)}, L_z^{(c)} | e^{ik_{op} \vec{r}} | L^{(v)}, L_z^{(v)} \rangle &= \sum_{L=0}^{\infty} \int_0^{\infty} R_{L^{(c)} n}^{(c)} R_{L^{(v)} n'}^{(v)} j_L(kr) r^2 dr \\
&\quad \left( 4\pi i^L \sqrt{\frac{2L+1}{4\pi}} \right) \int_0^{\pi} \int_0^{2\pi} Y_L^0 \left( Y_{L^{(c)}}^{L_z^{(c)}} \right)^* Y_{L^{(v)}}^{L_z^{(v)}} \sin(\theta) d\phi d\theta
\end{aligned}
$$

---

[1]Found using Mathematica, but the value does not matter in this case because it is obviously a constant

Next, we evaluate the integration of three spherical harmonics with the definition of the Gaunt coefficients which are defined in [29; 30]

$$\int_0^\pi \int_0^{2\pi} Y_L^m Y_{L'}^{m'} Y_{L''}^{m''} \sin(\theta) d\phi d\theta = \sqrt{\frac{(2L+1)(2L'+1)(2L''+1)}{4\pi}} \cdot$$
$$\begin{pmatrix} L & L' & L'' \\ 0 & 0 & 0 \end{pmatrix} \begin{pmatrix} L & L' & L'' \\ m & m' & m'' \end{pmatrix}$$

Where $\begin{pmatrix} L & L' & L'' \\ m & m' & m'' \end{pmatrix}$ is the Wigner 3-j symbol. They are related to the Clebsch Gordan coefficients by

$$\begin{pmatrix} L & L' & L'' \\ m & m' & m'' \end{pmatrix}_{cg} = (-1)^{m+L'-L''} \sqrt{2L+1} \begin{pmatrix} L & L' & L'' \\ m & m' & m'' \end{pmatrix}$$

For this element to be physical

$$m \in \{-L, \cdots, L\}, \; m' \in \{-L', \cdots, L'\}, \; m'' \in \{-L'', \cdots, L''\}$$

and the triangular inequality must also hold

$$|L' - L''| \le L \le L' + L''$$

In our case, we must account for the conjugation of the spherical harmonic from the conduction band. Using the conjugation rules for spherical harmonics

$$Y_L^{-m} = (-1)^m (Y_L^m)^*$$

we obtain

$$\int_0^\pi \int_0^{2\pi} Y_L^0 \left(Y_{L^{(c)}}^{L_z^{(c)}}\right)^* Y_{L^{(v)}}^{L_z^{(v)}} \sin(\theta)d\phi d\theta = (-1)^{L_z^{(c)}} \sqrt{\frac{(2L+1)(2L^{(c)}+1)(2L^{(v)}+1)}{4\pi}}$$

$$\cdot \begin{pmatrix} L & L^{(c)} & L^{(v)} \\ 0 & 0 & 0 \end{pmatrix} \begin{pmatrix} L & L^{(c)} & L^{(v)} \\ 0 & -L_z^{(c)} & L_z^{(v)} \end{pmatrix}$$

This result was checked in Mathematica and the left hand side and right hand side give the same answers. The Wigner 3-j symbol also has the important properties that $\begin{pmatrix} L & L' & L'' \\ m & m' & m'' \end{pmatrix}$ is non-zero if $L+L'+L''$ is an even number and $m+m'+m''=0$. In our case $m=0$ therefore the Gaunt coefficient is non zero if $L_z^{(c)} = L_z^{(v)}$ . Therefore, we use

$$\int_0^\pi \int_0^{2\pi} Y_L^0 \left(Y_{L^{(c)}}^{L_z^{(c)}}\right)^* Y_{L^{(v)}}^{L_z^{(v)}} \sin(\theta)d\phi d\theta = (-1)^{L_z^{(c)}} \sqrt{\frac{(2L+1)(2L^{(c)}+1)(2L^{(v)}+1)}{4\pi}}$$

$$\cdot \begin{pmatrix} L & L^{(c)} & L^{(v)} \\ 0 & 0 & 0 \end{pmatrix} \begin{pmatrix} L & L^{(c)} & L^{(v)} \\ 0 & -L_z^{(c)} & L_z^{(c)} \end{pmatrix} \delta_{L_z^{(c)},L_z^{(v)}}$$

We introduce the Kronecker delta function, because the Kronecker delta function will make the entire expression for $\left\langle L^{(c)}, L_z^{(c)} | e^{ik_{op} \vec{r}} | L^{(v)}, L_z^{(v)} \right\rangle = 0$ if $L_z^{(c)} \neq L_z^{(v)}$. Therefore we can use an "if-statement" for numerical evaluation to avoid unnecessary computation. Next, we combine these terms together

$$\left\langle L^{(c)}, L_z^{(c)} | e^{ik_{op} \vec{r}} | L^{(v)}, L_z^{(v)} \right\rangle = \delta_{L_z^{(c)},L_z^{(v)}} \sum_{L=0}^\infty \left[ \frac{2L+1}{4\pi} \sqrt{(2L^{(c)}+1)(2L^{(v)}+1)} (-1)^{L_z^{(c)}} 4\pi i^L \right.$$

$$\cdot \begin{pmatrix} L & L^{(c)} & L^{(v)} \\ 0 & 0 & 0 \end{pmatrix} \begin{pmatrix} L & L^{(c)} & L^{(v)} \\ 0 & -L_z^{(c)} & L_z^{(c)} \end{pmatrix}$$

$$\left. \cdot \int_0^\infty R_{L^{(c)},n}^{(c)} R_{L^{(v)}n'}^{(v)} J_L\left(\frac{2\pi}{\lambda}r\right) r^2 dr \right]$$

Finally we apply the inequality rule for the Wigner 3-j symbol

$$\left| L^{(c)} - L^{(v)} \right| \leq L \leq L^{(c)} + L^{(v)}$$

This changes the summation bounds over L and we obtain a final expression canceling out the $4\pi$ and obtain equation 4.20.

$$\left\langle L^{(c)}, L_z^{(c)} \middle| e^{ik_{op} \vec{r}} \middle| L^{(v)}, L_z^{(v)} \right\rangle = \delta_{L_z^{(c)}, L_z^{(v)}} \sum_{L=\left| L^{(c)} - L^{(v)} \right|}^{L^{(c)}+L^{(v)}} \left[ (2L+1) \sqrt{\left(2L^{(c)}+1\right)\left(2L^{(v)}+1\right)} \right.$$

$$(-1)^{L_z^{(c)}} i^L \cdot \begin{pmatrix} L & L^{(c)} & L^{(v)} \\ 0 & 0 & 0 \end{pmatrix} \begin{pmatrix} L & L^{(c)} & L^{(v)} \\ 0 & -L_z^{(c)} & L_z^{(c)} \end{pmatrix}$$

$$\left. \int_0^\infty R_{L^{(c)},n}^{(c)} R_{L^{(v)}n'}^{(v)} \jmath_L \left( \frac{2\pi}{\lambda} r \right) r^2 dr \right]$$

Also note that the $\left\langle L^{(c)}, L_z^{(c)} \middle| e^{ik_{op} \vec{r}} \middle| L^{(v)}, L_z^{(v)} \right\rangle$ is $\lambda$ dependent, which is also another numerical complication.

# Appendix B

# Useful Properties of Group III and V Elements

## B.1 Electron Structure of Group III and V Elements

Table B.1: Electron Structure of Group III and V Elements

| Group III | | Group V | |
|---|---|---|---|
| A | B | A | B |
| $B(\#5)$ $1s^2 2s^2 2p^1$ | | $N(\#7)$ $1s^2 2s^2 2p^3$ | |
| $Al(\#13)$ $[Ne]3s^2 3p^3$ | | $P(\#15)$ $[Ne]3s^2 3p^3$ | |
| | $Sc(\#21)$ $[Ar]3d^1 4s^2$ | | $V(\#23)$ $[Ar]3d^3 4s^2$ |
| $Ga(\#31)$ $[Ar]3d^{10}4s^2 4p^1$ | | $As(\#33)$ $[Ar]3d^{10}4s^2 4p^3$ | |
| | $Y(\#39)$ $[Kr]4d^1 5s^2$ | | $Nb(\#41)$ $[Kr]4d^4 5s^1$ |
| $In(\#49)$ $[Kr]4d^4 5s^2 5p^1$ | | $Sb(\#51)$ $[Kr]4d^4 5s^2 5p^3$ | |

Table B.2: Important Band Structure Parameters for various Group III and V Semiconductors*

| | Materials | | | | | | | | | | | |
|---|---|---|---|---|---|---|---|---|---|---|---|---|
| | GaAs | AlAs | InAs | GaP | InP | AlP | GaSb | AlSb | InSb | GaN | AlN | InN |
| Parameters | | | | | | | | | | | | |
| $a_o$(Å) | 5.6532 | 5.6611 | 6.0583 | 5.4505 | 5.8697 | 5.4672 | 6.0959 | 6.1355 | 6.4794 | 4.5 | 4.38 | 4.98 |
| $E_v$**(eV) | 0 | -0.53 | .21 | -0.47 | -0.14 | -0.94 | .77 | .39 | .8 | -1.84 | -2.64 | -1.58 |
| $E_g$(eV) | 1.424 | 3.03 | .354 | 2.777 | 1.4236 | 3.63 | .75 | 2.386 | .235 | 3.299 | 4.9 | 1.94 |
| $\triangle$(eV) | .341 | .28 | .39 | .08 | .108 | .07 | .76 | .676 | .81 | .017 | .019 | .006 |
| $E_p$(eV) | 28.8 | 21.1 | 21.5 | 31.4 | 20.7 | 17.7 | 27 | 18.7 | 23.3 | 25 | 27.1 | 25 |
| Effective | Masses | | | | | | | | | | | |
| $m_e^*/m_0$ | .067 | .15 | .026 | .13 | .0795 | .22 | .039 | .14 | .0135 | .15 | .25 | .12 |
| $m_{lh}^*/m_0$ | .090 | .185 | .027 | .199 | .121 | .210 | .044 | .134 | .015 | .240 | .350 | .160 |
| $m_{hh}^*/m_0$ | .350 | .471 | .333 | .326 | .531 | .518 | .25 | .357 | .263 | .855 | 1.02 | .833 |
| $m_{SO}^*/m_0$ | .176 | .281 | .107 | .254 | .211 | .301 | .136 | .217 | .110 | .376 | .523 | .270 |
| $\gamma_1$ | 6.98 | 3.76 | 20 | 4.05 | 5.08 | 3.35 | 13.4 | 5.18 | 34.8 | 2.67 | 1.92 | 3.72 |
| $\gamma_2$ | 2.06 | .82 | 8.5 | .49 | 1.6 | .71 | 4.7 | 1.19 | 15.5 | .75 | .47 | 1.26 |
| $\gamma_3$ | 2.93 | 1.42 | 9.2 | 2.93 | 2.1 | 1.23 | 6 | 1.97 | 16.5 | 1.1 | .85 | 1.63 |

*Data taken from[40; 24]

** Ev GaAs set to 0 and other Ev's are relative to it

Notes on using TableB.2:

- $E_c = E_v + E_g$

- $E_{so} = E_v - \Delta$

- $E_p$: Kanes Parameter used for optical matrix elements

- The effective masses given in their most common form (the effects of the conduction band are included)

- The spin-orbit effective mass is defined in[24] as

$$\frac{m_{so}^*}{m_0} = \left[\gamma_1 - \frac{E_p\Delta}{3E_g(E_g + \Delta)}\right]^{-1}$$

# Appendix C

# The Spherical Potential

Throughout this document, we frequently reference spherical Bessel functions of the first kind, $j_l$; and spherical Hankel functions of the first kind, $h_l^{(1)}$. These functions are closely related to Bessel functions. Problems with cylindrical symmetry frequently lead to Bessel functions and problems with spherical symmetry frequently lead to spherical or half-integer Bessel functions. Mathematicians, and mathematical publications such as [39] will usually refer to spherical Bessel functions as half-integer Bessel functions, perhaps because they came about first. In physics however, we refer to these functions as spherical Bessel functions because they relate to spherical problems. William Bell gives a very good description of these functions in chapter 4 of [41] (which is a very concise and inexpensive source).

## C.1   Spherical Bessel and Hankel Functions

Consider the equation

$$\left[ \frac{d}{dr^2} + \frac{2}{r}\frac{d}{dr} - \frac{l\,(l+1)}{r^2} + k^2 \right] R_l(r) = 0 \tag{C.1}$$

which has the general solution

$$R_l(kr) = A \cdot J_{l+\frac{1}{2}}(kr) + B \cdot Y_{l+\frac{1}{2}}(kr)$$

or

$$R_l(kr) = A' \cdot j_l(kr) + B' \cdot y_l(kr)$$

where J and Y are Bessel functions, and $j$ and $y$ are spherical Bessel functions of the first and second kinds. The spherical Bessel functions of the second kind call are often refereed to as spherical Neumann functions. The general solution can also have two additional particular solutions

$$h_l^{(1)}(kr) = j_l(kr) + iy_l(kr)$$

and

$$h_l^{(2)}(kr) = j_l(kr) - iy_l(kr)$$

These functions are called the spherical Hankel functions of the first and second kinds. Hankel functions of the first kind decay exponentially as $r \to \infty$. The relationship between any Bessel function and spherical Bessel function is

$$j_l(\rho) = \sqrt{\frac{\pi}{2\rho}} J_{l+\frac{1}{2}}(\rho)$$

$$y_l(\rho) = \sqrt{\frac{\pi}{2\rho}} Y_{l+\frac{1}{2}}(\rho)$$

$$h_l(\rho) = \sqrt{\frac{\pi}{2\rho}} H_{l+\frac{1}{2}}(\rho)$$

These Spherical Bessel functions have the recursion relations

$$j_l(\rho) = (-1)^l \rho^l \left(\frac{1}{\rho}\frac{d}{d\rho}\right)^l \frac{\sin \rho}{\rho}$$

$$y_l(\rho) = -(-1)^l \rho^l \left(\frac{1}{\rho}\frac{d}{d\rho}\right)^l \frac{\cos \rho}{\rho}$$

A few examples of these are

$$J_0(\rho) = \frac{\sin \rho}{\rho} \qquad , y_0(\rho) = \frac{-\cos \rho}{\rho} \qquad , h_0^{(1)}(\rho) = \frac{e^{i\rho}}{i\rho}$$

$$J_1(\rho) = \frac{\sin \rho}{\rho^2} - \frac{\cos \rho}{\rho}, y_1(\rho) = \frac{-\cos \rho}{\rho^2} - \frac{\sin \rho}{\rho}, h_1(\rho) = -\frac{e^{i\rho}}{\rho}\left(1 + \frac{i}{\rho}\right)$$

To solve these functions numerically, it is also important to note that any Bessel function $Z$, must have the two functional relations (Equation 8 471 of [39])

$$zZ_{l-1}(z) + zZ_{l+1}(z) = 2lZ_l(z)$$
$$Z_{l-1}(z) + Z_{l+1}(z) = 2\frac{d}{dz}Z_l(z)$$

From which we can see that

$$\frac{d}{dz}Z_l(z) = \frac{l}{z}Z_l(z) - Z_{l+1}(z)$$

If, as in our case, we have $J_l(kr)$, than (prime superscript denotes a derivative)

$$\frac{d}{dr}J_l(kr) = \frac{l}{kr}J_l(kr) - J_{l+1}(kr)$$
$$J_l'(kr) = k\left(\frac{l}{kr}J_l(kr) - J_{l+1}(kr)\right)$$
$$J_l'(kr) = \frac{l}{r}J_l(kr) - kJ_{l+1}(kr) \qquad (C\ 2)$$

Numerical solutions involving a ratio of Hankel functions can lead to problems because they are decaying exponential functions  We can alleviate this by canceling out the exponential terms with the following recursion relation (Equation 8 466 of [39])

$$h_l^{(1)}(\rho) = (-i)^{l+1}\frac{e^{i\rho}}{\rho}\sum_{m=0}^{l}\frac{i^m}{m!(2\rho)^m}\frac{(l+m)!}{(l-m)!} \qquad (C\ 3)$$

## C.2   Electron Motion under a Spherical Potential

We wish to solve $H\psi = E\psi$ for a bounded electron under the influence of a spherical potential (quantum dot) with a radius of $r_{well}$

$$V(r) = \begin{cases} 0 & r > r_{well} \\ -V_0 & r < r_{well} \end{cases} \qquad \text{(C 4)}$$

A good explanation of this problem is given in section 7 4 of [19]  In spherical coordinates our Hamiltonian $H = -\frac{\hbar^2}{2m}\nabla^2 + V(r)$ takes the form

$$H = -\frac{\hbar^2}{2m}\left[\frac{1}{r^2}\frac{\partial}{\partial r}\left(r^2\frac{\partial}{\partial r}\right) + \frac{1}{r^2\sin\theta}\frac{\partial}{\partial\theta}\left(\sin\theta\frac{\partial}{\partial\theta}\right) + \frac{1}{r^2\sin^2\theta}\frac{\partial^2}{\partial\phi^2}\right] + V(r)$$

We can substitute in the angular momentum operator $L^2$

$$L^2 = -\hbar^2\left(\frac{1}{\sin\theta}\frac{\partial}{\partial\theta}\left(\sin\theta\frac{\partial}{\partial\theta}\right) + \frac{1}{\sin^2\theta}\frac{\partial^2}{\partial\phi^2}\right)$$

and our Hamiltonian becomes

$$H = -\frac{\hbar^2}{2m}\left[\frac{1}{r^2}\frac{\partial}{\partial r}\left(r^2\frac{\partial}{\partial r}\right) - \frac{L^2}{\hbar^2 r^2}\right] + V(r)$$

In order to simplify this equation further, we first recall that the operators $L_x$, $L_y$, $L_z$, and $L^2$ do not operate on the the radial variable r  Hence, for our spherical potential which is only a function of r, we have $\left[V(r), \vec{L}\right] = [V(r), L^2] = 0$  The angular momentum operators also commute with the Hamiltonian

$$\left[H, \vec{L}\right] = [H, L^2] = 0$$

The operators $L_x$, $L_y$, and do not commute among them selves, so we choose the usual option of $L_z$, this gives us a complete set of $H$, $L_z$, and $L^2$  We know from $\left[H, \vec{L}\right] = [H, L^2] = 0$, that our set $H$, $L_z$, and $L^2$ must share the same eigenvalues and eigenvectors  The spherical harmonics are the the simultaneous eigenfunctions

of $L^2$ and $L_z$ and $L^2 Y_{lm}(\theta, \phi) = l(l+1)\hbar^2 Y_{lm}(\theta, \phi)$. Therefore we look for solutions of the Schrodinger equation having the separable form (using n for the index of a particular $E_n$

$$\psi_{nlm}(\vec{r}) = R_{ln}(r)Y_{lm}(\theta, \phi)$$

We know in advance that the radial component is independent of $m$. When our Hamiltonian operates on this state, $H\psi_{nlm} = E_n\psi_{nlm}$ becomes

$$\left( -\frac{\hbar^2}{2m} \left[ \frac{1}{r^2}\frac{\partial}{\partial r}\left( r^2\frac{\partial}{\partial r} \right) - \frac{L^2}{\hbar^2 r^2} \right] + V(r) \right) R_{ln}(r)Y_{lm}(\theta, \phi) = E_n R_{ln}(r)Y_{lm}(\theta, \phi)$$

$$\left( -\frac{\hbar^2}{2m}\frac{1}{r^2}\frac{\partial}{\partial r}\left( r^2\frac{\partial}{\partial r} \right) + \frac{l(l+1)\hbar^2}{2mr^2} + V(r) \right) R_{ln}(r) = E_n R_{ln}(r)$$

This verifies that $R_{ln}$ is independent of $m$. The consequence of this is that each particular $E_n$ depends on $n$ which is particular to a value for $l$; and because each $m \in [-l, ..., l]$ , each state will have a $(2l + 1)$ degeneracy. If we apply our potential from C.4 than inside our spherical potential we have

$$\left( -\frac{\hbar^2}{2m}\frac{1}{r^2}\frac{\partial}{\partial r}\left( r^2\frac{\partial}{\partial r} \right) + \frac{l(l+1)\hbar^2}{2mr^2} - V_0 \right) R_{ln}(r) = E_n R_{ln}(r)$$

$$\left( -\frac{1}{r^2}\frac{\partial}{\partial r}\left( r^2\frac{\partial}{\partial r} \right) + \frac{l(l+1)}{r^2} - \frac{2m}{\hbar^2}\left( V_0 + E_n \right) \right) R_{ln}(r) = 0$$

$$\left( +\frac{1}{r^2}\frac{\partial}{\partial r}\left( r^2\frac{\partial}{\partial r} \right) - \frac{l(l+1)}{r^2} + \frac{2m}{\hbar^2}\left( V_0 + E_n \right) \right) R_{ln}(r) = 0 \qquad \text{(C.5)}$$

Equation C.5 is in fact the spherical Bessel equation C.1. Where

$$k = \sqrt{\frac{2m}{\hbar^2}(E_n + V_0)}$$

therefore we have the solution

$$R_{ln}(kr) = A j_{ln}(kr) + B y_{ln}(kr)$$

However, the spherical Bessel functions of the second kind converge to -∞ at the origin, and $\psi_{nlm}$ must be finite. Therefore, inside the dot our solution has the form

$$R_{ln}(kr) = Aj_{ln}(kr) \qquad r < r_{well} \tag{C.6}$$

Outside the well our solution becomes

$$\left( +\frac{1}{r^2}\frac{\partial}{\partial r}\left(r^2\frac{\partial}{\partial r}\right) - \frac{l(l+1)}{r^2} + \frac{2m}{\hbar^2}(E_n) \right) R_{ln}(r) = 0$$

Note that under the formulation of our potential, our bounded energy values fall below 0. Therefore

$$i\lambda = \sqrt{\frac{2m}{\hbar^2}(E_n)}$$

so outside the well our "k" from C.1, must take the form $i\lambda$. Now considering a particular solution

$$R_{ln}(kr) = Cj_{ln}(i\lambda r) + Dy_{ln}(i\lambda r)$$

we know this solution must go to 0 at $r = \infty$, because the probability must be bounded Because we are outside the well we can consider a linear combination of these two functions. For large r the functions $j_{ln}(i\lambda r)$, $y_{ln}(i\lambda r)$, and $h_{ln}^{(2)}(i\lambda r)$ all increase exponentially. therefore the only type of solution outside the well is $h_{ln}^{(1)}(i\lambda r)$

$$R_{ln}(kr) = Bh_{ln}^{(1)}(i\lambda r) \qquad r > r_{well} \tag{C.7}$$

At this point we could solve the problem by noting that the function must be equal and continuous at $r = r_{well}$, and we obtain C and A from solving

$$\left[\frac{\frac{d}{dr}(j_{ln}(kr))}{j_{ln}(kr)}\right]_{r=r_{well}} = \left[\frac{\frac{d}{dr}\left(h_{ln}^{(1)}(i\lambda r)\right)}{h_{ln}^{(1)}(i\lambda r)}\right]_{r=r_{well}} \tag{C.8}$$

with normalization. However, in our case we are interested in a potential created by two materials with different effective masses and the condition in equation C.8 is not actually true. Physically we must check the probability current density $\vec{j}$. $(Im()$

means the imaginary component)

$$\vec{j} = \frac{-iq\hbar}{2m^*}\left((\nabla\psi)^*\psi - \psi^*\nabla\psi\right) = \frac{\hbar}{m^*}Im(\psi^*\nabla\psi)$$

which satisfies the continuity equation

$$\frac{\partial}{\partial t}|\psi|^2 + \nabla\cdot\vec{j} = 0$$

Therefore, if we have a heterojunction and assume that $\psi_{in}(r_{well}) = \psi_{out}(r_{well})$, and $\nabla\psi_{in}(r_{well}) = X\nabla\psi_{out}(r_{well})$. we can find X through $\vec{j}$.

$$\begin{aligned}
\frac{\hbar}{m^*_{in}}Im(\psi^*_{in}\nabla\psi_{in}) &= \frac{\hbar}{m^*_{out}}Im(\psi^*_{out}\nabla\psi_{out}) \\
\frac{1}{m^*_{in}}Im(X\psi^*_{out}\nabla\psi_{out}) &= \frac{1}{m^*_{out}}Im(\psi^*_{out}\nabla\psi_{out}) \\
X &= \frac{m^*_{in}}{m^*_{out}}
\end{aligned}$$

Next, we use equations C.6 and C.7; we can set $A = 1$, because we normalize later, and we must solve

$$\left[\frac{\frac{d}{dr}\left(j_{ln}(kr)\right)}{j_{ln}(kr)}\right]_{r=r_{well}} = \frac{m^*_{in}}{m^*_{out}}\left[\frac{\frac{d}{dr}\left(h^{(1)}_{ln}(i\lambda r)\right)}{h^{(1)}_{ln}(i\lambda r)}\right]_{r=r_{well}} \tag{C.9}$$

to find $B$. We first seek to find a more reasonable form of C.9. Starting with the LHS and using equation C.2

$$\begin{aligned}
\frac{\frac{d}{dr}\left(j_{ln}(kr)\right)}{j_{ln}(kr)} &= \frac{\frac{l}{r}j_{ln}(kr) - kj_{l+1,n}(kr)}{j_{ln}(kr)} \\
&= \frac{l}{r} - k\frac{j_{l+1,n}(kr)}{j_{ln}(kr)} \tag{C.10}
\end{aligned}$$

The RHS can be simplfied in the same way to

$$\frac{\frac{d}{dr}\left(h_{ln}^{(1)}(i\lambda r)\right)}{h_{ln}^{(1)}(i\lambda r)} = \frac{l}{r} - i\lambda\frac{h_{l+1,n}^{(1)}(i\lambda r)}{h_{ln}^{(1)}(i\lambda r)} \tag{C.11}$$

Now, we have two equations to help us numerically solve this problem. Equation C.10 behaves well numerically, but we recall from our formulation and section C.1 that equation C.11 contains a ratio or two rapidly decaying exponentials, and numerically this could give us problems. Therefore we use equation C.3 and further evaluate

$$
\begin{aligned}
i\cdot\frac{h_{l+1,n}^{(1)}(\rho)}{h_{ln}^{(1)}(\rho)} &= i\cdot\frac{(-i)^{l+1+1}\frac{e^{i\rho}}{\rho}\sum\limits_{m=0}^{l+1}\frac{i^m}{m!(2\rho)^m}\frac{(l+m+1)!}{(l-m+1)!}}{(-i)^{l+1}\frac{e^{i\rho}}{\rho}\sum\limits_{m=0}^{l}\frac{i^m}{m!(2\rho)^m}\frac{(l+m)!}{(l-m)!}} \\[2em]
&= i\cdot\frac{(-i)^{l+1+1}\sum\limits_{m=0}^{l+1}\frac{i^m}{m!(2\rho)^m}\frac{(l+m+1)!}{(l-m+1)!}}{(-i)^{l+1}\sum\limits_{m=0}^{l}\frac{i^m}{m!(2\rho)^m}\frac{(l+m)!}{(l-m)!}}
\end{aligned}
$$

where we have canceled out the exponential components that give us numerical problems and we can further simplify this to

$$
\begin{aligned}
i\cdot\frac{h_{l+1,n}^{(1)}(\rho)}{h_{ln}^{(1)}(\rho)} &= i\cdot\frac{(-i)^{l+1+1-l-1}\sum\limits_{m=0}^{l+1}\frac{i^m}{m!(2\rho)^m}\frac{(l+m+1)!}{(l-m+1)!}}{\sum\limits_{m=0}^{l}\frac{i^m}{m!(2\rho)^m}\frac{(l+m)!}{(l-m)!}} \\[2em]
&= \frac{\sum\limits_{m=0}^{l+1}\frac{i^m}{m!(2\rho)^m}\frac{(l+m+1)!}{(l-m+1)!}}{\sum\limits_{m=0}^{l}\frac{i^m}{m!(2\rho)^m}\frac{(l+m)!}{(l-m)!}}
\end{aligned}
$$

plugging back in $\rho = \imath\lambda r$

$$\imath \cdot \frac{h^{(1)}_{l+1,n}(\rho)}{h^{(1)}_{ln}(\rho)} = \frac{\sum\limits_{m=0}^{l+1} \frac{1}{m!(2\lambda r)^m} \frac{(l+m+1)!}{(l-m+1)!}}{\sum\limits_{m=0}^{l} \frac{1}{m!(2\lambda r)^m} \frac{(l+m)!}{(l-m)!}} \tag{C.12}$$

This may look complicated, but numerically this is fairly simple. We could note that this may be simplfied further

$$\imath \cdot \frac{h^{(1)}_{l+1,n}(\imath\lambda r)}{h^{(1)}_{ln}(\imath\lambda r)} = \frac{\sum\limits_{m=0}^{l+1} \frac{1}{m!(2\lambda r)^m} \frac{(l+m+1)!}{(l-m+1)!}}{\sum\limits_{m=0}^{l} \frac{1}{m!(2\lambda r)^m} \frac{(l+m)!}{(l-m)!}} = \frac{K_{l+\frac{3}{2}}(\lambda r)}{K_{l+\frac{1}{2}}(\lambda r)}$$

Where $K$ is a modified Bessel (not-spherical) function of the second kind, but that seems more complicated to implement numerically. Now we put these past few equations together and we rewrite equation C.9 into

$$\frac{l}{r} - k\frac{j_{l+1,n}(kr)}{j_{ln}(kr)} = \frac{m^*_{in}}{m^*_{out}} \left[ \frac{l}{r} - \lambda\frac{\sum\limits_{m=0}^{l+1} \frac{1}{m!(2\lambda r)^m} \frac{(l+m+1)!}{(l-m+1)!}}{\sum\limits_{m=0}^{l} \frac{1}{m!(2\lambda r)^m} \frac{(l+m)!}{(l-m)!}} \right] \tag{C.13}$$

(recall that this must be solve at $r = r_{well}$). For the case of a spherical single band effective mas equation we only need to solve C.13. Note that

$$k = \sqrt{\frac{2m^*_{in}}{\hbar^2}(E_n + V_0)} \quad \text{and} \quad \imath\lambda = \sqrt{\frac{2m^*_{out}}{\hbar^2}(E_n)}$$

# Bibliography

[1] I N Kaiander, R L Sellin, T Kettler, N N Ledentsov, D Bimberg, N D Zakharov, and P Werner, "1 24 mu m ingaas/gaas quantum dot laser grown by metalorganic chemical vapor deposition using tertiarybutylarsine," *Applied Physics Letters*, vol 84, no 16, pp 2992–2994, 2004 [Online] Available http //link aip org/link/?APL/84/2992/1

[2] R L Sellin, I Kaiander, D Ouyang, T Kettler, U W Pohl, D Bimberg, Λ D Zakharov, and P Werner, "Alternative-precursor metalorganic chemical vapor deposition of self-organized ingaas/gaas quantum dots and quantum-dot lasers," *Applied Physics Letters*, vol 82, no 6, pp 841–843, 2003 [Online] Available http //link aip org/link/?APL/82/841/1

[3] S Tsao, H Lim, W Zhang, and M Razeghi, "High operating temperature 320 x 256 middle-wavelength infrared focal plane array imaging based on an inas/ingaas/inalas/inp quantum dot infrared photodetector," *Applied Physics Letters*, vol 90, no 20, p 201109, 2007 [Online] Available http //link aip org/link/?APL/90/201109/1

[4] X Brokmann, E Giacobino, M Dahan, and J P Hermier, "Highly efficient triggered emission of single photons by colloidal cdse/zns nanocrystals," *Applied Physics Letters*, vol 85, no 5, pp 712–714, 2004 [Online] Available http //link aip org/link/?APL/85/712/1

[5] A. Luque and A. Martí, "Increasing the efficiency of ideal solar cells by photon induced transitions at intermediate levels," *Phys. Rev. Lett.*, vol. 78, no. 26, pp. 5014–5017, Jun 1997.

[6] W. Shockley and H. J. Queisser, "Detailed balance limit of efficiency of pn junction solar cells," *J. Appl. Phys*, vol. 32, no. 510, 1961.

[7] G. F Brown and J. Wu, "Third generation photovoltaics," *Laser and Photon*, vol. 3, no. 4, pp. 394–405, 2009.

[8] T. Soga, *Nanostructured Materials for Solar Energy Conversion*. Amsterdam, The Netherlands: Elsevier, 2006.

[9] A. D. Yoffe, "Semiconductors quantum dots and related systems: Electronic, optical, luminescense and related properties of low dimensional systems," *Advances in Physics*, vol. 50, no. 1, pp. 1–208, 2001.

[10] S. L. Chuang, *Physics of Photonic Devices, Second Edition*. Hoboken, NJ: Wiley, 2009.

[11] B. E. A. Saleh and M. C. Teich, *Fundamentals of Photonics*. Hoboken, NJ: Wiley, 2007.

[12] P. C. Sercel and K. J. Vahala, "Analytical formalism for determining quantum-wire and quantum-dot band structure in the multiband envelope-function approximation," *Physical Review B*, vol. 42, no. 6, pp. 3690–3710, August 1990.

[13] G. B. Grigoran, E. M. Kazaryan, A. L. Efros, and T. V. Yazeva, "Quantized holes and the absorption edge in spherical semiconductor microcrystals with a complex valence band structure," *Soviet Physics-Solid State*, vol. 32, no. 6, pp. 1031–1035, June 1990.

[14] E. P. Pokatilov and V. A. Fonoberov, "Development of an eight-band theory for quantum dot heterostructures," *Physical Review B*, vol. 64, no. 245328, December 2001.

[15] N. W. Ashcroft and N. D. Mermin, *Solid State Physics*. USA: Thomson Learning, Inc., 1976.

[16] L. E. Ballentine, *Quantum Mechanics: A Modern Development*. New Jersey: World Scientific, 1998.

[17] A. A. Abrikosov, L. P. Gorkov, and I. E. Dzyaloshinski, *Methods of Quantum Field Theory in Statistical Physics*. Mineola, NY: Dover, 1963.

[18] D. J. Griffiths, *Introduction to Quantum Mechanics, Second Edition*. Upper Saddle River, NJ: Prentice Hall, 2005.

[19] B. H. Bransden and C J. Joachain, *Quantum Mechanics, Second Edition*. New York: Prentice Hall, 2000.

[20] P. Lowdin, "A note on quantum-mechanical perturbation theory," *J. Chem. Phys*, vol. 19, no. 11, pp. 1396–1401, November 1951.

[21] D. P. Craig and T. Thirunamachandran, *Molecular Quantum Electrodynamics*. Mineola, NY: Dover, 1998.

[22] J. M. Luttinger and W. Kohn, "Motion of electrons and holes in preturbed periodic fields," *Physical Review*, vol. 97, no. 4, pp. 869–883, February 1955.

[23] J. M. Luttinger, "Quantum theory of cyclotron resonance in semiconductors: General theory," *Physical Review*, vol. 102, no. 4, pp. 1030–1041, May 1956.

[24] I. Vurgaftman, J. Meyer, and L. Ram-Mohan, "Band parameters for iii-v compound semiconductors and their alloys," *Journal of Applied Physics*, vol. 89, no 11, pp. 5815–5875, June 2001.

[25] S. Datta, *Quantum Phenomena (Modular Series on Solid State Devices, Vol 8) (Hardcover)*. Mineola, NY: Addison-Wesley, 1989.

[26] G. Dresselhaus, "Spin-orbit coupling effects in zinc blende structures," *Physical Review*, vol. 100, no. 2, pp. 580–586, October 1955.

[27] S. L. Chuang, "Spin-orbit-coupling effects in the valence-band structure of strained semiconductor quantum wells," *Physical Review B*, vol. 46, no. 7, pp. 4110–4122, August 1992.

[28] A. Gushterov, L. Lingys, and J. Reithmaier, "Control of dot geometry and photoluminescence linewidth of ingaas/gaas," *J. Crystal Growth*, vol. 311, pp. 1783–1786, 2009.

[29] A. R. Edmonds, *Angular Momentum in Quantum Mechanics*. Princeton, NJ: Princeton University Press, 1957.

[30] W. C. Chew, *Wave and Fields in Inhomogeneous Media*. Lexington, KY: IEEE Press, 1999.

[31] D. S. Boudreaux, F. Williams, and A. Nozik, "Hot carrier injection at semiconductor electrolyte junctions," *J. Appl. Phys.*, vol. 51, p. 2158, 1980.

[32] F. Williams and A. Nozik, "Solid state perspectives of the photoelectrochemistry of semiconductor-electrolyte junctions," *Nature*, vol. 311, p. 21, 1984.

[33] U. Bockelmann and G. Bastard, "Phonon scattering and energy relaxation in two-, one-, and zero-dimensional electron gases," *Phys. Rev. B*, vol. 42, no. 14, pp. 8947–8951, Nov 1990.

[34] J. L. Blackburn, R. J. Ellington, and A. Nozik, "Electron relaxation in colloidal inp quantum dots with photogenerated excitons or chemically injected electrons," *J. Phys. Chem.*, vol. 107, p. 102, 2003.

[35] R. J. Ellingson, J. L. Blackburn, J. Nedeljkovic, G. Rumbles, M. Jones, H. Fu, and A. J. Nozik, "Theoretical and experimental investigation of electronic structure and relaxation of colloidal nanocrystalline indium phosphide quantum dots," *Phys. Rev. B*, vol. 67, no. 7, p. 075308, Feb 2003.

[36] V. Aroutiouian, S. Petrosyan, and A. Khachatryan, "Quantum dot solar cells," *J. Appl. Phys.*, vol. 89, no. 4, pp. 2268–2271, 15 February 2001.

[37] Y. Shoji, R. Oshima, and Y. Okada, "Structural properties of multi-stacked self-organized ingaas quantum dots grown on gaas (3 1 1)b substrate," *J. Crystal Growth*, vol. 312, pp. 226–230, 2010.

[38] A. Takata, R. Oshima, and Y. Okada, "Optical studies on inas/ingaas/ganas strain-compensated quantum dots grown on gaas (001) by molecular beam epitaxy," *J. Crystal Growth*, vol. 311, pp. 1774–1777, 2009.

[39] I. S. Gradshteyn and I. Ryzhik, *Table of Integrals, Series, and Products, Seventh Edition*. Burlington, MA: Elsevier, 2007.

[40] O. Madelung, *Semiconductors–Basic Data*. New York: Springer, 1996.

[41] W. W Bell, *Special Functions for Scientists and Engineers*. Mineola, NY: Dover, 2004.

[42] S. L. Chuang, "Efficient band-structure calculations of strained quantum wells," *Physical Review B*, vol. 43, no. 12, pp. 9649–9661, April 1991.

[43] I. Kang and F. W. Wise, "Electronic structure and optical properties of pbs and pbse quantum dots," *Journal of the Optical Society of America*, vol. 14, no. 7, pp. 1632–1646, July 1997.

[44] K. J. Vahala, "Quantum box fabrication tolerance and size limits in semiconductors and their effect on optical gain," *IEEE Journal of Quantum Electronics*, vol. 24, no. 3, pp. 523–533, March 1988.

# Index